OPTIMIZATION OF A TECHNIQUE FOR PHOSPHORESCENCE LIFETIME IMAGING OF OXYGEN TENSION IN THE MOUSE RETINA

by

Amanda C. Kight

A Thesis

Submitted to the Faculty

of the

WORCESTER POLYTECHNIC INSTITUTE

in partial fulfillment of the requirements for the

Degree of Master of Science

in

Biomedical Engineering

by

April 2002

APPROVED:

Ross D. Shonat, Ph.D., Major Advisor

Karl G. Helmer, Ph.D., Committee Member

Elizabeth Ryder, Ph.D., Committee Member

ACKNOWLEDGEMENTS

Funding for this project was provided, in part, by a pilot an feasibility grant from the Diabetes and Endocrinology Resource Center (DERC) at the University of Massachusetts Medical School, Worcester, MA, and by a biomedical engineering research grant from the Whitaker Foundation, Rosslyn VA.

I would like to extend my thanks to my family and friends for their support throughout my academic career, and to:

Kevin Hawkins and Daniel Traviglia, for their help with hardware and software issues, respectively, and for keeping the lab fun;

Karl Helmer and Elizabeth Ryder, my thesis committee, for taking interest in this project and providing constructive criticism;

Ross Shonat, my advisor and role model, for having tremendous faith in me and continuously encouraging me to reach my fullest potential.

ABSTRACT

Retinal hypoxia and inadequate oxygen delivery have been implicated as causal for the development of several eye diseases, including diabetic retinopathy, glaucoma, and retinopathy of prematurity. The imaging of oxygen tension in the retina, generated from a measure of the phosphorescence lifetimes of bolus-injected palladium-porphyrin probes, has been used successfully to study retinal oxygen dynamics in numerous animal models. However, the specific parameters for applying this technique in the mouse have not been thoroughly investigated. The goals of this project were to calibrate a newly-constructed phosphorescence lifetime imaging instrument and data analysis software against known oxygen concentrations, to determine specific parameters for probe excitation and image collection and analysis in the mouse eye, and to assess any damage caused to the eye by the technique using histological analysis. An *in vitro* system was developed for calibration of the probe and for estimation of power of excitation light and camera settings necessary to produce acceptable oxygen maps. *In vivo* experiments were then performed, and plots indicating camera settings necessary for producing varying qualities of oxygen maps were constructed. Trypsin digestion of retinal tissue was used in an attempt to assess any damage to experimental subjects, but this histological technique was deemed inadequate for analyzing the capillary structures of the mouse eye. Alternatively, damage was assessed using the instrument itself to calculate changes in oxygen tension during the experimental process. The results of this work will allow the phosphorescence lifetime imaging system to be used in the mouse to study how changes in retinal oxygen tension correlate with the progression of eye diseases where oxygen is implicated, including diabetic retinopathy.

TABLE OF CONTENTS

LIST OF TABLES AND FIGURES

1. INTRODUCTION

Retinal hypoxia has been implicated as a causal factor in the development of numerous eye diseases, including diabetic retinopathy, retinopathy of prematurity, and glaucoma. Recently, a phosphorescence lifetime imaging technique has been developed for measuring oxygen tension in the eye that has important implications for the study retinal oxygenation in mouse models of these serious diseases. Optimizing this phosphorescence lifetime imaging technique for use in the mouse eye will allow for more complete, accurate, and useful studies of the oxygen tension in normal and diseased mouse retinas.

Phosphorescence lifetime imaging has received considerable attention in the literature as a method for measuring oxygen tension *in vivo* [Shonat, 1997]. This technique involves the injection of a phosphorescent probe into animal vasculature and the subsequent excitation of this probe with light. From its excited state, the probe phosphoresces and can be quenched by oxygen. The degree of quenching and, hence, the concentration of oxygen, can be determined by measuring the phosphorescence lifetime. When the excitation light is modulated sinusoidally, the phosphorescence is emitted at the same frequency, but with a phase delay resulting from the finite lifetime of the phosphorescence. Using a phase-sensitive detector, such as a camera's image intensifier, phase and, therefore, lifetime, can be determined. Using the intensity of phosphorescence reaching the camera at a series of intensifier phase delay values, phase shift maps can be created. When known equations are applied to each pixel in these maps, the phase shift maps can be converted to oxygen tension (PO_2) maps.

Despite the recognition of this technique in the literature [Wilson, 1991 and Shonat, 1992, 1997, 1998], the specific parameters for data collection and analysis in the mouse eye have not been thoroughly investigated. The goal of this project was to examine these parameters in an effort to optimize the phosphorescence lifetime imaging technique for measuring oxygen tension in the mouse retina. The specific aims for achieving the goal of optimization were:

1. To calibrate the phosphorescence lifetime imaging system *in vitro* using a probe solution equilibrated at different oxygen concentrations.
2. To determine appropriate parameters for optimal excitation of the probe, including wavelength, bandwidth, energy, and power of the excitation light.
3. To determine optimal procedures for image collection and analysis, including camera exposure time, intensifier gain, and number of images necessary for fitting.
4. To examine, using histological techniques, any potential microvascular damage induced by this measurement.

2. BACKGROUND

Phosphorescence lifetime imaging is the marriage of techniques in physiology, imaging, and microscopy. Understanding its application to the normal or diseased eye requires study of eye structure, retinal oxygenation, and the basics of imaging and microscopy. The following sections provide background in these areas, as well as an overview of phosphorescence lifetime imaging in general.

Oxygen Delivery and Consumption in the Retina

The eye is a unique organ requiring a complex vasculature to deliver adequate oxygen for visual and neural function, while maintaining visual clarity and transparency. Oxygenation in the various parts of the eye, including the retina, reflects the distinctive demands of ocular vascularization.

The retina is located on the back surface of the eye, behind the vitreous. All vertebrate retinas have a layered structure [Dowling, 1987 and Moses, 1987] (Figures 2.1 and 2.2). Two synaptic layers, known as the outer and inner plexiform layers, are stacked between three cellular layers, termed the outer and inner nuclear layer and the ganglion cell layer [Dowling, 1987]. These layers are capped by the pigmented epithelial layer and the inner limiting membrane. The outer nuclear layer contains the cell bodies of the photoreceptors, which are sensitive to light and initiate all visual responses in the retina and the brain [Dowling, 1987 and Moses, 1987]. The inner nuclear layer contains the neuron and glial cell bodies (not shown in the figure), while the ganglion cell layer contains the ganglion cell bodies. The outer plexiform layer is the site of the synaptic reactions of photoreceptors, horizontal cells, and bipolar neurons. The inner plexiform layer houses the synaptic interactions involving bipolar neurons, amacrine cells, and ganglion cells [Moses, 1987].

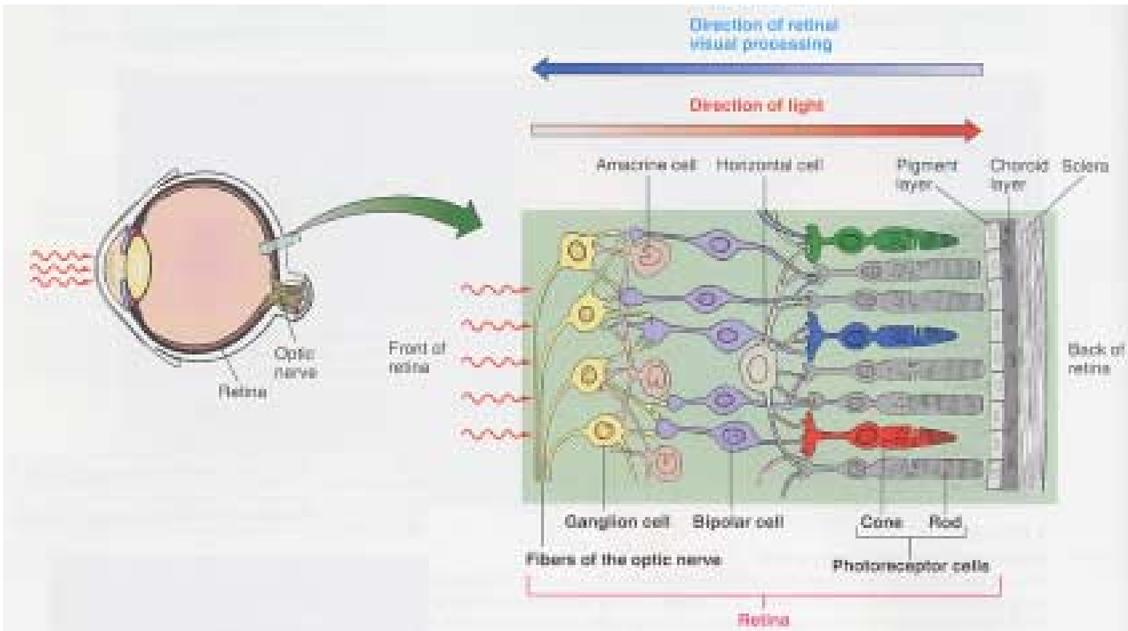

Figure 2.1-Cutaway view of retinal layers. Light enters from the front of the retina and travels through the layers to the photoreceptors. Visual information travels from the photoreceptors to the bipolar cells and the ganglion cells before traveling down the fibers of the optic nerve to the brain [Sherwood, 2001].

When light enters the eye, it passes through the retina and is captured by the photoreceptors and the outer segments of the pigment-containing cells in the pigment epithelium [Dowling, 1987]. Visual processing then occurs in the opposite direction, passing through the retina to the optic nerve at the front of the retina. The fibers of the optic nerve then transmit the visual signal to the brain.

The retina requires adequate amounts of oxygen for normal function [Linsenmeier, 1989 and Yu, 2001]. The photoreceptors responsible for collecting light and converting it to an electrical signal contain a large concentration of mitochondria,

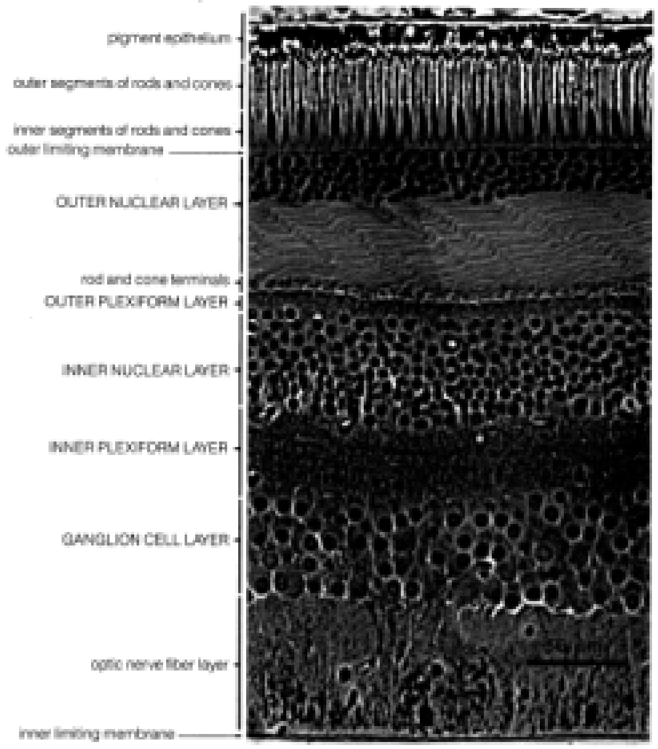

Figure 2.2—The layered structure of the retina [Dowling, 1987].

necessary for producing energy to carry out this function. This large production of energy makes the retina one of the highest oxygen consuming tissues in the body [Yu, 2001]. However, the necessity of transparency in the retina limits extensive vascularization, and the retina has only a simple vasculature radiating from the optic nerve; [Yu, 2001]. This constraint dictates that the extensive oxygen requirements of the retina be met in part by adjacent vasculatures. The avascular parts of the retina, including the photoreceptors and the outer regions, are preferentially supplied with oxygen by the choroidal vasculature, which lies behind the retina [Delori, 1988 and Yu, 2001] (Figure 2.1). This vasculature is characterized by a low vascular resistance and high blood flow rate, with an average PO_2 very close to arterial PO_2 [Linsenmeier, 1989 and 2000] and significantly greater than the PO_2 in the retinal vasculature.

Retinal oxygen consumption is heterogeneous through the different layers of the tissue [Yu, 1999]. Oxygen tension is relatively uniform in the inner retina, reaches a minimum within the outer retina, and rises to a maximum at the tips of the outer segments near the choroid [Linsenmeier, 1986] (Figure 2.2). In regards to oxygen consumption modeling, the avascular outer retina can be broken into three layers: layer 1, consisting of the pigment epithelium and outer segments of the photoreceptors; layer 2, consisting of the inner segments of the photoreceptors; and layer 3, consisting of the outer plexiform layer. Of these three layers, only layer 2 consumes oxygen, as oxygen-dependent mitochondria are most abundant in the inner segments of the photoreceptors [Linsenmeier, 1986 and 2000]. The oxygen consumption of the other two layers is modeled most accurately with values near zero.

The oxygen demands of the inner retina are supplied directly by the retinal circulation. The retinal circulation differs from the choroidal circulation in terms of flow rate and control mechanisms [Linsenmeier, 1986]. There exist two capillary beds in the retina, the outer bed being more venous in nature than the inner layer [Alder, 1983]. The oxygen tension is relatively low between these two beds [Yu, 1999]. The retinal circulation has no autonomic innervation, relying totally on local control mechanisms to regulate distribution of blood flow [Alder, 1997]. The capillary system in the retina is sparse to allow for minimal optical interference and, as such, has a large arteriovenous oxygen difference [Alder, 1997].

The high oxygen demands of the retina, along with its delicate supply mechanisms, make it more vulnerable to vascular deficiencies than most other organs [Yu, 2001]. Neither the retinal nor the choroidal circulation is capable of adequately compensating for impairment to the other [Alder, 1983]. Thus, damage to either the retinal or choroidal vasculature can be devastating, often resulting in complete loss of vision [Yu, 2001]. Problems with retinal oxygen supply are often treated with panretinal photocoagulation. This technique, in which a laser is applied to broad areas of the retina, destroys photoreceptors in the peripheral retina and is thought to increase the oxygen flux from the choroid to the inner retina and thereby compensate for a decrease in retinal circulation. Less oxygen is consumed in the partially burned outer retina, allowing for increased oxygen supplied to the inner retina [Stefansson, 1981].

Oxygen Measurements in the Eye

Many different techniques have been developed for measuring oxygen tension in the eye. However, most of these techniques have significant limitations, particularly in applications to the small mouse eye.

Oxygen-sensitive microelectrodes have been used extensively in animal models for generating oxygen profiles in the eye. While their use has offered many insights into ocular oxygenation, this method is highly invasive; the insertion of the electrode into the eye and the subsequent withdrawal of the electrode with oxygen tension measurements taken at specified points can cause significant trauma. Each introduction of the electrode offers only a one-dimensional oxygen profile for the region of insertion. Electrodes must also be recalibrated following each profile measurement. The invasive nature of the microelectrode prevents its ready application in clinical settings (due to the necessity of surgical intervention), or to mice (due to the small size of the eye) [Ito, 2001].

Retinal vessel oximetry has been used in humans to determine oxygen saturation of blood [Delori, 1988]. This technique is based on the fact that the light absorbing properties of blood (absorbance spectrum) depends on the amount of oxygen bound to hemoglobin. While the technique may be used to accurately determine oxygen tensions under ideal conditions, measurements are adversely affected by a number of factors including eye pigmentation, turbidity of ocular media, and irregular retinal topography [Delori, 1988]. It is also an indirect measure of oxygen tension.

MRI-based methods have also been used to survey oxygen characteristics of the retinal surface [Ito, 2001]. This method is unhindered by optical properties and eye size, but it requires the use of a perfluorocarbon droplet situated in the preretinal vitreous space, thus limiting its application in human subjects.

Light-based methods for exploring oxygen tensions in the eye have gained recent prominence. Some fluorescent and phosphorescent compounds (see Fig. 2.4) have been discovered to be sensitive to oxygen; when oxygen collides with a light-emitting compound in its excited state, it quenches the molecule and prevents light emission. The use of fluorescence to determine PO_2 is limited due to relatively low sensitivity of fluorescent molecules to oxygen [Vanderkooi, 1987]; fluorophores remain in the excited state for a relatively short period of time (nanoseconds to microseconds), and thus have limited opportunity to collide with oxygen molecules, particularly at low PO_2s. Changes in turbidity of the suspending medium also affect fluorescence measurements. In contrast, phosphorescent probes are not affected by blood flow, and have relatively long lifetimes (microseconds to seconds), thereby increasing the likelihood of collision with oxygen molecules in the blood.

Imaging and Microscopy

Standard research microscopes and low power objectives can be used for viewing the small mouse eye and its vasculature. Major parts of the microscope optical train include the light source, a dichromatic beam splitter (for fluorescence and phosphorescence microscopy), the objective lens, the ocular, and the camera or observer's eye (Figure 2.3). An image is produced and focused to infinity by the

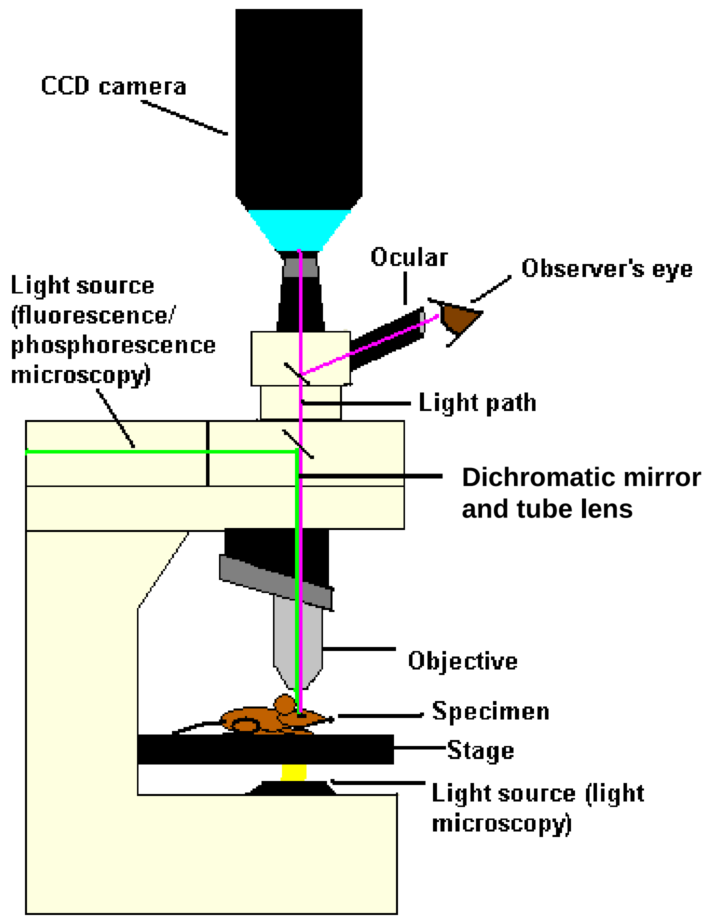

Figure 2.3-Optical train of a microscope. The specimen is illuminated by one of the light sources, and the image of the specimen travels along the optical train to the camera and/or the observer's eye.

objective lens conjugate with the specimen. A very high quality, diffraction-limited image is produced with a modern, high-numerical aperture plan-apochromatic objective lens [Inoue, 1997]. A tube lens then focuses the image onto a target. When a charge-coupled device (CCD) camera is used, that target consists of a large array of photodiodes deposited on a silicon substrate. Each sensor element on the CCD camera is a silicon photodiode built into the silicon chip, isolated electrically from its neighbors by a channel stop [Inoue, 1997]. The image may also be projected to the eye.

Phosphorescence Lifetime Imaging of Oxygen Tension

Phosphorescence lifetime imaging has been recognized in the literature as a technique for measuring oxygen tension in the vasculature [Wilson, 1991 and Shonat, 1992, 1997, 1998]. This technique can be applied to determine oxygen tensions in the mouse retina and in such a case is based on excitation of a phosphorescent probe and subsequent quenching of phosphorescence by intravascular oxygen. The probe is bolus-injected intravenously, and equilibrates in the bloodstream. It may then be excited by light delivered through the eye. When excited, the probe molecules phosphoresce, and are quenched when they collide with oxygen molecules. The frequency of collision and, hence, the oxygen concentration, may then be determined by computing the lifetime of the phosphorescence decay. The probe remains exclusively in the vasculature in the eye due to the blood-retinal barrier.

The phosphorescent probe generally used is palladium *meso-tetra* [4 carboxyphenyl] porphrine. This probe is sensitive to oxygen in physiological concentrations when bound to excess albumin. It is excited at 422 and 524 nm, and emits phosphorescence at 698 nm, a wavelength in the near-infrared range where the retinal tissue absorbs minimally [Shonat, 1992 and Lo, 1996].

Phosphorescence lifetime imaging requires a unique microscopic instrument (Figure 2.4). An illuminating beam is emitted by a xenon arc lamp, sinusoidally modulated using an optical chopper, and a particular wavelength (524 ± 20 nm) is selected by a monochromator. The light is then low-pass filtered and reflected down into the objective by a dichromatic mirror (pass>575 nm). This light excites phosphorescent molecules in the vasculature to their triplet states, and phosphorescence is emitted during the decay of these molecules back to the ground state. This emitted light then passes

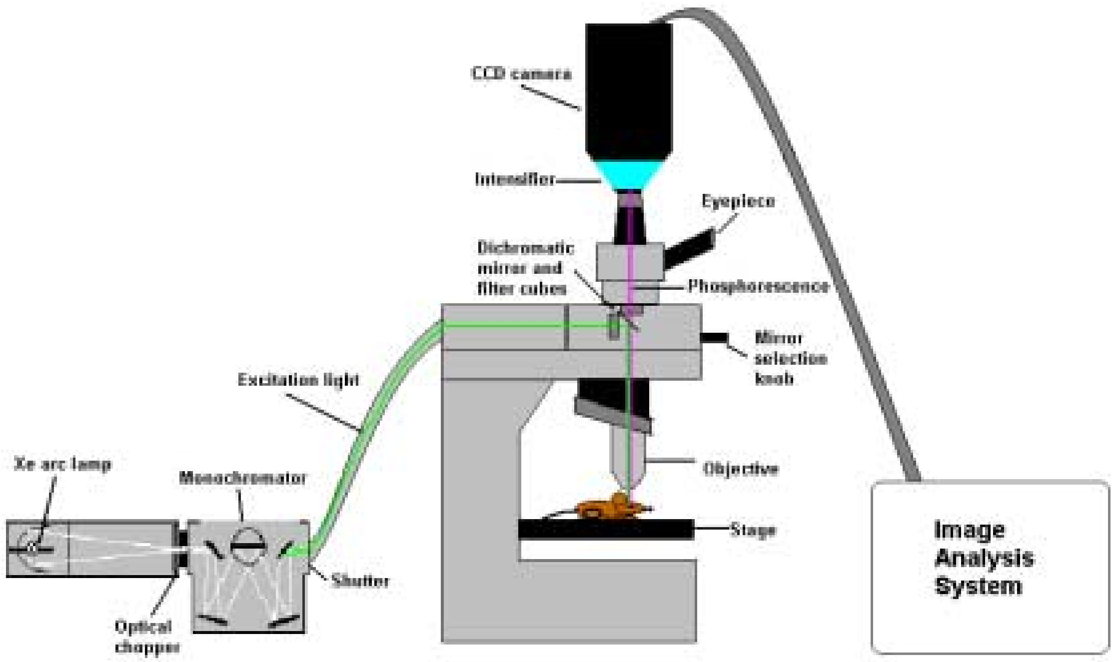

Figure 2.4-The phosphorescence lifetime imaging system. White light is emitted by the xenon arc lamp and sinusoidally modulated by the optical chopper. The monochromator selects a particular wavelength of light, which is directed to the eye by a dichromatic mirror. Phosphorescence is produced by probe in the eye, and travels to the CCD camera.

straight through the dichromatic mirror to the intensifier, which amplifies the relatively weak phosphorescent signal before transmitting it to the CCD camera. The intensifier is also used for the phase-sensitive detection of phosphorescence lifetimes, which will be explained below. The image is then conducted to the PC-based image analysis system. This technique represents one of the few modes of microscopy in which the illuminating excitation wavelength differs from the wavelength of emitted light [Inoue, 1997]. Due to the relative weakness of the emitted light, high-sensitivity photodetectors and high light-gathering optics are required. These include objectives with high numerical aperture-to-magnification ratios and high transmission for the relevant wavelengths [Inoue, 1997]. Phosphorescence is defined as the emission of light during a transition from an excited triplet state to the ground state. The energy diagram in Figure 2.5 illustrates this phenomenon. The three singlet states (ground, first, and second) are depicted by S_0, S_1, and S_2, respectively. In each of these states, the molecule may exist in a number of vibrational energy levels, indicated by 0, 1, 2, etc. [Lakowicz, 1999]. Photons are depicted by lightning bolts. The vertical lines represent possible transitions between states, illustrating the instantaneous nature of light absorption.

When a fluorescent or phosphorescent molecule absorbs a photon, it is excited to a higher vibrational level of S_1 or S_2. Fluorophores then rapidly relax to the lowest vibrational level of S_1, a process called internal conversion (Figure 2.4) [Lakowicz, 1999]. The molecule will then return to the ground state at any of the vibrational energy levels, quickly relaxing to the lowest level. During the decay to the ground state, the molecule emits of photon in the form of fluorescence.

Excitation to the triplet state (T_1) involves a spin conversion from the S_1 state, resulting in a state with unpaired spins—a phenomenon termed intersystem crossing (Figure 2.4) [Turro, 1978 and Lakowicz, 1999]. In this excited state, the two electrons are each in a different orbital, and thus the Pauli exclusion principle does not require their

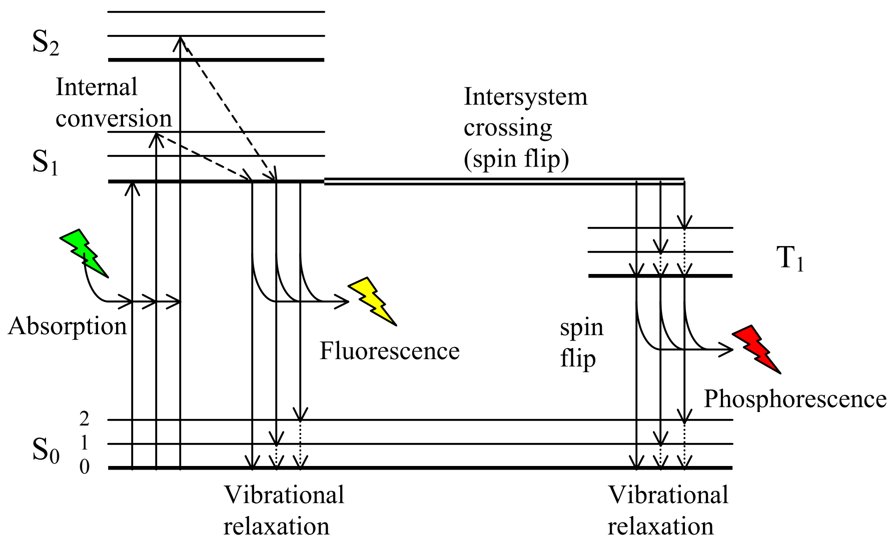

Figure 2.5—Energy diagram for fluorescent and phosphorescent molecules. S_0, S_1, and S_2, depict ground, first, and second singlet states, respectively. T_1 depicts the triplet state. Each state has representative vibrational states indicated by 0, 1, and 2. Solid vertical lines arrows represent transitions between states, dashed arrows represent vibrational relaxation within states, and lightning bolts represent photons. A molecule is excited from the ground state to any of the vibrational levels of the singlet state, and then decays to the lowest vibrational state in S_1. Fluorescent molecules will then decay down to the ground state with the emission of fluorescence, with a total reaction time on the order of ns to µs. Phosphorescent molecules undergo a spin flip to the triplet state, then decay to the ground state with a spin flip and phosphorescence emission, with a total reaction time of the order of µs to s. Once in the ground state, molecules will relax to the lowest energy level (0). Adapted from Lakowicz, 1999 and Vanderkooi, 1990.

spins to be paired. The energy required to produce this excited state is determined by the equation

$$\Delta E = E_2 - E_1 = h\upsilon$$

where h is Planck's constant, υ is the frequency of the excitation light, and E_2 and E_1 are the energies of a single molecule in the initial and final states [Turro, 1978]. Like the singlet state, the triplet state is a metastable species, and will decay to the ground state after a finite time, emitting a photon in the form of phosphorescence. However, the decay from the triplet state takes a relatively long time (microseconds to seconds) when compared with decay from the singlet state (nanoseconds to microseconds) due to the quantum mechanically forbidden spin flip completed during the decay.

When a large number of phosphorescent molecules are excited simultaneously, the resultant light emission is the sum of the individual photon emissions, and can be represented by the function:

$$I(t) = I_0 \exp(-t/\tau)$$

where I(t) is the phosphorescence intensity as a function of time (t), I_0 is the initial, maximum intensity at t = 0, and τ is the lifetime of the decay [Shonat, 1995].

In phosphorescence the excitation and emission wavelengths differ, and neither is exact; the numerous possible vibrational states create a range of wavelengths that may be absorbed or emitted, with a relative maximum wavelength resulting from conversions between the most common states. The excitation spectrum for palladium *meso-tetra* [4-carboxyphenyl] porphrine, the phosphorescent probe used in this study, has maxima at 420 and 524 nm. Due to the absorption of excitation light by blood, the volume of excitation, defined as the excitation area times the penetration depth, is ten times smaller at 420 nm than at 524, and the total quantity of probe excited is reduced [Shonat, 1995]. The emission is maximal at 687 nm, regardless of what wavelength is used for excitation; decay always occurs from the lowest vibrational level of the triplet state resulting in a consistent emission spectrum [Lo, 1996 and Vanderkooi, 1990].

When the phosphorescent probe is excited by light that has been sinusoidally modulated, the phosphorescence emitted will have the same frequency, but will have lower amplitude and be delayed in phase by an angle θ. θ is related to the probe lifetime, τ, by the following equation:

$$\tan \theta = \omega\tau$$

where ω is the excitation frequency [Shonat, 1997].

A phosphorescent molecule that has been excited to the triplet state may transfer its energy to another molecule without light emission, a phenomenon termed *quenching* (Figure 2.6). Such interactions between phosphors and their environment are common; the spin-forbidden transition from the triplet state to the ground has a relatively long lifetime, and increases the probability of contact between molecules [Vanderkooi, 1990].

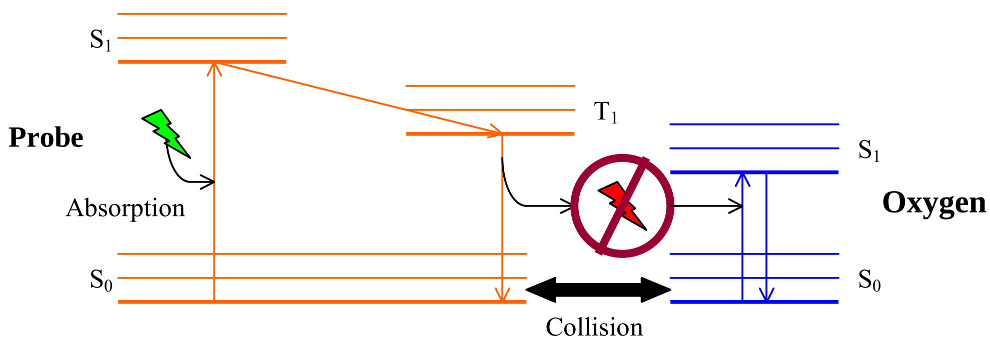

Figure 2.5—Quenching of the phosphorescent probe by oxygen. 6When the two molecules collide, the decaying probe gives its energy to oxygen instead of giving it off as phosphorescence. This results in a singlet oxygen molecule, which decays to the ground state within microseconds.

In blood, the only significant quenching agent is oxygen [Wilson, 1991]. The degree of quenching of the phosphorescent molecule depends on the concentration of oxygen in its vicinity [Shonat, 1992]. The efficiency of phosphorescence quenching is governed by the frequency of collision between the excited triplet state molecule and the quencher before the phosphor returns to the ground state. This relationship is represented by the Stern-Volmer equation:

$$\tau_o / \tau = 1 + k_Q \tau_0 [PO_2]$$

where τ_o is the lifetime in the absence of oxygen, k_Q is the bimolecular rate constant (or quenching constant), and $[PO_2]$ is the oxygen concentration [Vanderkooi, 1987, Shonat, 1995 and 1997, and Lo, 1996]. In a zero oxygen environment, $\tau = \tau_o$ and the lifetime is a maximum.

Quenching reactions form excited singlet oxygen (Figure 2.5), which may react with unsaturated double bonds in lipids to form peroxides. These peroxides destructively alter amino acids and nucleic acids. However, destruction of biological tissue by these reactions is mitigated by the fact that singlet oxygen decays to the ground state within microseconds, and any chemical reactions must occur by collision with the singlet-state molecule before it decays [Vanderkooi, 1987]. However, the potential for vascular damage must always be considered when using these probes for *in vivo* applications.

Palladium meso-tetra porphrine must be mixed with excess albumin prior to injection for phosphorescence quenching studies. This complex has several properties essential to accurate phosphorescence lifetime imaging: the sensitivity to quenching of albumin-bound probe by oxygen is independent of the suspending medium or probe concentration in solution, self-quenching of the probe is eliminated, and the sensitivity to oxygen is increased since the binding to albumin decreases k_Q [Vanderkooi, 1987 and Shonat, 1995]. As long as albumin is present in excess of the probe, the probe/albumin complex may be suspended in saline and injected directly into the femoral vein, and will show no decrease in phosphorescence intensity over several hours [Wilson, 1991].

Calibration of the probe for determining oxygen concentration in the vasculature is absolute—calibration depends only on the phosphor and its molecular environment, which remain constant for such experiments [Lo, 1996]. Once τ_0 and k_Q are known *ex vivo*, they apply *in vivo* and recalibration is not necessary [Vanderkooi, 1987].

From phosphorescence lifetime, PO_2 can be calculated. A phase-sensitive measure of this phosphorescence lifetime is possible when the delivered excitation light and the sensitivity of the collection system (intensifier) can be independently modulated and the phase relationship between these two elements can be accurately varied [Shonat, 1997]. Intensity images may then be taken with increasing intensifier phase delays relative to excitation phase, and a graph of intensity versus phase delay constructed. This graph may be used in conjunction with the following equation to determine the phosphorescence phase delay, θ:

$$I(\theta_D) = k[Pd]\{1+ m_D m\cos(\theta - \theta_D)\}$$

where $I(\theta_D)$ is the intensity as a function of known phase delay, k is a constant, [Pd] is the probe concentration, θ_D is the phase delay of the intensifier sensitivity, m_D is the modulation of the emission, and

$$m = (1 + \omega^2\tau^2)^{-1/2}.$$

However, since this equation is nonlinear, applying it to each pixel in an image is computationally difficult. A linearized form of the equation was developed by Lakowicz [1992] by applying the trigonometric identity for subtraction of cosine terms and combining the fitting parameters into linear coefficients:

$$I(\theta_D) = a_0 + a_1\cos\theta_D + b_1\sin\theta_D$$

where a fit to the equation can be determined by the evaluation of a_0, a_1, and b_1 using linear regression. θ is then determined as:

$$\tan^{-1}(b_1/a_1)$$

and may be used to determine τ for each pixel. This value of τ is used in the Stern-Volmer equation to calculate PO_2 maps (Figure 2.7).

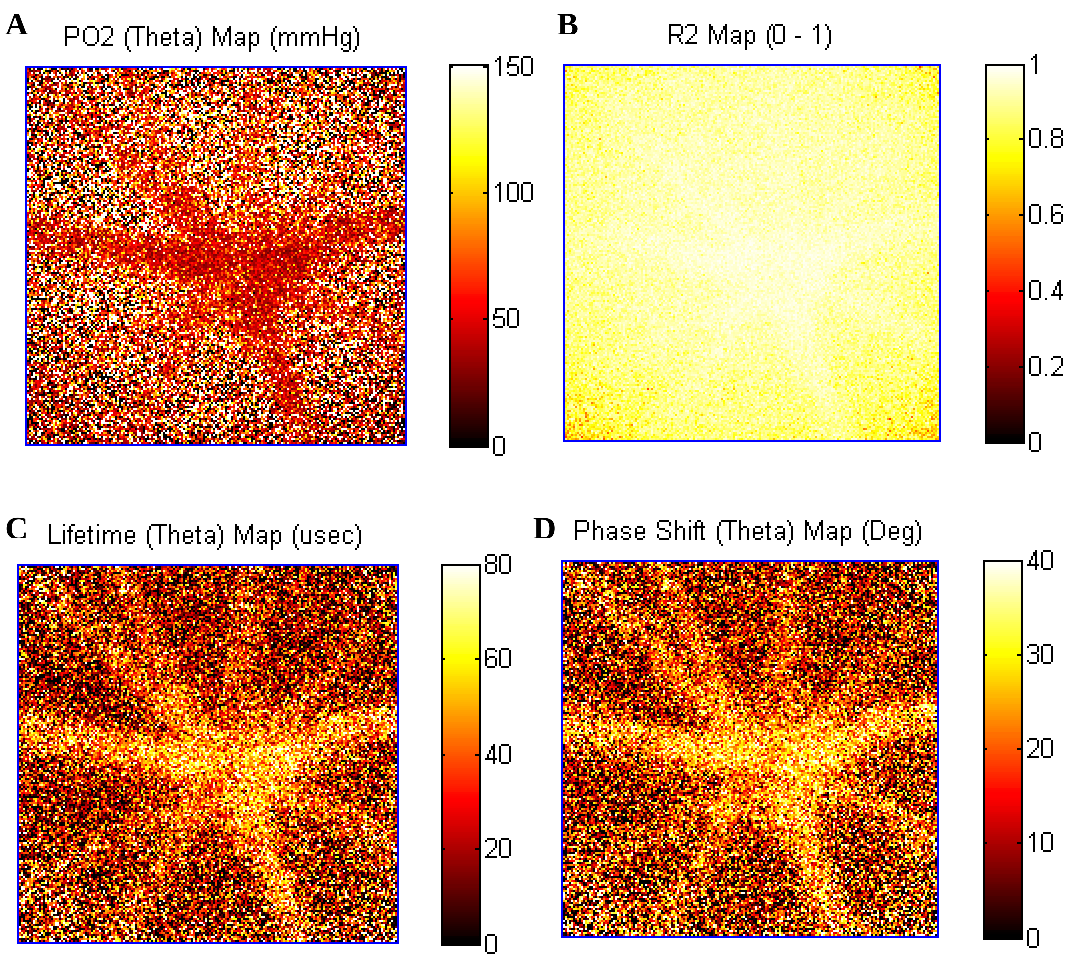

Figure 2.7—Maps of the mouse retina. The PO_2 map (A) is created using the Stern-Volmer equation. The parameters for the equation are calculated by fitting a series of intensity images to a linear equation (B shows the R^2 for this fit in every pixel), which is used to determine phase shift (D). Phase shift is then used to calculate lifetime (C).

Certain hardware and software elements and an electronic interface are required for the generation of PO_2 maps (Figure 2.8). The program used for data collection,

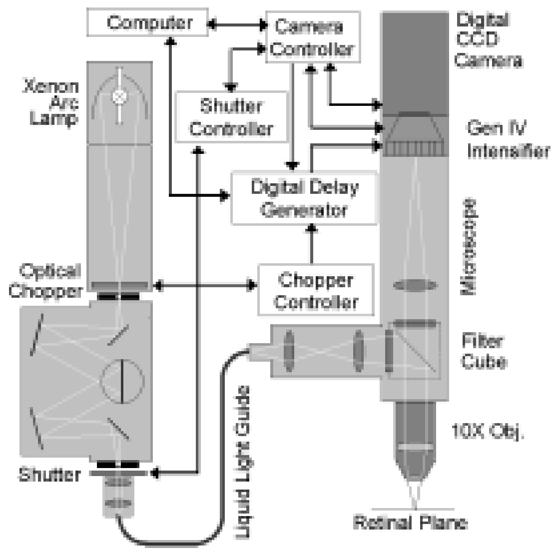

Figure 2.8—Schematic diagram of the phosphorescence lifetime imaging system.

WinViewNT (Roper Scientific, Trenton, NJ), allows for control of the digital delay generator (Stanford Research Systems, Sunnyvale, CA) and the camera and its intensifier (Roper Scientific, Trenton, NJ). The delay generator sets the phase delay of the intensifier relative to the optical chopper. The optical chopper controller (Photon Technology, Brunswick, NJ) rotates the chopper disc at 1.6 kHz, and sinusoidally modulates the light produced by the Xenon arc lamp. The light passes through a monochromator (Photon Technology), which selects the wavelength used for excitation (524±20 nm). A shutter (Vincent Associates, Rochester, NY), which is directly connected to the camera control mechanism, operates in parallel with the camera, opening only during camera exposure and blocking the excitation light when the camera shutter is closed. The light passes through a focusing lens and an interference filter, is reflected off a dichromatic mirror, and is concentrated by an infinity-corrected objective to reach the retinal plane [Shonat, 1992 and 1995]. Light emitted from the eye is collected by the objective and sent to the dichromatic mirror, where wavelengths longer than the cut-off wavelength of 630 nm pass through to the intensifier to the CCD camera [Shonat, 1992]. The camera delivers each image to the WinViewNT program, where the entire series may be stored as a single binary data file.

Advantages of phosphorescence lifetime imaging of oxygen tension are numerous. Recalibration of the probe is not required. The response time is very short, and signal acquisition and calculation are rapid. Data analysis is also relatively simple, since the dependence of phosphorescence lifetime on oxygen pressure follows a well-defined physical relationship, which can be expressed with simple equations [Lo, 1996].

Difficulties with the phosphorescence lifetime imaging technique mainly involve the possible effects of the excitation on the tissue. The excitation of the phosphorescent probe within the blood vessels of the eye and subsequent quenching by oxygen creates oxygen free radicals, which are toxic to the vessels and tissue. Extensive excitation of the probe decreases the amount of oxygen available to the eye, and can cause significant damage. To limit tissue damage, the concentration of the probe and the duration of exposure to excitation light should be kept to a minimum [Shonat, 1995].

To utilize the phosphorescence lifetime imaging system to its fullest potential, the existing structure was calibrated using an *in vitro* system to ensure that oxygen maps report accurate PO_2 values. Acquisition parameters, including camera exposure time, intensifier settings, power of excitation light, and number of images necessary for determining phase shift were determined for *in vivo* experiments. Histological techniques were used in an attempt to assess any microvascular damage induced by the measurement.

3. METHODS

Despite its potential usefulness in the characterization of oxygen tensions in diabetic retinopathy and other oxygen-related eye diseases, the specific parameters for phosphorescence lifetime imaging in the mouse eye have not yet been determined. The primary goal of this project was to determine these parameters. To this end, *in vitro* and *in vivo* experiments were conducted, and appropriate gains, exposure times, and other imaging considerations were examined.

Data Acquisition and Analysis

Phosphorescence intensity images were collected using the WinViewNT software package (see Background). For each data set, a series of 15 to 30 images was taken at increasing phase delays, and stored as a single binary data file. Data analysis for all *in vitro* and *in vivo* experiments was done using Microsoft Excel, SigmaPlot, and a program in MatLab called "Retina," developed by Ross Shonat (see Appendix B).

Three experiments at each gain and exposure time were performed. Map R^2 values, indicating the fit to the equation $I(\theta_D) = a_0 + a_1\cos\theta_D + b_1\sin\theta_D$, were used as an indication of the quality of the oxygen maps. PO_2 means and standard deviations for specified regions were calculated using the "Retina" program.

In Vitro Experiments

An *in vitro* system was constructed to calibrate the phosphorescence lifetime imaging system and to determine approximate gain settings and exposure times required to produce acceptable oxygen maps. The system, pictured in Figure 3.1, included a

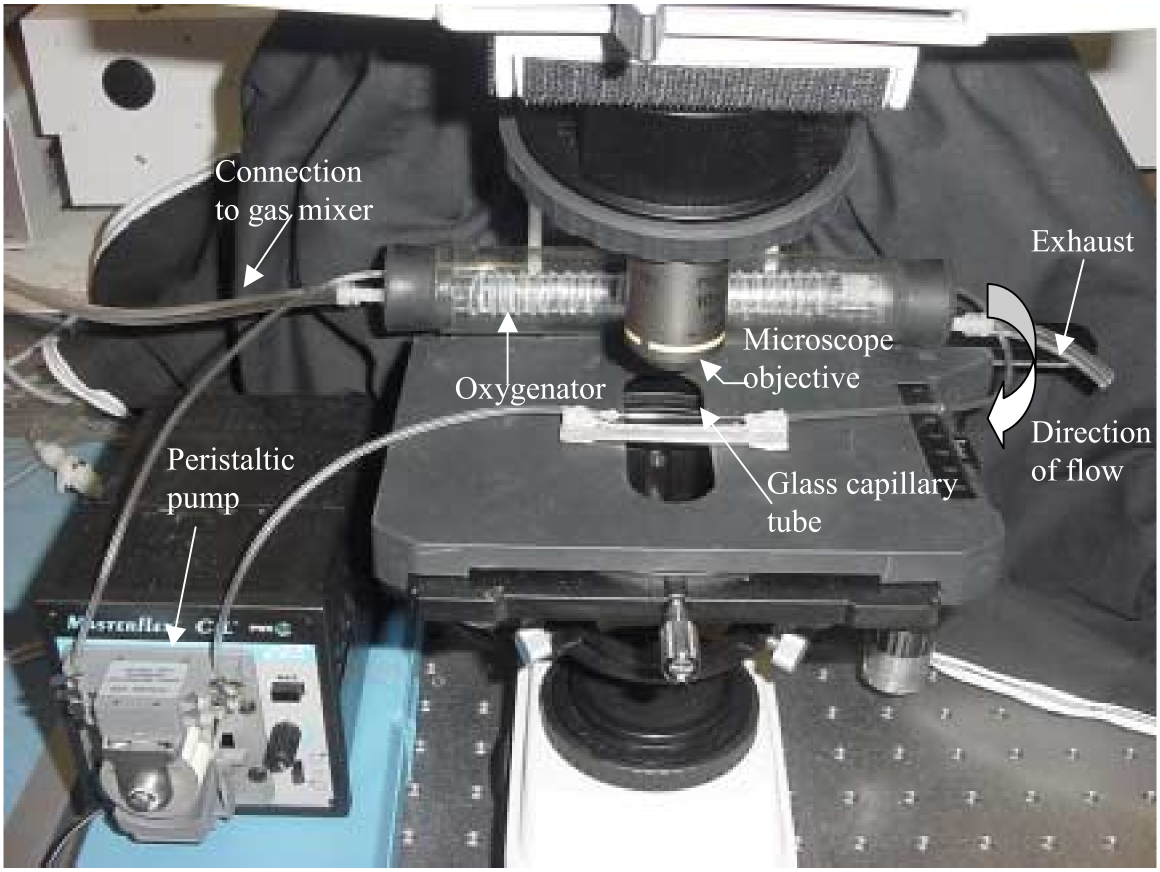

Figure 3.1—*In vitro* system. The system consists of an oxygenator connected to a gas mixer, a peristaltic pump used for circulating probe solution inside the system, and a square glass capillary tube situated under the microscope objective used for measuring the PO_2 of the solution. The parts are connected with Tygon® microbore tubing, which may be disconnected at various junctions and injected with solution using a 22-gauge needle and syringe.

length of Tygon® tubing, into which a probe solution, consisting of 12 ml albumin stock solution, 148 mg NaCl, 216 mg glucose, and 10 μl probe was injected. A peristaltic pump was used to circulate the fluid through the system. The phosphorescent solution flowed through an oxygenator (consisting of a length of plastic tubing, inlaid with a Plexiglas rod wrapped with oxygen-permeable silastic tubing, and capped at each end by a rubber stopper with an inlet connector for the gas mixer and an outlet for exhaust), used to apply gas mixtures with known oxygen concentrations. Upon leaving the oxygenator, the solution flowed through a square glass capillary tube situated under the phosphorescence lifetime imaging system. The phosphorescence lifetime was then measured as previously described, and a PO_2 map was generated. The correspondence between the PO_2 values indicated by the map and those applied using the gas mixer and oxygenator was used to calibrate the system to provide accurate measures of PO_2 within the vasculature.

Signal-to-noise ratios (SNR) were used to determine appropriate gain settings and exposure times. The probe was equilibrated at a physiological oxygen concentration of 40 mm Hg (5% oxygen applied using the gas mixer and oxygenator). Exposure times were tested at random in an attempt to achieve a maximal range of SNR for camera intensifier gain settings 10, 100, and 255. Exposure times yielding SNR of approximately 2 and approximately 225 were noted for each gain. Phosphorescence lifetime images were then taken at a range of ten exposure times equally spaced between the time yielding SNR ≈ 2 and the time yielding SNR ≈ 225. R^2 maps, which demonstrate the integrity of the fit between the phosphorescence intensity data and the equation $I(\theta_D) = a_0 + a_1\cos\theta_D + b_1\sin\theta_D$, were then created. From these maps, the average R^2 value for the entire capillary tube was determined. These values were plotted versus SNR for each gain setting

The *in vitro* system was also used to calibrate the phosphorescence lifetime imaging system against known oxygen concentrations. Oxygen concentrations in the physiological range of zero to 100 mm Hg were tested. To obtain concentrations in this range, the oxygenator was used to apply gas mixtures between one and 12 percent O_2 balanced with N_2. A zero oxygen environment was obtained by adding probe solution and a pinch of glucose oxidase to a closed cuvette to prevent leakage of environmental oxygen into the system (Figure 3.2). At each oxygen concentration, ten image sets were taken at each of four gain settings (100, 70, 40 and 10). Exposure times were 0.23, 0.47, 0.83, and 1.0 seconds, respectively, and were selected based on the fact that they yield SNRs between 3 and 15. After each exposure, the objective was blocked with white paper to produce intensity images with a theoretical phase delay of zero and a modulation of one (reflected images). These data were used to determine the intrinsic phase delay and modulation of the instrument.

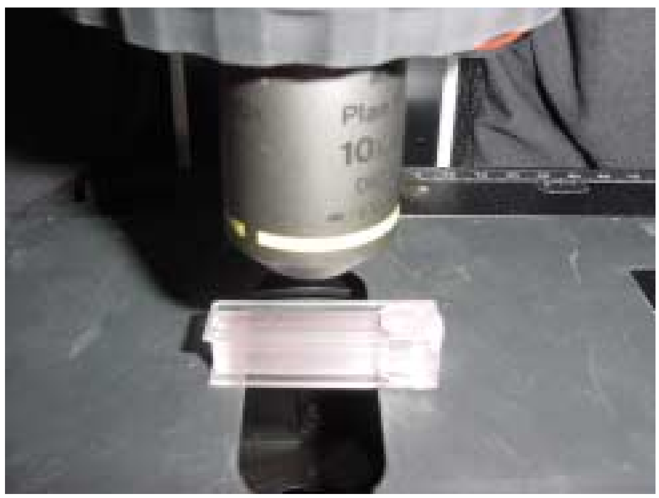

Figure 3.2—Zero-oxygen *in vitro* testing system. Cuvette is filled with glucose-containing probe solution, to which glucose oxidase is added to remove all oxygen.

In Vivo *Oxygen Mapping*

All animal experiments were performed in accordance with WPI's Institutional Animal Care and Use Committee (IACUC) protocols and the Association for Research in Vision and Ophthalmology statement for the Use of Animals in Ophthalmic and Vision Research. Mice were anesthetized prior to all experiments with a solution of 125 µl

Avertin and 4.875 ml saline, in the amount of 0.25 ml/10 g body weight (adjusted as needed). When fully anesthetized, one eye per mouse was dilated with Mydriacyl (1%). Mice were fixed in a stereotaxic head holder (Figure 3.3) to prevent movement and assist placement during experimentation. A drop of Goniosoft ophthalmic ointment was placed on the dilated eye, and a small piece of microscope coverglass was situated on top of the layer of Goniosoft to negate the refractive power of the cornea.

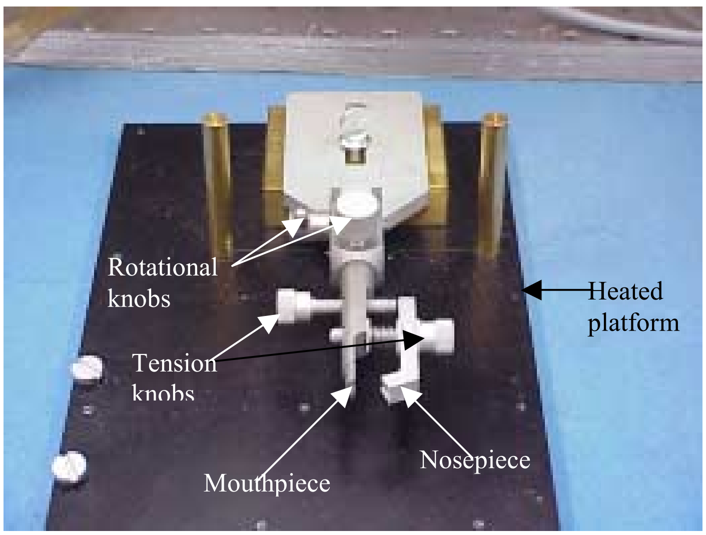

Figure 3.3—Stereotaxic head holder. Mouse rests on a heated platform, designed to maintain body heat while animal is under anesthesia. The mouthpiece is inserted into the animal's mouth, and the nosepiece is tightened onto the nose with the tension knobs. The rotational knobs are loosened to allow proper positioning of the head so the eye may be viewed, and tightened to prevent movement once the proper position is achieved.

Probe solution was introduced through the femoral vein by venous puncture. A small patch of skin was removed above the vessel, and a solution of 10 mg/ml Pd *meso-tetra* [4-carboxyphenyl] porphrine in bovine serum albumin was bolus injected in the amount of 10 mg/kg body weight[1]. Following injection, the vein was cauterized to

[1] Dosages of 5 mg/kg and 15 mg/kg were also tested; however, the lower dose yielded relatively faint intensity images, while the higher dose resulted in damage to the retinal vessels with relatively little light exposure.

prevent bleeding. The mouse was then placed under a dissecting microscope, and the position of the head was adjusted such that the retinal blood vessels radiating from the optic nerve were visible. Power density of the excitation light (mJ/cm^2) was measured prior to data collection using a photodetector and power/energy meter (Newport Corporation, Irvine, CA).

Eight mice, labeled 1a-8a, were prepared and tested at gains 10, 40, 70, and 100, as determined by the *in vitro* experiments. Exposure times were selected based on preliminary *in vivo* tests; times yielding signal-to noise ratios between 3 and 15 without exceeding 1.0 second were used (Table 3.1). Fifteen images per set, determined during *in vitro* experiments to be adequate, were taken beginning with an intensifier delay of 5 μs and continuing at 20 μs increments. Experiments were performed in triplicate for each gain and exposure time setting. The sequence of data collection was varied in each mouse (see Appendix E).

Gain	Exposure Times (seconds)
100	0.6, 0.145, 0.23, 0.315, 0.4
70	0.15, 0.31, 0.47, 0.63, 0.79
40	0.32, 0.49, 0.66, 0.83, 1.0
10	0.4, 0.55, 0.7, 0.85, 1.0

Table 3.1—Gain settings and exposure times used for *in vivo* experiments.

Regions of interest in a vein, an artery, and a section of tissue were then selected for each mouse. The “Retina” program (Appendix B) was used to analyze these different and distinct regions. A maximum PO_2 of 150 was used in the analysis, and all pixels exceeding this value were rejected as physiologically impossible. The following parameters were noted for each region:

- Fitting parameters a_0, a_1, and b_1
- Phase shift (θ)
- Modulation (m)
- PO_2 mean and standard deviation
- R^2 mean and standard deviation
- Number of pixels in the selected region of interest
- Number of pixels from the selected region of interest used for calculations

Signal-to-noise was calculated as a_0 (the DC fitting term) divided by the average intensity with the microscope objective's shutter closed (camera dark noise). Accumulated energy deposition at each point in the experiment was calculated as excitation light power (measured with a power/energy meter) divided by excitation light area multiplied by cumulative exposure time. The analysis was then repeated using a smaller number of the images (7), beginning with the first and continuing with every other image in each set to maintain uniform phase delay increments.

Histology

Histology was used as a potential method for determining any damage to the mouse eye incurred during phosphorescence lifetime imaging, and, potentially, as a method for correlating physical damage caused by disease with the PO_2 maps. No standard technique for conducting histology on the mouse retina exists, so the assistance of Dr. Robert Frank of the Kresge Eye Institute, Wayne State University, Detroit, MI, was sought. His expertise in performing trypsin digestion and periodic acid solution (PAS)/hematoxylin staining on rat retinas was well known, and personal communication with him and personnel in his lab indicated that this technique could be successfully applied to the mouse retina. A visit to his lab allowed the intricacies of the technique to be learned, and a protocol for conducting trypsin digestion and PAS/Hematoxylin staining on the mouse retina was developed (see Appendices C and D).

To induce damage following *in vivo* calibration experiments, probe-injected (10 mg/kg) mice were exposed continuously to 524 nm excitation light for an extended period of time on a single eye. Following continuous exposure for an hour, mice were removed to a dissecting microscope. Complete retinal vascular damage was confirmed by the absence of blood flow in retinal vessels (vessels appearing white in color, rather than the normal red). Eyes were removed and retinas were digested and stained, with the non-exposed eye serving as a control.

4. RESULTS

Phosphorescence Intensity

Phosphorescence intensity images were acquired, and graphs of intensity vs. phase delay created for each *in vitro* and *in vivo* experiment. Sample data appears in Tables 4.1 and 4.2, and sample images and curves appear in Figures 4.1 and 4.2.

Image Number	Phase Delay (Radians)	Intensity Average	Intensity Standard Dev.
2	14.4	941	213
3	25.9	975	222
4	37.4	987	224
5	49.0	985	224
6	60.5	980	224
7	72.0	950	218
8	83.5	923	212
9	95.0	886	203
10	106.6	840	194
11	118.1	788	184
12	129.6	719	170
13	141.1	665	159
14	152.6	604	146
15	164.2	549	134

Table 4.1—Sample data for *in vitro* image set.

Image Number	Phase Delay (Radians)	Artery Intensity Average	Artery Intensity St. Dev.	Vein Intensity Average	Vein Intensity St. Dev.	Tissue Intensity Average	Tissue Intensity St.Dev.
2	14.4	655	30	1150	114	372	32
3	25.9	654	41	1164	121	370	28
4	37.4	640	31	1165	119	357	29
5	49.0	619	35	1135	112	342	31
6	60.5	594	29	1106	109	323	28
7	72.0	564	30	1052	105	302	267
8	83.5	532	27	1008	102	279	24
9	95.0	482	30	936	98	254	22
10	106.6	444	29	878	94	228	20
11	118.1	403	24	810	82	202	20
12	129.6	353	22	730	80	178	16
13	141.1	325	24	655	73	155	16
14	152.6	275	16	589	63	134	13
15	164.2	248	19	522	57	118	12

Table 4.2—Sample data for *in vivo* image set.

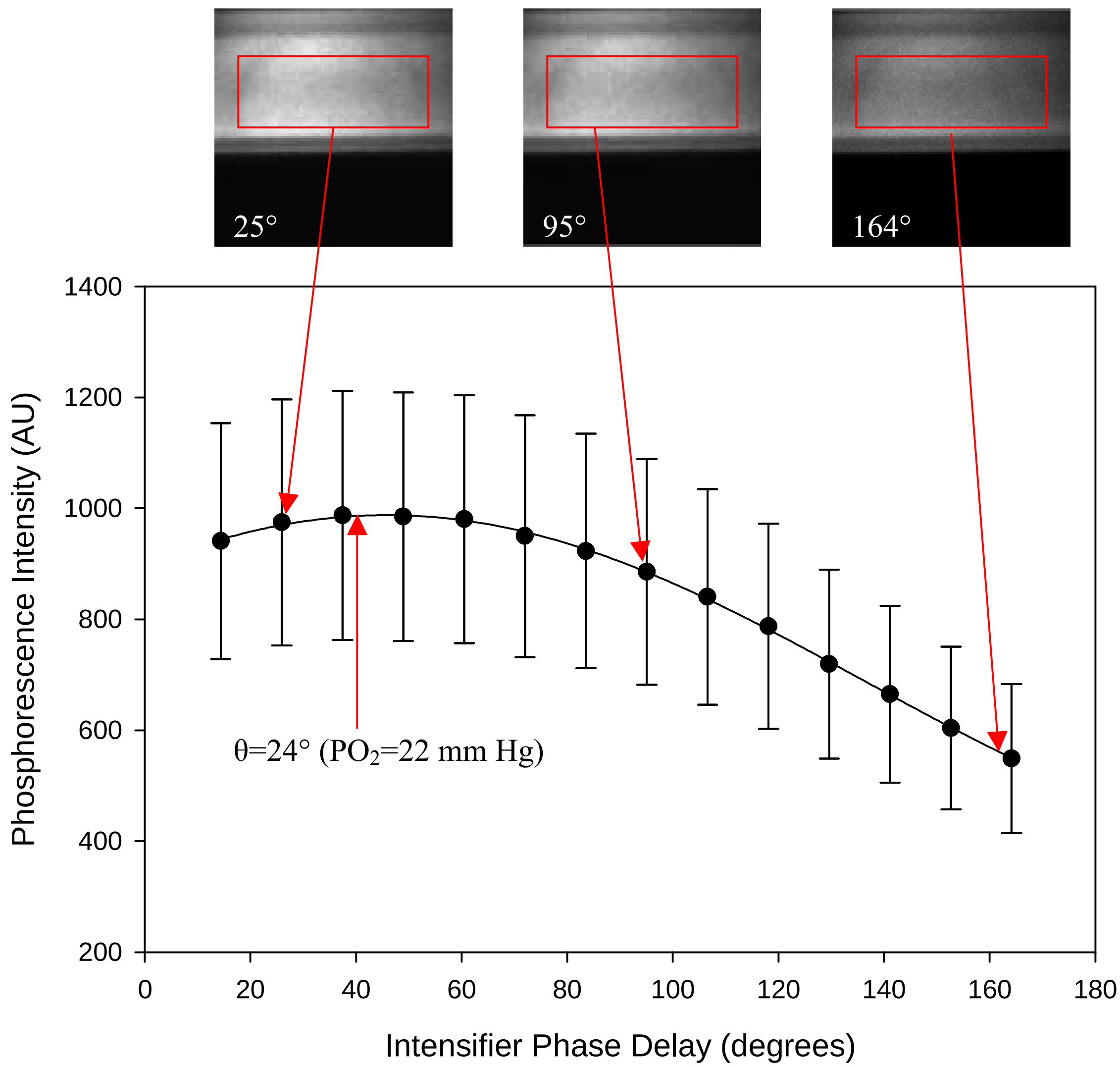

Figure 4.1—Sample intensity images and intensity vs. phase delay graph for *in vitro* experiments. Intensity images corresponding to phase delays of 25°, 95°, 25°, and 164°, are shown. The region of interest used for intensity averaging is indicated by the red line in each image. The maximum value on the graph, corresponding to the phase delay, and used to calculate PO_2, is also indicated.

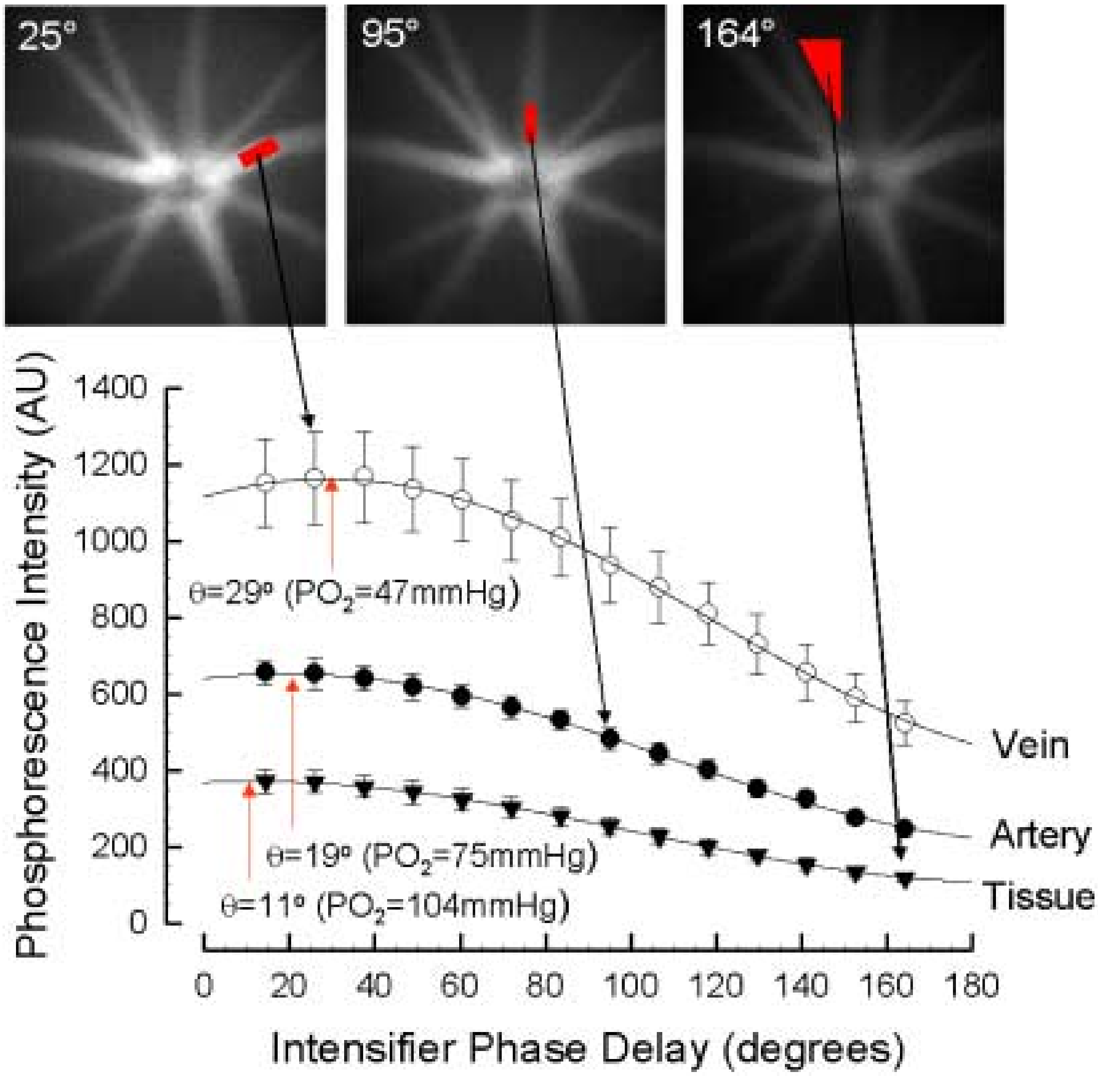

Figure 4.2—Sample intensity images and intensity vs. phase delay graph for *in vivo* experiments. Intensity images corresponding to phase delays of 25°, 95°, 25°, and 164°, are shown. The region of interest used for intensity averaging is indicated by the red region in each image—vein, artery, and tissue were selected for each animal tested. The maximum value on the graph, corresponding to the phase delay, and used to calculate PO_2, is also indicated.

In Vitro Tests

The phosphorescence lifetime imaging system was calibrated using the *in vitro* testing system, described in the methods section. Early experiments identified a drift in the optical chopper phase, which was rectified with a change in hardware. Experiments with a blocked objective and no phosphorescence verified that the instrument did not produce significantly different results at different gains, exposure times, or total experiment times. However, an intrinsic phase error of 0.80 and modulation error of 0.67 were discovered. The phase error was subtracted from all subsequent data sets, and the modulation error was divided. Following this correction, PO_2 and R^2 maps (where R^2 is a measure of the fit of the intensity images to the specified equation) were created for each image set, a sample of which appears Figure 4.3, and a final calibration curve was generated (Figure 4.4).

To determine if map fit was affected by intensity signal-to-noise ratio, average R^2 value for the capillary tube was plotted versus SNR (with SNR calculated as the average intensity of images taken at a series of 30 delay settings between 10 and 300 µs divided by the average intensity of images taken with no light entering the camera). The results appear in Figure 4.5.

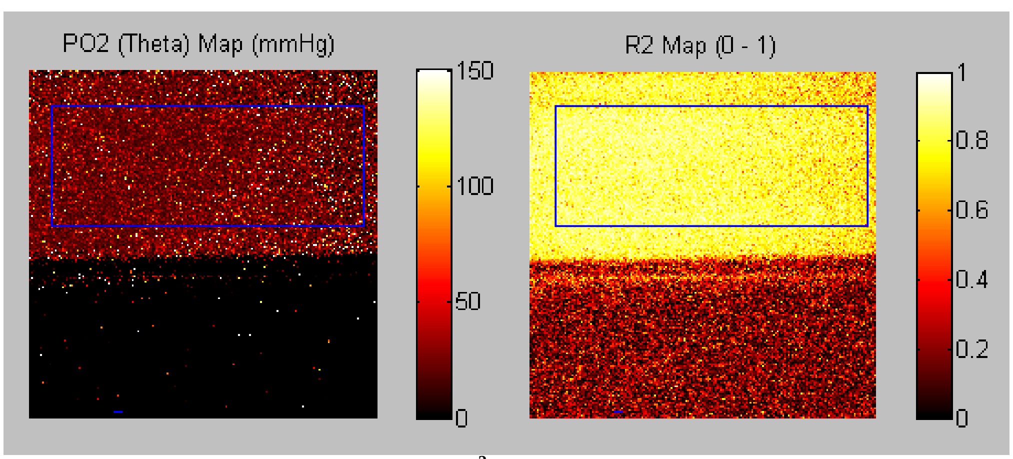

Figure 4.3—Sample PO_2 and R^2 maps for *in vitro* experiments. Regions of interest selected for data analysis in the "Retina" program are delimited by the blue lines.

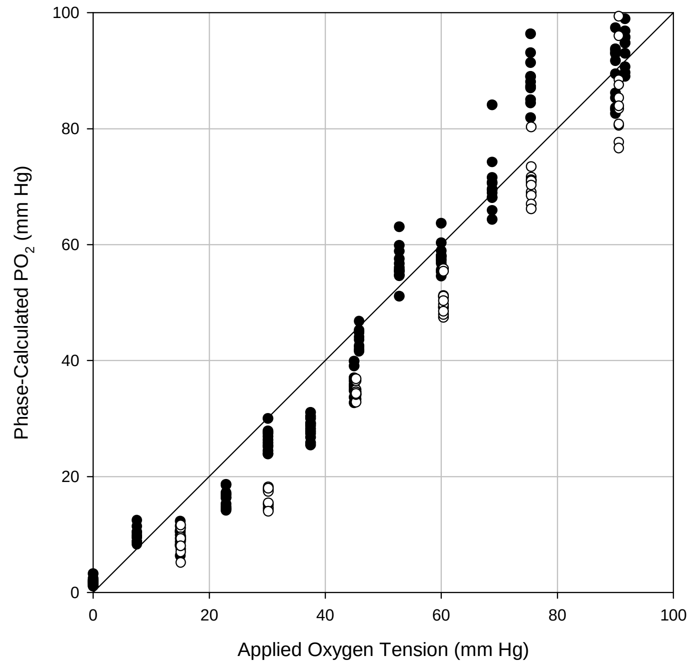

Figure 4.4—*In vitro* calibration curve. The x-axis represents oxygen concentrations applied with the gas mixer. The y-axis indicated PO_2 as determined by the phosphorescence lifetime imaging system. A line of identity intersects the data, indicating that the system produced accurate PO_2 maps.

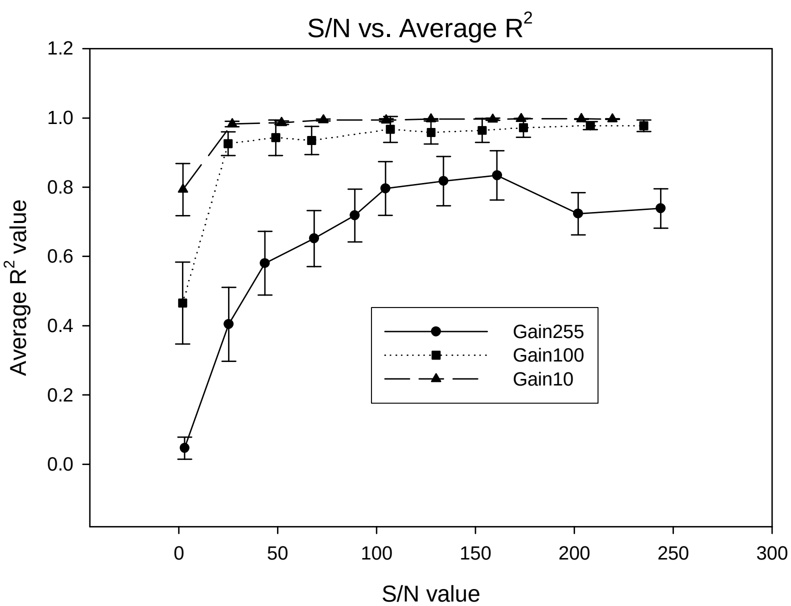

Figure 4.5—Average R^2 value versus SNR for gain settings 10, 100, and 255. Gain 255 gave less than acceptable R^2 values regardless of signal-to noise ratio. Gains 10 and 100 yielded very high R^2 values at SNR>50.

These data indicate that a gain setting of 255 did not produce images with acceptable R^2 values (>0.9), even at high signal-to-noise ratios. In contrast, R^2 values of greater than 0.9 were obtained with gain settings 10 and 100 for all SNR > 50. These results were verified in subsequent experiments (data not shown). As a result, all subsequent experiments were conducted at gain settings between 10 and 100. Since the data indicated that all SNR>50 yield similarly high R^2 values, exposure times resulting in signal-to-noise ratios of 50 or less were used, thereby minimizing excitation light exposure.

In Vivo Tests

For all image sets with 15 images each, a vein, an artery, and a section of tissue were analyzed (Figure 4.6). In general, PO_2 was highest in the tissue region, and lowest in the veins. For each of these regions, graphs were created for R^2 vs. SNR, PO_2 vs. accumulated energy deposition, and PO_2 vs. SNR. The raw data for each animal appear in Appendix E, and sample data and graphs for a single mouse (Mouse 1a) are shown in Table 4.3 and Figure 4.7. Figure 4.8 contains summary plots of R^2 vs. signal-to-noise ratio for the three regions in all mice. Each data point represents an individual image set.

For all regions, lower gains produced better fits at lower signal-to-noise ratios. All gain settings yielded R^2 values of approximately 0.95, but a gain setting of 100 requires an SNR of greater than 10 to produce this good fit. Conversely, a gain setting of 10 requires an SNR of only 4 to produce an excellent fit. However, it must be considered that achieving an SNR 4 at gain 10 requires an exposure time of 1.0 seconds, while achieving an SNR of 10 at gain 100 requires an exposure time of only 0.4 seconds.

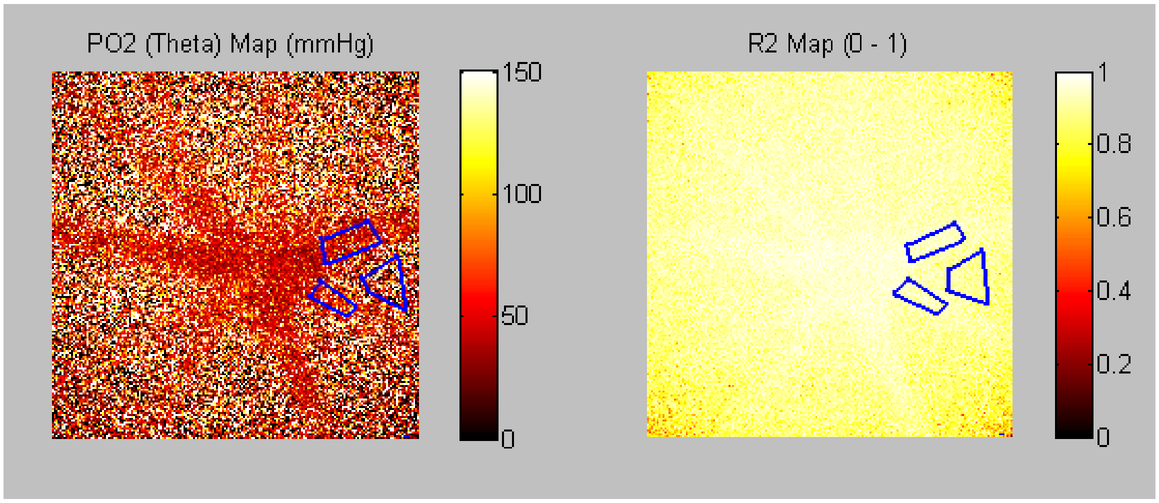

Figure 4.6—Sample PO_2 and R^2 maps for *in vivo* experiments. Regions of interest for vein (top), artery (bottom) and tissue (center) are indicated by the blue lines.

Gain	Exposure Time	Relative Image Number	Cumulative Image Number	Accumulated Energy Deposition (mJ/cm^2)	SNR	PO2 Mean	PO2 St. Dev	R2 Mean	R2 St. Dev
100	0.06	1	1	4.5	3.1	31.3	25.5	0.71	0.11
100	0.06	2	2	9.1	3.1	33.2	24.6	0.70	0.12
100	0.06	3	3	13.6	3.1	39.4	29.7	0.72	0.11
100	0.145	1	4	24.6	6.6	37.3	22.3	0.86	0.06
100	0.145	2	5	35.6	6.2	38.1	23.5	0.85	0.06
100	0.145	3	6	46.6	5.9	35.2	20.7	0.85	0.06
100	0.23	1	7	64.1	8.9	40.2	22.2	0.90	0.04
100	0.23	2	8	81.5	8.4	39.4	21.6	0.91	0.04
100	0.23	3	9	99.0	8.3	37.7	19.5	0.90	0.04
100	0.315	1	10	122.8	11.7	36.4	16.2	0.93	0.03
100	0.315	2	11	146.7	11.1	40.4	20.7	0.93	0.03
100	0.315	3	12	170.6	10.7	43.4	19.4	0.93	0.03
100	0.4	1	13	200.9	14.4	37.0	14.1	0.98	0.03
100	0.4	2	14	231.3	14.2	37.1	14.4	0.95	0.02
100	0.4	3	15	261.6	13.0	39.7	17.0	0.94	0.02
70	0.15	1	16	273.0	2.7	47.8	30.2	0.83	0.07
70	0.15	2	17	284.4	2.6	44.2	28.1	0.84	0.07
70	0.15	3	18	295.7	2.6	39.0	25.3	0.84	0.07
70	0.31	1	19	319.2	4.3	41.2	20.9	0.91	0.04
70	0.31	2	20	342.7	4.2	43.5	22.8	0.91	0.04
70	0.31	3	21	366.2	4.3	41.4	22.2	0.91	0.04
70	0.47	1	22	401.9	5.8	41.7	18.6	0.94	0.03
70	0.47	2	23	437.5	5.6	43.4	19.4	0.94	0.03
70	0.47	3	24	473.2	5.8	43.6	20.2	0.94	0.03

70	0.63	1	25	520.9	7.1	44.5	17.8	0.95	0.02
70	0.63	2	26	568.7	7.0	46.1	20.9	0.95	0.02
70	0.63	3	27	616.5	7.3	47.8	19.1	0.95	0.02
70	0.79	1	28	676.4	8.5	46.4	18.0	0.96	0.02
70	0.79	2	29	736.3	8.3	46.9	20.6	0.96	0.02
70	0.79	3	30	796.2	8.6	41.7	15.2	0.96	0.02
40	0.32	1	31	820.4	2.4	42.1	24.5	0.88	0.05
40	0.32	2	32	844.7	2.5	44.2	26.1	0.89	0.05
40	0.32	3	33	869.0	2.4	47.2	26.5	0.89	0.05
40	0.49	1	34	906.1	3.1	41.2	20.9	0.92	0.04
40	0.49	2	35	943.3	3.1	46.8	24.3	0.92	0.03
40	0.49	3	36	980.4	3.0	48.4	25.6	0.92	0.04
40	0.66	1	37	1030.5	3.7	45.5	22.2	0.95	0.03
40	0.66	2	38	1080.5	3.9	43.4	18.8	0.94	0.03
40	0.66	3	39	1130.6	3.7	45.9	20.9	0.94	0.03
40	0.83	1	40	1193.5	4.3	48.0	20.9	0.95	0.02
40	0.83	2	41	1256.4	4.4	44.8	21.1	0.95	0.02
40	0.83	3	42	1319.4	4.4	45.3	19.3	0.95	0.02
40	1	1	43	1395.2	5.2	45.1	18.3	0.96	0.02
40	1	2	44	1471.0	5.1	42.4	16.3	0.95	0.02
40	1	3	45	1546.9	5.2	44.0	18.1	0.96	0.02
10	0.4	1	46	1577.2	1.8	42.3	24.6	0.86	0.06
10	0.4	2	47	1607.5	1.9	44.6	26.7	0.87	0.05
10	0.4	3	48	1637.9	1.9	45.6	27.3	0.86	0.06
10	0.55	1	49	1679.6	2.1	43.8	22.8	0.90	0.04
10	0.55	2	50	1721.3	2.1	38.2	19.7	0.90	0.04
10	0.55	3	51	1763.0	2.1	42.9	23.9	0.90	0.04
10	0.7	1	52	1816.1	2.4	42.3	21.3	0.91	0.04
10	0.7	2	53	1869.1	2.5	40.6	21.4	0.92	0.03
10	0.7	3	54	1922.2	2.4	44.4	21.3	0.92	0.04
10	0.85	1	55	1986.7	2.6	43.8	21.1	0.93	0.03
10	0.85	2	56	2051.1	2.8	41.7	19.7	0.93	0.03
10	0.85	3	57	2115.6	2.8	43.3	20.2	0.93	0.03
10	1	1	58	2191.4	3.0	43.5	20.2	0.94	0.03
10	1	2	59	2267.2	3.1	45.1	19.5	0.94	0.03
10	1	3	60	2343.0	2.9	46.1	20.9	0.94	0.03

Table 4.3—Sample raw data for *in vivo* experiments, from Mouse 1a vein. Data were calculated from PO_2 and R^2 maps and intensity images using the "Retina" program.

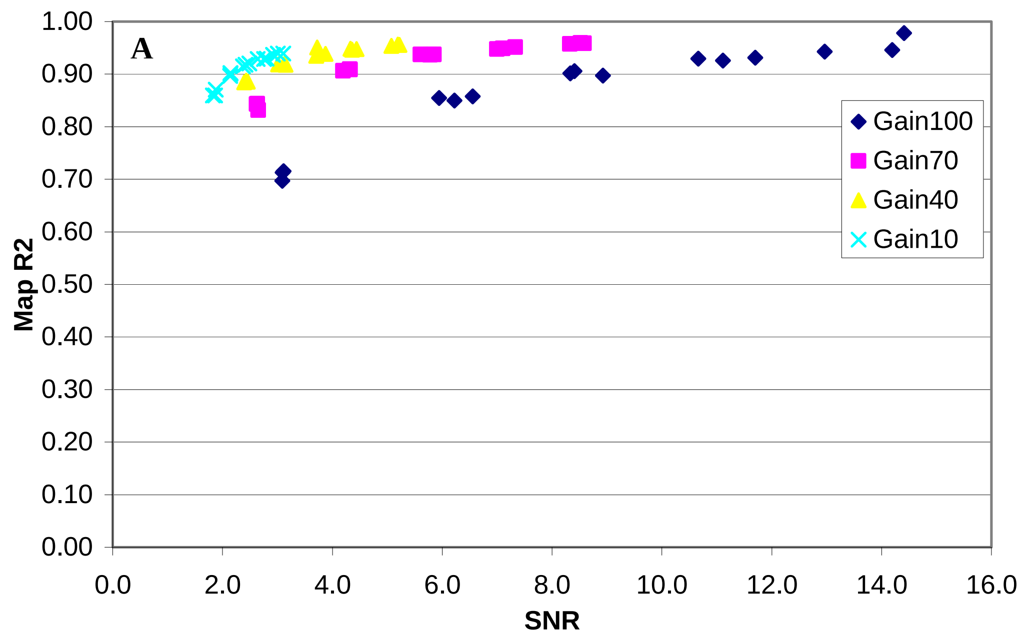

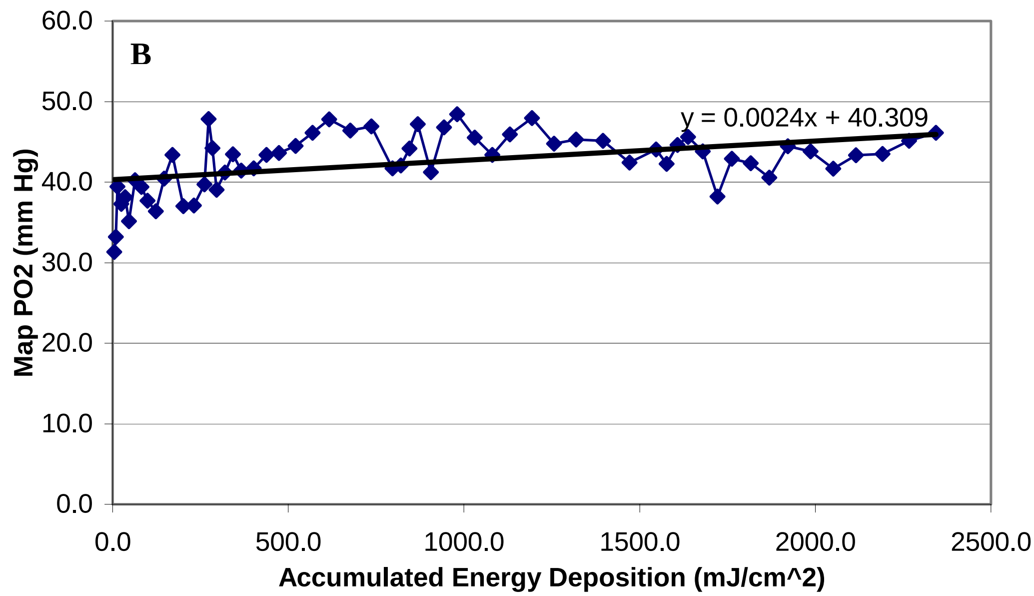

Figure 4.7—Sample graphs of *in vivo* data, taken from Mouse 1a vein. Panel A represents a typical graph of R^2 value vs. SNR, where R^2 value increases slightly with increasing SNR. Panel B shows a typical map PO_2 vs. accumulated energy deposition graph, where the slope of the trendline is not statistically different from zero in the negative direction (one-tailed Student's t-test, $p>0.05$).

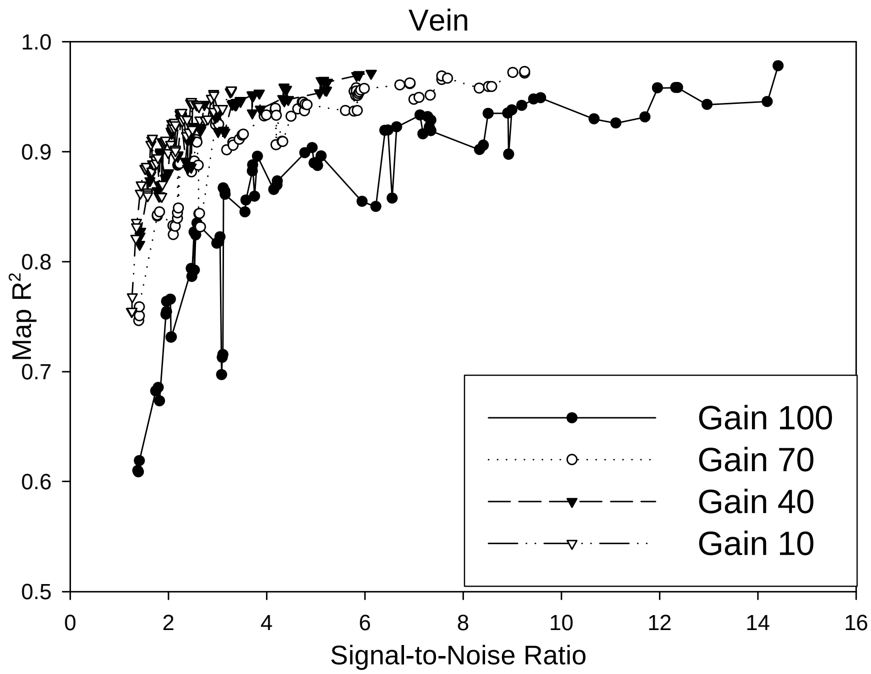
Vein
1.0
0.9
0.8
0.7
0.6
0.5
Map R2
0
2
4
6
8
10
12
14
16
Signal-to-Noise Ratio
Gain 100
Gain 70
Gain 40
Gain 10

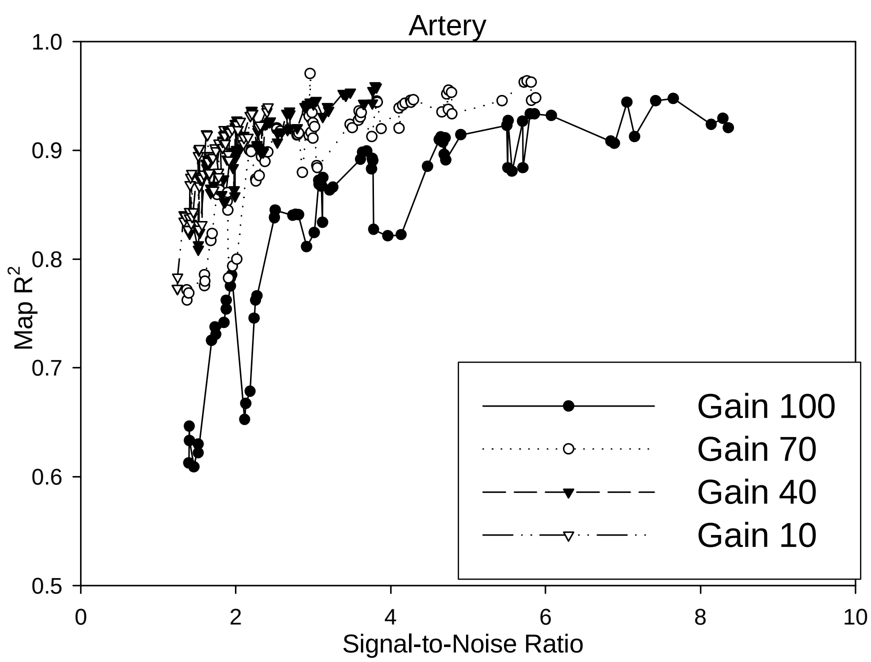
Artery
1.0
0.9
0.8
0.7
0.6
0.5
Map R2
0
2
4
6
8
10
Signal-to-Noise Ratio
Gain 100
Gain 70
Gain 40
Gain 10

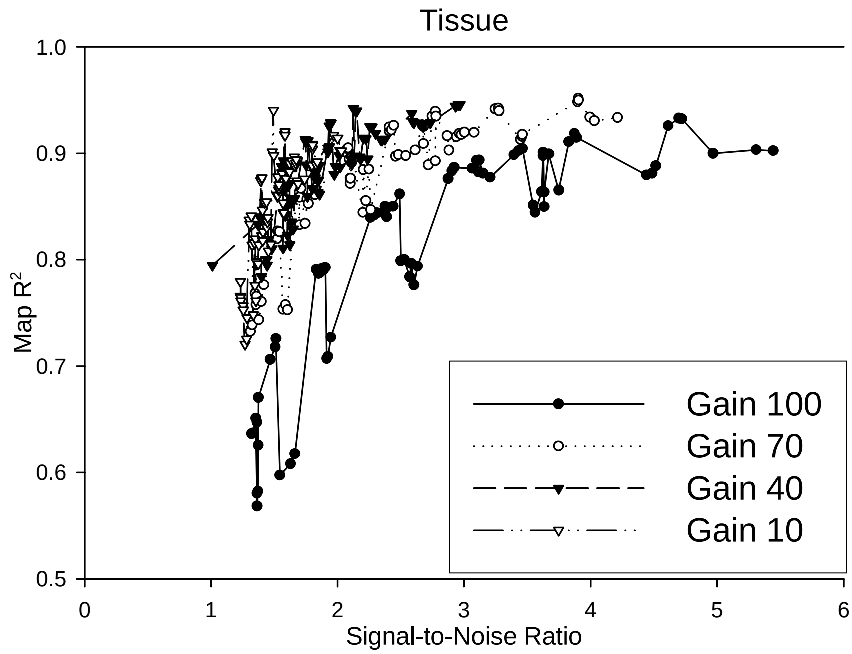

Figure 4.8—Map R^2 value versus SNR in vein, artery, and tissue for all animals tested. Each point represents an individual image set and R^2 map.

Composite graphs of PO_2 vs. accumulated energy deposition and vs. signal-to-noise were not created, as differences in oxygen tensions in individual mice made such general comparisons inappropriate. However, graphs of these parameters for individual mice appear in Appendix E. For all animals, the slope of the linear best-fit lines on these plots is not significantly different from zero in the negative direction (one-tailed Student's t-test, $p>0.05$), indicating that PO_2 was not affected by increasing energy deposition or SNR.

Results of analysis of image sets with seven images were compared to those obtained with 15 images to determine if fewer images (which would result in decreased light exposure and less possible physiological damage) could produce accurate maps. A parameter termed "Delta PO_2," defined as the PO_2 calculated with 15 images minus that

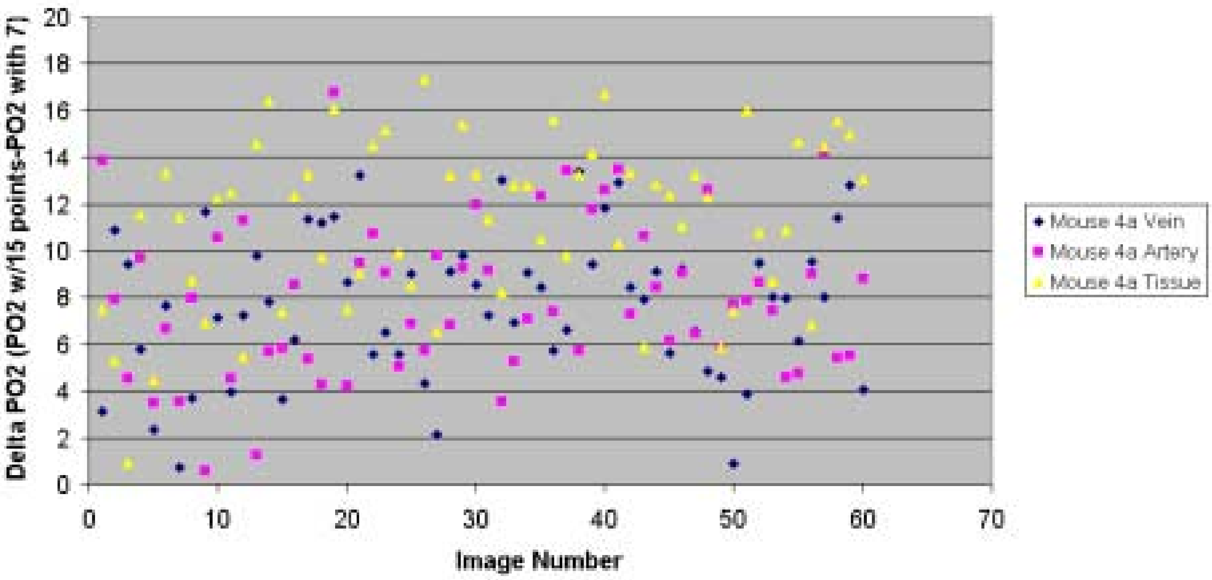

Figure 4.9—Delta PO_2 versus image number for Mouse 4a. PO_2 differs by as much as 17 mm Hg when calculated with the fewer number of images, indicating that seven images are too few for calculating PO_2 accurately.

Mouse	Vessel	Average Delta PO2	Delta PO2 St.Dev.
1	Vein	-0.6	3
1	Artery	2.1	3.9
1	Tissue	5.7	3.3
3	Vein	3.7	2.8
3	Artery	7.1	2.5
3	Tissue	9.8	1.8
4	Vein	7.7	3.1
4	Artery	7.9	3.3
4	Tissue	11.3	3.6

Table 4.4—Summary of delta PO_2 mean and standard deviation for Mice 1a, 3a, and 4a. Delta PO_2 is significantly different from zero in most cases, indicating that the use of seven images does not produce accurate PO_2 values.

calculated with seven, was used to examine possible error incurred using fewer images. Sample results appear in Figure 4.9 and Table 4.4. PO_2 differed significantly when calculated with seven images in some cases, indicating that seven images is too few for calculating accurate PO_2 values.

Histology

Trypsin digestion and PAS/Hematoxylin staining (see Appendices C and D) were performed on mouse eyes visibly damaged by light exposure, and on unexposed control eyes from the same mouse. No apparent differences were observed between the two types of retinas during the digestion procedure, with the exception that the photoreceptors of the damaged retinas appeared darker in color than those of the controls.

Trypsin digestion of the mouse retina proved to be an extremely difficult, lengthy, and frustrating process with little reproducibility. The retinas often did not digest completely, requiring extensive mechanical dissection to remove the inner limiting membrane and cellular debris, often resulting in damage to the vessel bed. Digesting for longer periods in an attempt to correct this problem resulted in the dissolution of the entire retina, including the vasculature. A mounting of the entire, intact vascular bed onto a slide was never accomplished.

Even somewhat successful digestions, in which large sections of the vasculature were mounted onto slides, yielded questionable results when stained (Figure 4.10). While the photographs in the first row appear to show flatter, denser arteries and veins in the damaged eye (panel B) when compared with the control (panel A), this phenomenon cannot be seen in the second or third rows (photographs of different mice). The large, dark blue areas in these photographs represent sections of cellular debris that were not cleared away. As is evident in the pictures, these sections interfere with visualization of the vessels, particularly the capillary beds. However, removing such debris was often impossible without destroying the vessels themselves. While it may be stated that the large vessels in eyes exposed to large amounts of excitation light had a flatter appearance than those of their unexposed counterparts, the evidence is largely inconclusive. Additionally, no apparent changes in the capillary structure are visible.

As faulty technique may have been responsible for the poor quality of the mounts, the procedure was also performed on a healthy rat retina. Trypsin digestion of the rat retina is a widely accepted procedure, yielding excellent results when performed properly. Results of this digestion appear in Figure 4.11. The entire vascular bed was successfully mounted in nearly intact form, and the capillary structure is more clearly visible at high magnification. The success of this digestion indicates that faulty technique is not the cause of the poor quality of the mouse digests.

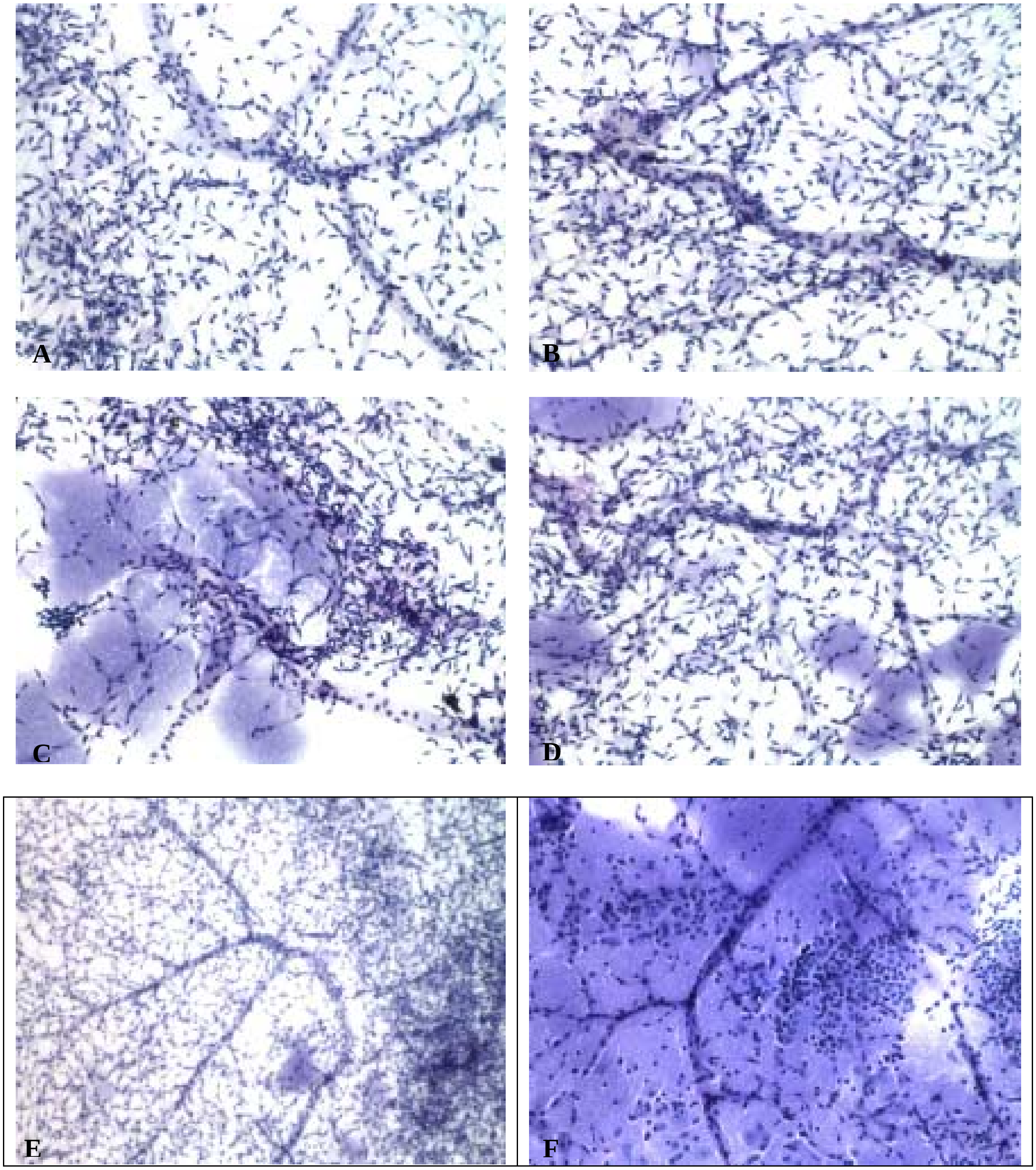

Figure 4.10—Trypsin digestion slides of control (left column) and damaged (right column) mouse retinas. The damaged retina in panel B appears to have lost some of its structural integrity when compared with its control in panel A—the large vessels appear flatter, and the nuclei (blue stain) appear denser within the vessels. However, the same direct comparison is not possible in the subsequent panels due to damage to the retinal vessels incurred during dissection, and dark staining of the cellular debris not removed during the trypsin digestion procedure.

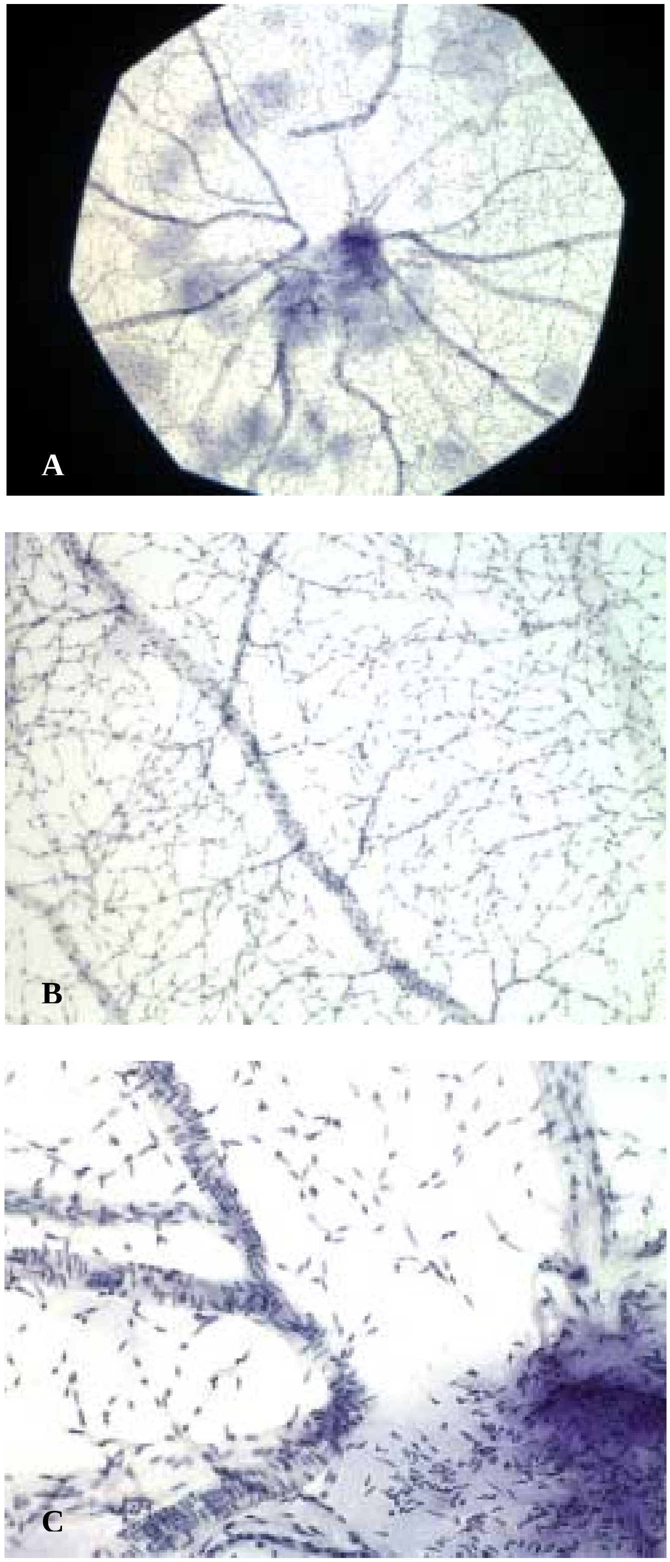

Figure 4.11—Trypsin digestion of the rat retina, viewed at 4x (A), 10x (B), and 20x (C) magnification. The vessel bed is nearly intact, and the capillaries are significantly more visible when compared with the mouse digests (Figure 4.1).

5. DISCUSSION

Significance of Results

The first aim of this project was to calibrate the phosphorescence lifetime imaging system against known oxygen concentrations. This was achieved using the *in vitro* calibration system, shown in Figure 4.1. For the physiologic range of oxygen concentrations, the instrument and data analysis program produce accurate PO_2 maps.

The second aim of determining optimal parameters for probe excitation was achieved during *in vivo* experiments. Wavelength and bandwidth of 524±20 nm, as recommended in the literature, yielded acceptable maps. A decrease in PO_2 was used as an indicator of vessel damage; vessels damaged using this technique demonstrate a decrease in blood flow, which would subsequently decrease PO_2. Setting energy and power to keep accumulated energy deposition below 2500 mJ/cm^2 prevented damage in the eye, as analyzed using observation of vessels and lack of a decrease in average PO_2 over the course of image collection.

Qualitatively, the relationship between PO_2 values in the different regions analyzed (vein, artery, and tissue) made logical sense. The physiological structure of the retina, with the high-PO_2 choroidal vasculature lying behind the lower-PO_2 retinal vasculature, caused some interference in phosphorescence images. In the major blood vessels, the light-absorbing properties of hemoglobin prevented the excitation light from reaching the probe within the choroidal vasculature, so the true PO_2 of the retinal vessels was determined. However, this effect was reduced in the capillary beds, which lie in the tissue sections analyzed—the excitation light was allowed to reach the choroid, and phosphorescence was emitted from this oxygen-rich vasculature, yielding high PO_2 map values.

Relationships between camera exposure time, intensifier gain, and the quality of oxygen maps was also achieved with *in vivo* experiments. Signal-to-noise ratios of phosphorescence intensity images were determined to be dependent on camera intensifier gain settings. Low gain settings yielded better fits, and, therefore, better oxygen maps at lower signal-to-noise ratios, but at the cost of longer exposure times. When creating oxygen maps, the quality of the maps necessary must be weighed against the ability of the eye to withstand lengthy exposure to excitation light, the effect of longer exposure times on total experiment time, and the necessity for following rapid physiological changes.

The minimum number of images necessary to produce acceptable oxygen maps was determined to be near 15. Using 15 intensity images at incremented phase delays produced fits comparable to those obtained using 30 images. Seven images proved to be too few, as the delineation between vessels in the oxygen maps grew faint.

It was not possible to determine the level of damage caused by experimentation using trypsin digestion. This histological technique did not allow for viewing of the capillary structure in sufficient detail to analyze damage to vessel walls. The inability to see any changes in the capillary structure in retinal vasculatures that are decisively damaged renders trypsin digestion an unacceptable method for study of the mouse eye.

Future Work

Additional *in vitro* calibration studies should be performed to explain the variation in instrument PO_2 readings for identical applied oxygen concentrations. While the calibration curve shows relatively good correlation between instrument and applied oxygen, additional experiments may identify areas for improvement. Some non-linearity in the calibration curve may be present, and must be accounted for.

Data from three individual mice (2a, 6a, and 7a) were not included in summary analyses due to inadequate physiological control during experimentation. Likely changes in blood pressure and respiration rate during the course of experiments caused variations in intensity images, and, hence, inadequate sine-wave fits and poor oxygen maps. Such problems may have been prevented by a physiological control system to monitor blood pressure, ensure adequate respiration, and continuously maintain level of anesthesia. Implementing such a system will increase efficiency of experiments by allowing for greater frequency of experimental success.

Experiments determining the threshold of accumulated energy deposition for damage to retinal blood vessels would be beneficial. In this study, no experiments were carried out in which damage to blood vessels occurred—all animals maintained blood vessel structure and oxygen levels. Determining the level of light exposure needed to cause damage would allow for recommendations for maximum light exposure levels to be made. Additionally, the issue of excitation light modulation frequency was not addressed. Changes in modulation frequency could cause significant changes in quality of oxygen maps, and should be investigated.

Further analysis of the number of images necessary for creating good quality oxygen maps would be beneficial. It was determined that seven images are too few for producing accurate maps when compared with results using 15 images; however, numbers between seven and 15 were not examined. Additional *in vivo* experiments using different image numbers would allow the determination of the absolute minimum number of images necessary for accurate maps, and possibly allow for a decrease in light exposure to animals during experiments.

As trypsin digestion proved to be an unacceptable method for histologically examining the mouse eye, other methods should be investigated. Changes in capillary structure are of particular interest in diabetic retinopathy, a disease whose first clinical signs manifest in these minute vessels. The lack of capillary definition in the photographs shown in Figure 4.5 makes it unlikely that trypsin digestion and PAS/Hematoxylin staining will be of use in further mouse model study. Laver et al [1993] confirm that while retinal mounts of the type used in this study demonstrate the microaneurysms present in diabetic retinopathy, they did not provide a clear view of the capillaries. They also claim that, even under ideal conditions, it is difficult to obtain good quality trypsin digestions of mouse retinas. Cuthbertson et al [1986] also verify this claim. Both of these studies recommend the use of elastase, rather than trypsin, for digesting the mouse retina. Analysis of eyes subjected to the phosphorescence lifetime imaging technique using elastase digestion and staining may be of benefit.

Conclusions

The specific aims for achieving the goal of optimization of the phosphorescence lifetime imaging system for the mouse eye were calibration of the system, determination of probe excitation parameters, determination of image collection and analysis parameters, and examination of microvascular damage using histology. Calibration was accomplished using an *in vitro* system to correlate instrument-derived oxygen tensions with known concentrations. Probe excitation parameters were studied indirectly through the determination of accumulated energy deposition during series of phosphorescence lifetime imaging experiments. Image collection and analysis parameters were studied in depth, with the final determination that lower intensifier gains produced better maps at lower signal-to-noise ratios, but higher gain settings allowed reasonably good maps to be created with shorter exposure times. Gain and exposure time settings for specific experiments may be determined using the graphs in Figure 4.8 as a guide. Seven was determined to be too few images for creating clear, precise oxygen maps—the number necessary is closer to fifteen. The aim of using histology to examine damage caused by probe excitation was not achieved, but recommendations for performing this procedure more effectively were made.

This work demonstrates that the phosphorescence lifetime imaging instrumentation and technique may be used for studying oxygen tensions in the mouse eye. The determination of the optimal parameters for conducting such experiments will allow for the investigation of how changes in retinal oxygen tensions correlate with the progression of numerous ocular diseases, such as diabetic retinopathy, retinopathy of prematurity, and glaucoma.

References

Aiello, L.P., T.W. Gardner, G.L. King, G. Blankenship, J.D. Cavallerano, F.L. Ferris, R. Klein. 1998. Diabetic Retinopathy. *Diabetes Care,* 21:143-156.

Aiello, L.P., E.A. Pierce, E.D. Foley, H. Takagaki, H. Chen, L. Riddle, N. Ferrara, G.L. King, and L.E.H. Smith. 1995. Suppression of retinal neovascularization *in vivo* by inhibition of vascular endothelial growth facto (VEGF) using soluble VEGF-receptor chimeric proteins. *Proceedings of the National Academy of Science, USA*, 92:10457-10461.

Alder, V.A., S.J. Cringle, and M. Brown. 1987. The effect of regional retinal photocoagulation on vitreal oxygen tension. *Ivestigative Ophthalmology and Visual Science*, 28:1078-1085.

Alder, V.A., S.J. Cringle, and I.J. Constable. 1983. The retinal oxygen profile in cats. *Investigative Ophthalmology and Visual Science,* 24:30-36.

Alder, V.A., E.N. Su, D.Y. Yu, S.J. Cringle, P.K. Yu. 1997. Diabetic retinopathy: Early functional changes. *Clinical and Experimental Pharmacology and Physiology,* 24:785-788.

Alm, A. and A. Bill. 1972. The oxygen supply to the retina, I. Effects of changes in intraocular and arterial blood pressures, and in arterial pO_2 and pCO_2 on the oxygen tension in the vitreous body of the cat. *Acta Physiologica Scandanavia,* 84:261-274.

Amin, R.H., R.N. Frank, A. Kennedy, D. Eliott, J.E. Puklin, G.W. Abrams. 1997. Vascular endothelial growth factor is present in glial cells of the retina and optic nerve of human subjects with nonproliferative diabetic retinopathy. *Investigative Ophthalmology and Visual Science,* 38:36-47.

Andreani, D., G. Crepaldi, U. DiMario, G. Pozza. Diabetic Complications: Early Diagnosis and Treatment. 1987. Chichester: John Wiley & Sons, Inc.

Araki, E., M.A. Lipes, M.-E. Patti, J.C. Bruning, B. Haag, III, R.S. Johnson, and C.R. Kahn. 1994. Alternative pathway of insulin signaling in mice with targeted disruption of the IRS-1 gene. *Nature,* 372:186-190.

Benson, W., G. Brown, W. Tasman. 1988. Diabetes and its Ocular Complications. Philadelphia: Harcourt Brace Jovanovich, Inc.

Berkowitz, B.A., R.A. Kowluru, R.N. Frank, T.S. Kern, T.C.Hohman, M. Prakash. 1999. Subnormal retinal oxygenation response precedes diabetic-like retinopathy. *Investigative Ophthalmology and Visual Science,* 40:2100-2105.

Crabbe, M.J.C. 1987. Diabetic Complications: Scientific and Clinical Aspects. London: Churchill Linvingstone.

Cuthbertson, R.A., T.E. Mandel. 1986. Anatomy of the mouse retina: Endothelial cell-pericyte ratio and capillary distribution. *Investigative Ophthalmology and Visual Science,* 27:1659-1664.

Davison, J.K. 2000. Clinical Diabetes Mellitus: A Problem-Oriented Approach. New York: Thieme Medical Publishers, Inc.

Delori, F.C. 1988. Noninvasive technique for oximetry of blood in retinal vessels. *Applied Optics,* 27:1113-1125.

Diabetes Control and Complications Trial Research Group. 1998. Early worsening of diabetic retinopathy in the diabetes control and complications trial. *Archives of Ophthalmology*, 116:874-886.

Ditzel, J. and E. Standl. 1975. The problem of tissue oxygenation in diabetes mellitus I. Its relation to the early functional changes in the microcirculation of diabetic subjects. *Acta Medica Scandanavia*, 578 (Supplementum):49-58.

Dowling, J.E. The Retina: An Approachable Part of the Brain. 1987. Cambridge: The Belknap Press of Harvard University Press.

Ernest, J.T., T.K. Goldstick, and R.L. Engerman. 1983. Hyperglycemia impairs retinal oxygen autoregulation in normal and diabetic dogs. *Investigative Ophthalmology and Visual Science,* 24:985-989.

Frank, R.N. 1991. On the pathogenesis of diabetic retinopathy: A 1990 update. *Ophthalmology,* 98:586-593.

Grunwald, J.E., C.E. Riva, J.Baine, and A.J. Brucker. 1992. Total retinal volumetric blood flow rate in diabetic patients with poor glycemic control. *Investigative Ophthalmology and Visual Science,* 33:356-363.

Grunwald, J.E., C.E. Riva, A.J. Brucker, S.H. Sinclair, and B.L. Petrig. 1984. Altered retinal vascular response to 100% oxygen breathing in diabetes mellitus. *Ophthalmology*, 91:1447-1452.

Grunwald, J.E., C.E. Riva, A.J. Brucker, S.H. Sinclair, and B.L. Petrig. 1986. Effect of panretinal photocoagulation on retinal blood flow in proliferative diabetic retinaopathy. *Ophthalmology*, 93:590-595.

Guillan, M.-T., E. Hummler, E. Schaerer, J.-Y. Wu, M.J. Birnbaum, F. Beerman, A. Schmidt, N. Deriaz, and B. Thorens. 1997. Early diabetes and abnormal postnatal pancreatic islet development in mice lacking Glut-2. *Nature Genetics,* 17:327-330.

Hawes, N.L., R.S. Smith, B. Chang, M. Davisson, J.R. Hackenlively, S.W.M. John. 1999. Mouse fundus photography and angiography: a catalogue of normal and mutant phenotypes. *Molecular Vision,* 5:22-29.

Inoue, S. and K.R. Spring. 1997. *Video Microscopy: The Fundamentals,* Second Edition. New York: Plenum Press.

Ito, Y. and B.A. Berkowitz. 2001. MR studies of retinal oxygenation. *Vision Research,* 41:1307-1311.

Kern, T.S., R.L. Engerman. 1995. Galactose-induced retinal microangiopathy in rats. *Investigative Ophthalmology and Visual Science,* 36:490-496.

Kern, T.S., R.L. Engerman. 1996. A mouse model of diabetic retinopathy. *Archives of Ophthalmology*, 114:986-990.

Kern, T.S., J. Tang, M. Mizutani, R.A. Kowluru, R.H. Nagara, G. Romeo, F. Podesta, M. Lorenzi. 2000. Response of capillary cell death to aminoguanidine predicts the development of retinopathy: Comparison of diabetes and galactosemia. *Investigative Ophthalmology and Visual Science,* 41:3972-3978.

Kuwabara, T., D.G. Cogan. Studies of retinal vascular patterns: Part I, Normal architecture. 1960. *Archives of Ophthalmology,* 64:904-911.

Lakowicz, J.R. 1999. Principles of Fluorescence Spectroscopy, Second Edition. New York: Kluwer Academic/Plenum Publishers.

Lakowicz, J.R., and K.W. Berndt. 1991. Lifetime-selective fluorescence imaging using an rf phase-sensitive camera. *Review of Scientific Instruments,* 62:1727-1734.

Lakowicz, J.R., H. Szmacinski, K. Nowaczyk, K.W. Brerndt, and M. Johnson. 1992. Fluorescence lifetime imaging. *Analytical Biochemistry,* 202:316-330.

Laver, N.M., W.G. Robison, B.A. Pfeffer. 1993. Novel procedures for isolating intact retinal vascular beds from diabetic humans and animal models. *Investigative Ophthalmology and Visual Science*, 34:2097-2104.

Linsenmeier, R.A. 1986. Effects of light and darkness on oxygen distribution and consumption in the cat retina. *Journal of General Physiology,* 88:521-542.

Linsenmeier, R.A., R.D. Braun, M.A. McRipley, L.A. Padnick, J. Ahmed, D.L. Hatchell, D.S. McLeod, G.A. Lutty. 1998. Retinal hypoxia in long-term diabetic cats. *Investigative Ophthalmology and Visual Science,* 39:1647-1657.

Linsenmeier, R.A., L. Padnick-Silver. 2000. Metabolic dependence of photoreceptors on the choroids in the normal and detached retina. *Investigative Ophthalmology and Visual Science,* 41:3117-3123.

Linsenmeier, R.A. and C.M. Yancey. 1989. Effects of hyperoxia on the oxygen distribution in the intact cat retina. *Investigative Ophthalmology and Visual Science,* 30:612-618.

Lo, L.-W., C.J. Koch, and D.F. Wilson. 1996. Calibration of oxygen-dependent quenching of the phosphorescence of Pd-meso-tetra(4-carboxyphenyl) porphine: A phosphor with general application for measuring oxygen concentration in biological systems. *Analytical Biochemistry,* 236:153-160.

Molnar, I., S. Poitry, M. Tsacopoulos, N. Gilodi, and P.M. Leuenberger. 1985. Effect of laser photocoagulation on oxygenation of the retina in miniature pigs. *Investigative Ophthalmology and Visual Science,* 26:1410-1414.

Moses, R.A., Hart, W.A. 1987. Adler's Physiology of the Eye: Clinical Applications. St. Louis: The C.V. Mosby Company.

Patz, A. 1980. Studies on retinal neovascularization: Fiedenwald lecture. *Investigative Ophthalmology and Visual Science*, 19:1133-1138.

Pierce, E.A., R.L. Avery, E.D. Foley, and L.H. Smith. 1995. Vascular endothelial growth factor/vascular permeability factor expression in a mouse model for retinal neovascularization. *Proceedings of the National Academy of Science, USA*, 92:905-909.

Sakagami, K., T. Kodama, D.G. Puro. 2001. PDGF-induced coupling of function with metabolism in microvascular pericytes of the retina. *Investigative Ophthalmology and Visual Science,* 42:1939-1944.

Sherwood, L. 2001. Human Physiology: From Cells to Systems. Pacific Grove, CA: Brooks/Cole.

Shonat, R.D. Personal communication. 1/15/01-4/1/01.

Shonat, R.D. and P.C. Johnson. 1997. Oxygen tension gradients and heterogeneity in the venous microcirculation: A phosphorescence quenching study. *American Journal of Physiology,* 272:H2233-H2240.

Shonat, R.D., K.N. Richmond, P.C. Johnson. 1995. Phosphorescence quenching and the microcirculation: An automated mutilpoint oxygen tension measuring instrument. *Review of Scientific Instruments.* 66:5075-5084.

Shonat, R.D., E.S. Wachman, W. Niu, A.P. Koretsky, D.L. Farkas. 1997. Near-simultaneous hemoglobin saturation and oxygen tension maps in the mouse brain using an AOTF microscope. *Biophysical Journal,* 73:1223-1231.

Shonat, R.D., E.S. Wachman, W. Niu, A.P. Koretsky, D.L. Farkas. 1998. Near-simultaneous hemoglobin saturation and oxygen tension maps in the mouse cortex during amphetamine stimulation. *Oxygen Transport to Tissue,* 20:149-158.

Shonat, R.D., D.F. Wilson, C.E. Riva, and S.D. Cranstoun. 1992. Effect of acute increases in intraocular pressure on intravascular optic nerve head tension in cats. *Investigative Ophthalmology and Visual Science*, 33:3174-3180.

Shonat, R.D., D.F. Wilson, C.E. Riva, M. Pawlowski. 1992. Oxygen distribution in the retinal and choroidal vessels of the cat as measured by a new phosphorescence imaging method. *Applied Optics,* 31:3711-3718.

Stefansson, E. 1990. Oxygen and diabetic eye disease. *Graefe's Archive of Clinical and Experimental Ophthalmology,* 228:120-123.

Stefansson, E., D.L. Hatchell, B.L. Fisher, F.S. Sutherland, and R. Machemer. 1986. Panretinal photocoagulation and retinal oxygenation in normal and diabetic cats. *American Journal of Ophthalmology,* 101:657-664.

Stefansson, E. M.B. Landers, III, and M.L. Wolbarsht. 1981. Increased retinal oxygen supply following pan-retinal photocoagulation and vitrectomy and lensectomy. *Transactions of the American Ophthalmological Society,* 79:307-334.

Stefansson, E., R.L. Novack, and D.L. Hatchell. 1990. Vitrectomy prevents retinal hypoxia in branch retinal vein occlusion. *Investigative Ophthalmology and Visual Science,* 31:284-289.

Stenbit, A.E., T.-S. Tsao, J. Lu, R. Burcelin, D.L. Geenen, S.M. Factor, K. Houseknecht, E.B. Katz, and M.J. Charron. 1997. GLUT4 heterozygous knockout mice develop muscle insulin resistance and diabetes. *Nature Medicine*, 3:1096-1101.

Sussman, K.E., B. Draznin, W.E. James. 1987. Clinical Guide to Diabetes Mellitus. New York: Alan R. Liss, Inc.

Tamemoto, H., T. Kadowaki, K. Tobe, T. Yagi, H. Sakura, T. Hayakawa, Y. Terauchi, K. Veki, Y. Kaburagi, S. Satoh, H. Sekihara, S. Yoshioka, H. Horikoshi, Y. Furuta, Y. Ikawa, M. Kasuga, Y. Yazaki, and S. Alzawa. 1994. Insulin resistance and growth retardation in mice lacking insulin receptor substrate-1. *Nature,* 372:182-186.

Terauchi, Y., K. Iwamoto, H. Tamenoto, K. Komeda, C. Ishii, Y. Kanazawa, N. Asanuma, T. Aizawa, Y. Akanuma, K. Yasuda, T. Kodama, K, Tobe, Y. Yazaki, and T. Kadowaki. 1997. Development of non-insulin-dependent diabetes mellitus in the double knockout mice with disruption of insulin substrate-1 and β-cell glucokinase genes: Genetic reconstitution of diabetes as a polygenic disease. *The Journal of Clinical Investigation,* 99:861-866.

Vanderkooi, J.M. 1990. Fluorescence and Phosphorescence. Lecture notes, University of Pennsylvania, Philadelphia, PA.

Vanderkooi, J.M., G. Maniara, T.J. Green, and D.F. Wilson. 1987. An optical method for measurement of dioxygen concentration based upon quenching of phosphorescence. *The Journal of Biological Chemistry,* 262:5476-5482.

Wachman, E.S., W.-H. Niu, and D.L. Farkas. 1996. Imaging acousto-optic tunable filter with 0.35-micrometer spatial resolution. *Applied Optics,* 35:5220-5226.

Watkins, P.J., P.L. Drury, S.L. Howell. 1996. Diabetes and its Management. Oxford: Blackwell Science, Ltd.

Wilson, D.F., A. Pastuszko, J.E. DiGiacomo, M. Pawlowski, R. Schneiderman, and M. Delivoria-Papadopoulos. 1991. Effect of hyperventilation on oxygenation of the brain cortex of newborn piglets. *Journal of Applied Physiology,* 70:2691-2696.

Withers, D.J., J.S. Gutierrez, H. Towery, D.J. Burks, J.M. Ren, S. Previs, Y. Zhang, D. Bernal, S. Pons, G.I. Shulman, S. Bonner-Weir, M.F. White. 1999. Disruption of IRS-2 causes type 2 diabetes in mice. *Nature,* 391:900-904.

Yamaoka, T., C. Nishimura, K. Yamashita, M. Itakura, T. Yamada, J. Fujimoto, and Y. Kokai. 1995. Acute onset of diabetic pathological changes in transgenic mice with human aldose reductase cDNA. *Diabetologia,* 38:255-261.

Yu, D.-Y. and S.J. Cringle. 2001. Oxygen distribution and consumption within the retina in vascularized and avascular retinas and in animal models of retinal disease. *Progress in Retinal and Eye Research,* 20:175-208.

Yu, D.-Y., S.J. Cringle, V. Alder, E.N. Su. 1999. Intraretinal oxygen distribution in the rat with graded systemic hyperoxia and hypercapnia. *Investigative Ophthalmology and Visual Science*, 40:2082-2087.

Appendix A: Pd-Meso-Tetra (4-carboxyphenyl) Porphrine Probe Solution

1. Measure 50mg Pd-meso-tetra (4-carboxyphenyl) porphrine (Porphryin Products, Logan, UT) in a 1.5 ml microcentrifuge tube.

2. Add 500 µl 0.5N NaOH—probe dissolves in basic solution.

3. Warm under tap water until dissolved. Centrifuge.

4. Make a 1.25x albumin salt solution (25 ml)
    a. Weigh 253.8 mg NaCl (FW = 58.44).
    b. Add distilled/deionized water to 25 ml.
    c. Pour salt water into a wide-mouth container, ad stirring rod and place on magnetic stir plate.
    d. Add 1.88g albumin, bovine fraction V (Sigma, St. Louis, MO), taking care not to let the albumin touch the sides of the container.
    e. Stir gently to dissolve (takes a few hours).

5. Slowly mix 4 ml albumin salt solution and all of the probe/NaOH solution.

6. Adjust pH to 7.4 with Tris(hydroxymethyl)aminomethane base (Aldrich Chemical Company, Milwaukee, WI) and HCl as needed. If albumin precipitates, pH is too low and Tris should be added.

7. Aliquot into 100 µl portions and store at -20°C.

8. Final solution is Pd-porphyrin (10 mg/ml) in BSA (60 mg/ml) 0.9% NaCl (Shonat 2001).

Appendix B: "Retina" Program

The front panel of this program accepts as inputs τ_o, k_Q, modulation frequency and pulse time of excitation light, the name of the file containing the series of intensity images, and the number of intensity images to be used for fitting. It also allows the user to input a phase error, which is subtracted from the calculated phase delay, and a modulation error, which is divided into the calculated modulation. Averaging filters may be applied using the "Phos Filter" box. A region of interest (ROI) may then be selected within the intensity images, and a graph of phosphorescence intensity versus phase shift may be calculated and fit to the equation $I(\theta_D) = a_0 + a_1\sin\theta_D + b_1\cos\theta_D$. The parameters θ, τ, and $[PO_2]$ are calculated (see Background), and the fitting parameters k, m_D, m, and R^2 are also output. The program may also be used to create a number of maps using the intensity images, including PO_2 and R^2 maps. The mapping function also allows ROI selection, and outputs the mean, standard deviation, maximum, and minimum values within the ROI.

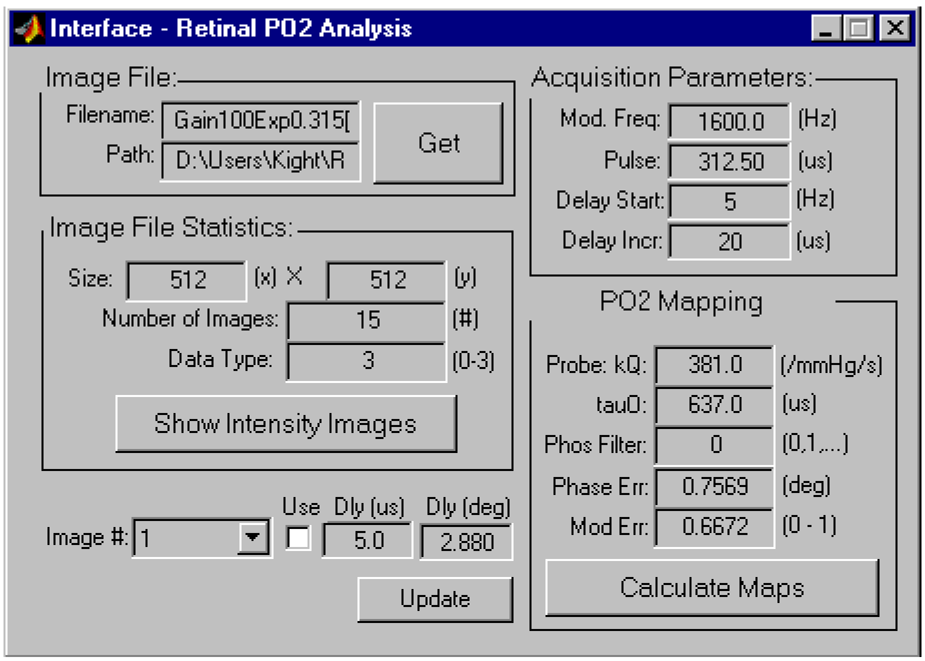

Figure B.1—"Retina" front panel. Phosphorescence intensity image files are input using the "Get" button. Individual images used for graphing and mapping are selected at the bottom of the panel—in this particular case, image #1 is not selected. The mapping parameters may be input using the PC keyboard. Once all parameters are correct, the "Show Intensity Images" and "Calculate Maps" buttons may be used.

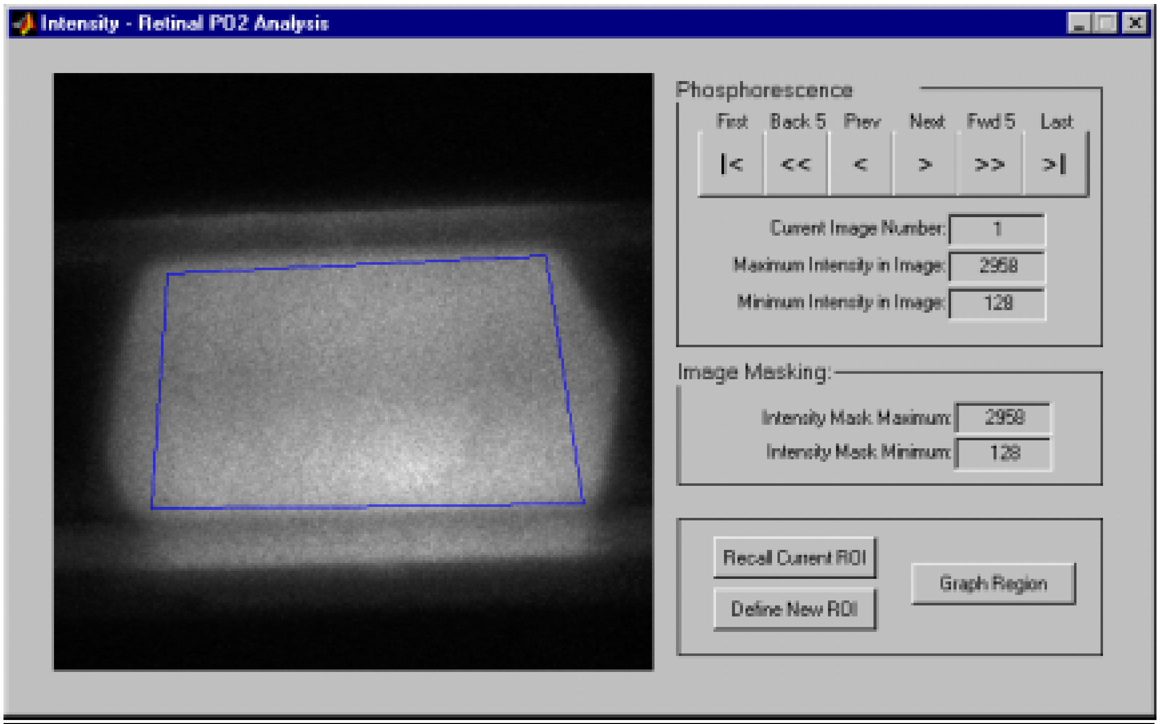

Figure B.2—"Show Intensity Images" screen. Individual intensity images may be viewed using the buttons at the top of the screen. An ROI may be selected by pressing one of the buttons at the bottom, and using the mouse to define a region on the image—the ROI selected in this image appears in blue. A graph of intensity versus phase delay for the ROI may be created by pressing the "Graph Region" button.

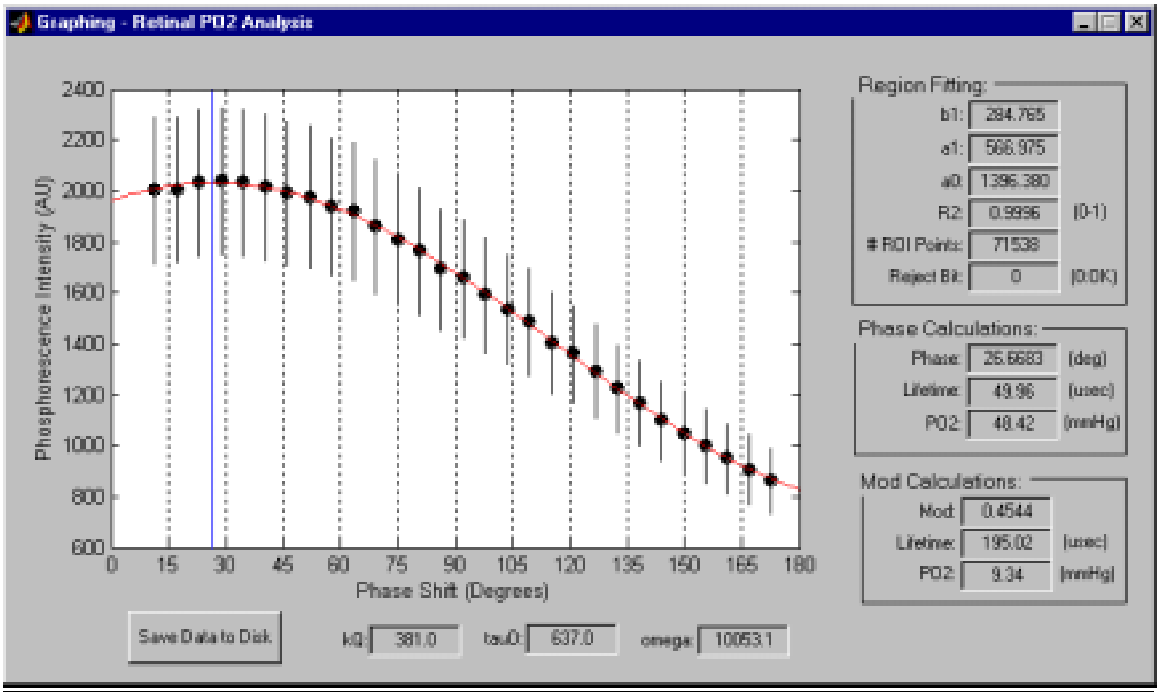

Figure B.3—"Graph Region" screen. Phosphorescence is plotted versus phase delay for the images and ROI selected. Relevant fitting and calculated parameters are output on the right. The blue line represents the curve maximum, which indicates the phosphorescence phase delay (θ) also output on the right.

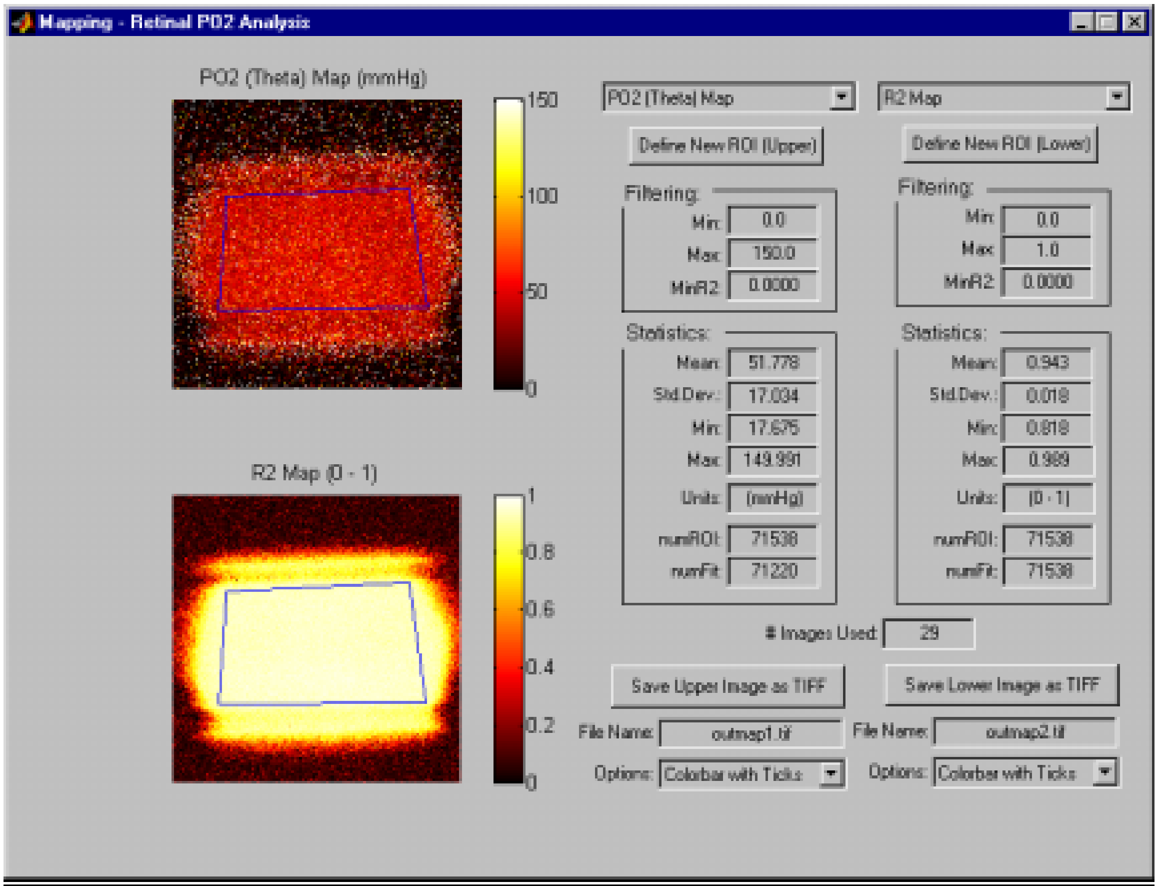

Figure B.4—"Calculate Maps" screen. A number of different maps may be created using the pull-down menus at the top. Filtering parameters may be input to reduce extraneous pixels in the images. Statistics are output in the right center of the screen.

Appendix C: Procedure for Trypsin Digestion of the Retina

Note: All procedures should be performed in a clean, dust-free environment to prevent contamination of samples. Procedures on the eye and retina should be performed under a dissecting microscope when necessary.

1. Remove eyes from animal and fix in 10% buffered formalin for a minimum of 5 days and a maximum of 10-12 days. After 10-12 days, transfer eyes from the fixative into phosphate-buffered saline and store at 4°C.

2. Prepare trypsin digestion buffer:
    a. Weigh out 18.2 g Tris base (MW 121).
    b. Add approximately 800 ml deionized water.
    c. Create a 0.2 M NaF (MW 42) solution using the following formula to determine the weight of NaF to be added:

       42 x (volume of tris/water solution in L) x 0.2 = weight of NaF in grams

    d. Add this measured weight of NaF to the tris/water solution.
    e. Bring this solution to pH 7.8 using concentrated HCl.
    f. Store refrigerated.

3. Prepare trypsin digestion solution:
    a. Weigh out 0.3 g crude trypsin 1:250 powder (it is absolutely necessary to use crude trypsin—pure trypsin will not digest the retina).
    b. Add trypsin digestion buffer to make 10 ml. Shake or vortex to completely dissolve the trypsin in the buffer.
    c. Centrifuge or filter the solution to remove the sediment.
    d. Either make this solution fresh each day, or aliquot 5-10 ml portions and store frozen.

4. Transfer eyes to a 50-ml beaker of distilled water. Change the water once by carefully pouring the water out of the beaker (do not pour out the eyes), and refilling the beaker.

5. Place one eye in a petri dish filled with distilled water, and remove excess tissue from around the eyeball.

6. Place the eye in a sized tray to hold it in place, and use a razor blade to make a small initial cut just below the limbus, as indicated on the diagram below:

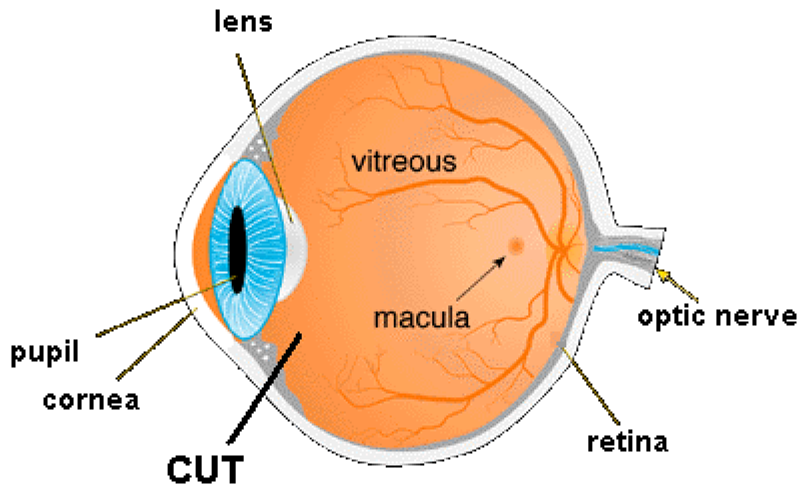

7. Beginning at the initial cut, use tweezers and scissors to completely remove the anterior segment from the eyes, leaving only a cup containing the retina:

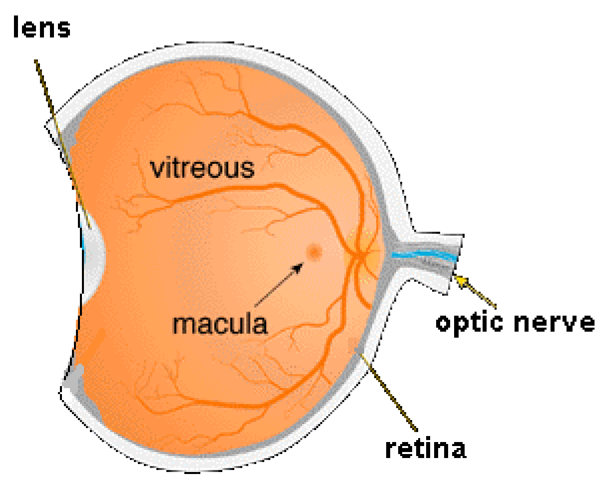

8. Return the eye to the water-filled petri dish, and pop out the lens with a sweep of curved scissors or forceps.

9. Hold the sclera (the outside cup of the remaining eyeball) with a pair of forceps, and use curved scissors or forceps to carefully free the retina from the eye. Take care not to tear the retina during this process. The sclera may be cut to facilitate removal of the retina.

10. Use an appropriately sized piece of glass tubing with a pipet bulb on the end to aspirate the retina and transfer it to a 50-ml beaker of distilled water.

11. Allow the retina to soak for 1-2 hours, changing the water 4 or 5 times. Take care not to pour the retina down the drain when changing the water.

12. Transfer the retina to a glass test tube (NOT plastic—the retina will stick to it) using the Pasteur pipette, and remove the water with a dropper. Add 5-10 ml trypsin digestion solution to the test tube. Place the tube in a 37°C shaker water bath at 40-60 cycles per minute.

13. Allow the retina to digest for and hour and a half to an hour and forty-five minutes. Diseased or damaged retinas may take longer to digest. Avoid over-digestion—this will cause the vessels in the retina to fall apart. If under-digested, the retina may be returned to the trypsin solution for further digestion.

14. Transfer the retina to a petri dish of distilled water with the Pasteur pipette. Do not throw away the trypsin solution. Three layers of the retina should be visible: the jelly-like inner limiting membrane (which is clear, and may not be visible unless the petri dish is agitated), the clear/whitish vascular layer, and the tan photoreceptor layer. Grasp the inner limiting membrane with forceps, and use scissors to free it from the retina. The membrane will be sticky and difficult to deal with. Be sure all of this membrane is removed, and wipe it away from the forceps on a paper towel.

15. Use a Pasteur pipette with an eyelash cemented to the tip to beat the photoreceptors away from the retina. Use the curved surface of the eyelash, never the tip, as the tip may damage the blood vessels. Continue manipulating the retina with the eyelash to remove all cellular debris, frequently dipping the eyelash in the trypsin solution to prevent it from sticking to the retina.

16. Once all debris is removed, the vasculature will remain. It will be nearly transparent. Place a microscope slide in a separate petri dish, and fill the dish with enough water adequately cover the slide. Aspirate the retinal vessels and deposit them on the slide. Using the eyelash, carefully unfold the vessels and very gently press them onto the slide. If necessary, cut the vessels so they lie flat. Slowly remove the water from the petri dish using a peristaltic pump set a low speed.

17. Allow the vessels to air-dry overnight.

18. Mount and stain the retinas using the Procedure for Hematoxylin Staining of Trypsin Digests.

Appendix D: Procedure for Hematoxylin Staining of Trypsin Digests

1. After mounting retinas onto slides, allow to air-dry overnight.

2. Prepare periodic acid solution:
   a. Weigh out 0.8 g reagent grade periodic acid.
   b. Add 20 ml distilled water. Agitate to dissolve.
   c. Add 10 ml 0.2M sodium acetate.
   d. Add 70 ml 95% ethanol (66.5 ml EtOH + 3.5 ml water).
   e. Swirl to mix. Make this solution fresh each day it is used. Store refrigerated when not in use.

3. Place slides in slide staining tray.

4. Stain the slides with the following solutions by using one reagent bottle for each step. Pour the reagent into the staining tray, allow to sit for the specified time, and then return the reagent to the bottle (except where specified).
   a. 70% ethanol—5 minutes
   b. Periodic acid solution—5 minutes
   c. 70% ethanol, 3 changes (3 reagent bottles)—2 minutes each
   d. Rinse in distilled water (discard water)
   e. Schiff's reagent—25 minutes (Schiff's reagent is light sensitive. Place slides in a drawer or other dark area when soaking in this reagent.)
   f. Running tap water—20 minutes
   g. Hematoxylin—10 minutes (Hematoxylin is light sensitive. Place slides in a drawer or other dark area when soaking in this reagent)
   h. Running tap water—20 minutes
   i. 95% ethanol, 3 changes—2 minutes each
   j. 100% ethanol, 3 changes—2 minutes each
   k. Xylene, 3 changes—2 minutes each
   l. Drop Permount or Histoclad onto each stained retina and apply a cover glass.

Vessel walls will appear magenta, and nuclei will be blue.

Appendix E: Data Tables and Graphs

The following are Microsoft Excel spreadsheets used for analysis of data obtained during *in vivo* experiments. Data are organized by animal number and vessel type, and listed in the order images were taken. Map R^2 vs. SNR graphs were not created for Mouse 6a because the animal died during experimentation, and insufficient data were acquired at each gain setting to allow for statistical significance. The data from this mouse are not included in the summary graphs in the Results section. Additionally, data from Mice 2a and 7a are not included, as excessive head movement and drastic changes in the blood flow during image acquisition prevented the creation of satisfactory oxygen maps

Gain	Exposure T	Relative Im	Cumulative	Accumulat	SNR	PO2 Mean	PO2 St. De	R2 Mean	R2 St. Dev
100	0.06	1	1	4.549606	3.095793	31.3381	25.532	0.7126	0.1108
100	0.06	2	2	9.099213	3.085443	33.1828	24.6421	0.697	0.1198
100	0.06	3	3	13.64882	3.108929	39.4319	29.6684	0.7154	0.1148
100	0.145	1	4	24.6437	6.557214	37.3026	22.3232	0.8576	0.0617
100	0.145	2	5	35.63858	6.222086	38.115	23.4717	0.85	0.0649
100	0.145	3	6	46.63346	5.941643	35.1657	20.675	0.8547	0.0612
100	0.23	1	7	64.07362	8.92515	40.231	22.1909	0.8975	0.0415
100	0.23	2	8	81.51378	8.409721	39.3985	21.5983	0.9058	0.0409
100	0.23	3	9	98.95394	8.334536	37.6933	19.4958	0.9017	0.0428
100	0.315	1	10	122.8394	11.70094	36.3694	16.1542	0.9314	0.0289
100	0.315	2	11	146.7248	11.11096	40.4209	20.7441	0.926	0.0333
100	0.315	3	12	170.6102	10.66342	43.3651	19.3882	0.9297	0.0312
100	0.4	1	13	200.9409	14.40799	37.0123	14.0576	0.9778	0.0252
100	0.4	2	14	231.2717	14.19239	37.0853	14.4383	0.9456	0.0246
100	0.4	3	15	261.6024	12.96509	39.713	17.0262	0.9426	0.0249
70	0.15	1	16	272.9764	2.651029	47.847	30.1669	0.8315	0.0711
70	0.15	2	17	284.3504	2.6225	44.2218	28.1264	0.8433	0.0681
70	0.15	3	18	295.7244	2.635986	39.0434	25.3113	0.8436	0.0667
70	0.31	1	19	319.2307	4.325664	41.1906	20.8689	0.9089	0.0392
70	0.31	2	20	342.737	4.196321	43.4629	22.788	0.9061	0.0389
70	0.31	3	21	366.2433	4.317443	41.4235	22.1984	0.9092	0.0389
70	0.47	1	22	401.8819	5.8495	41.7067	18.6205	0.9373	0.0283
70	0.47	2	23	437.5205	5.606057	43.386	19.3558	0.9371	0.0266
70	0.47	3	24	473.1591	5.777164	43.5985	20.2452	0.9367	0.0277
70	0.63	1	25	520.9299	7.105086	44.4771	17.7629	0.9491	0.0221
70	0.63	2	26	568.7008	6.995464	46.1181	20.8784	0.9474	0.0219
70	0.63	3	27	616.4717	7.332793	47.8064	19.0871	0.9513	0.0209
70	0.79	1	28	676.3748	8.517693	46.3823	17.9728	0.959	0.0173
70	0.79	2	29	736.278	8.327271	46.9208	20.5558	0.9576	0.0183
70	0.79	3	30	796.1811	8.581879	41.7116	15.173	0.9589	0.0173
40	0.32	1	31	820.4457	2.3966	42.0659	24.4672	0.8847	0.0493
40	0.32	2	32	844.7102	2.461529	44.1889	26.0651	0.8858	0.0484
40	0.32	3	33	868.9748	2.430371	47.2164	26.4607	0.8874	0.0481
40	0.49	1	34	906.1299	3.124143	41.2365	20.8511	0.9193	0.0359
40	0.49	2	35	943.285	3.148657	46.8152	24.2926	0.9178	0.0346
40	0.49	3	36	980.4402	3.011221	48.4096	25.5742	0.9182	0.0351
40	0.66	1	37	1030.486	3.724993	45.5322	22.1523	0.951	0.0285
40	0.66	2	38	1080.531	3.875971	43.3804	18.7779	0.9388	0.0255
40	0.66	3	39	1130.577	3.704214	45.9238	20.9077	0.9352	0.0282
40	0.83	1	40	1193.513	4.3264	47.9599	20.8675	0.9482	0.0235
40	0.83	2	41	1256.45	4.359643	44.7594	21.1474	0.9464	0.0231
40	0.83	3	42	1319.386	4.439157	45.2842	19.3097	0.9476	0.0228
40	1	1	43	1395.213	5.221529	45.1115	18.2914	0.9558	0.0199
40	1	2	44	1471.039	5.075257	42.44	16.2557	0.9535	0.0196
40	1	3	45	1546.866	5.1926	44.0404	18.0572	0.9561	0.019
10	0.4	1	46	1577.197	1.826257	42.2584	24.6142	0.8597	0.0586
10	0.4	2	47	1607.528	1.8781	44.597	26.6512	0.8703	0.0548
10	0.4	3	48	1637.858	1.867364	45.5887	27.2643	0.8593	0.0611
10	0.55	1	49	1679.563	2.143657	43.8342	22.756	0.9022	0.0408
10	0.55	2	50	1721.268	2.144786	38.2199	19.6557	0.9008	0.0416
10	0.55	3	51	1762.972	2.13575	42.8878	23.885	0.8968	0.0432
10	0.7	1	52	1816.051	2.370264	42.3321	21.2545	0.9146	0.0377
10	0.7	2	53	1869.13	2.490007	40.5599	21.3576	0.9205	0.0334
10	0.7	3	54	1922.209	2.416929	44.4406	21.3127	0.9176	0.0351
10	0.85	1	55	1986.661	2.640707	43.8111	21.1277	0.9287	0.0305
10	0.85	2	56	2051.114	2.756536	41.6892	19.7134	0.9286	0.0303
10	0.85	3	57	2115.567	2.802221	43.3271	20.2275	0.9296	0.0308
10	1	1	58	2191.394	3.005229	43.5173	20.1546	0.9393	0.0267
10	1	2	59	2267.22	3.105014	45.124	19.5174	0.9392	0.0268
10	1	3	60	2343.047	2.921743	46.1122	20.9077	0.9368	0.0286

Mouse 1a Vein

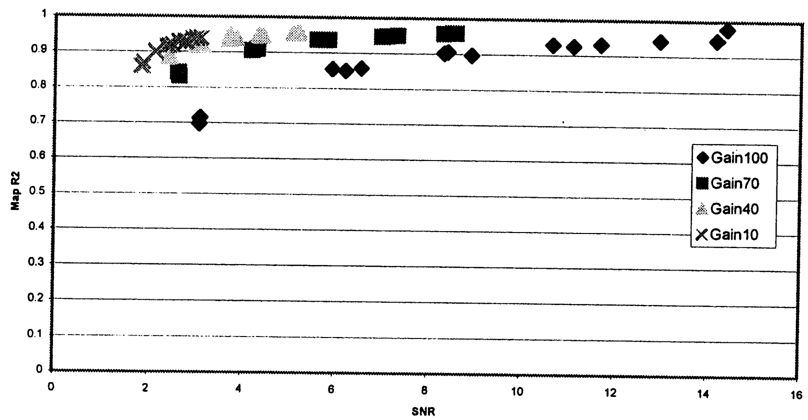

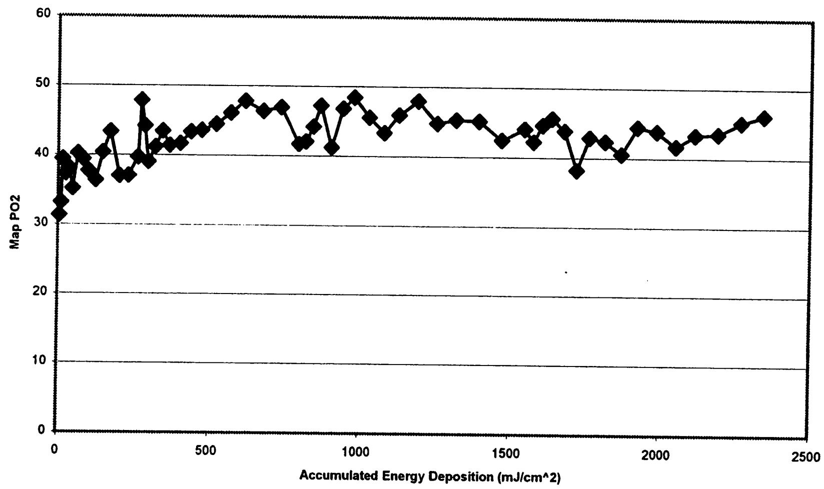

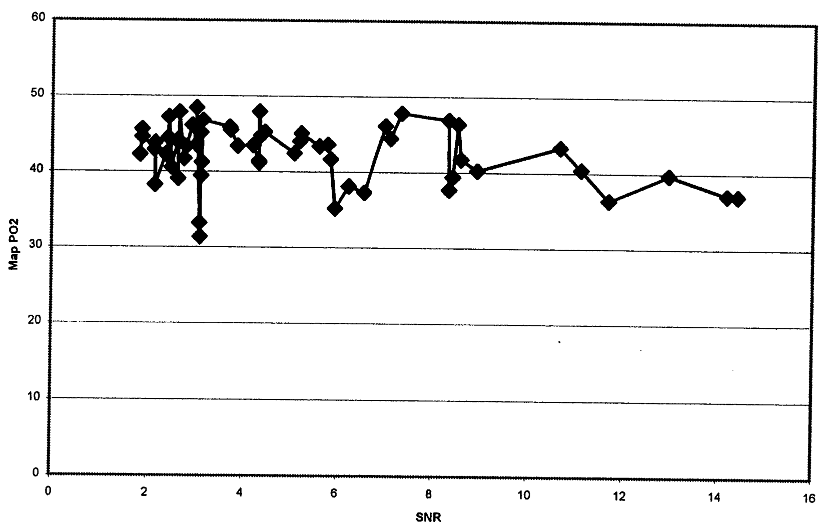

Gain	Exposure T	Relative Im	Cumulative	Accumulate	SNR	PO2 Mean	PO2 St. De	R2 Mean	R2 St. Dev
100	0.06	1	1	4.549606	2.114821	39.6745	29.2787	0.6522	0.1285
100	0.06	2	2	9.099213	2.18555	40.0248	30.7703	0.6784	0.1227
100	0.06	3	3	13.64882	2.132386	38.1474	29.1068	0.6672	0.1207
100	0.145	1	4	24.6437	4.135036	47.0121	26.6557	0.8224	0.0674
100	0.145	2	5	35.63858	3.961193	50.7693	28.0794	0.8212	0.0728
100	0.145	3	6	46.63346	3.781429	45.7589	27.8362	0.8271	0.0678
100	0.23	1	7	64.07362	5.706393	47.8422	24.8418	0.8838	0.0517
100	0.23	2	8	81.51378	5.56675	51.5178	27.2305	0.8808	0.0527
100	0.23	3	9	98.95394	5.513643	50.132	27.91	0.8838	0.0496
100	0.315	1	10	122.8394	7.148736	54.7994	26.7813	0.9127	0.0367
100	0.315	2	11	146.7248	6.889557	45.6133	22.3398	0.9061	0.0425
100	0.315	3	12	170.6102	6.84275	53.9341	28.3479	0.9082	0.0406
100	0.4	1	13	200.9409	8.358679	52.4021	24.9794	0.9206	0.0339
100	0.4	2	14	231.2717	8.287757	47.7886	24.5135	0.9293	0.03
100	0.4	3	15	261.6024	8.137771	51.3911	22.8888	0.9238	0.0354
70	0.15	1	16	272.9764	1.956836	49.7236	30.6369	0.7933	0.0876
70	0.15	2	17	284.3504	2.010964	49.6578	29.4232	0.7997	0.0844
70	0.15	3	18	295.7244	1.907214	49.0474	30.8991	0.7826	0.0909
70	0.31	1	19	319.2307	3.046629	47.4786	25.4282	0.8859	0.0464
70	0.31	2	20	342.737	3.05295	55.3046	29.7117	0.8839	0.0535
70	0.31	3	21	366.2433	2.8612	53.6004	28.1099	0.8794	0.0496
70	0.47	1	22	401.8819	4.10985	55.3252	27.091	0.9201	0.0345
70	0.47	2	23	437.5205	3.877786	55.4945	27.3316	0.9197	0.0359
70	0.47	3	24	473.1591	3.758521	52.6991	26.1164	0.9123	0.0397
70	0.63	1	25	520.9299	4.792414	57.5879	25.8847	0.9333	0.0287
70	0.63	2	26	568.7008	4.745214	53.3979	26.6935	0.9374	0.0255
70	0.63	3	27	616.4717	4.660943	58.5217	25.3551	0.9352	0.0295
70	0.79	1	28	676.3748	5.870486	58.8598	24.5303	0.9481	0.024
70	0.79	2	29	736.278	5.816621	61.0782	27.4807	0.9457	0.0256
70	0.79	3	30	796.1811	5.4385	51.7926	22.0157	0.9454	0.0249
40	0.32	1	31	820.4457	1.861457	48.0736	27.1763	0.8527	0.0637
40	0.32	2	32	844.7102	1.979321	53.192	29.4465	0.8637	0.0571
40	0.32	3	33	868.9748	1.989986	55.9282	30.5722	0.8579	0.0615
40	0.49	1	34	906.1299	2.353907	51.4996	28.2755	0.8985	0.0459
40	0.49	2	35	943.285	2.353586	59.2062	30.1828	0.9001	0.0429
40	0.49	3	36	980.4402	2.325614	53.1608	27.416	0.8982	0.0471
40	0.66	1	37	1030.486	2.6682	56.065	27.771	0.9191	0.035
40	0.66	2	38	1080.531	2.794857	54.8396	25.4769	0.9208	0.0351
40	0.66	3	39	1130.577	2.702571	57.9637	27.121	0.9205	0.0344
40	0.83	1	40	1193.513	3.196864	58.3452	26.2303	0.9365	0.0274
40	0.83	2	41	1256.45	3.124921	54.3426	25.1233	0.9312	0.028
40	0.83	3	42	1319.386	3.185336	57.3821	25.6143	0.9399	0.0309
40	1	1	43	1395.213	3.765514	57.7478	24.1372	0.9435	0.0244
40	1	2	44	1471.039	3.648779	55.7926	25.5267	0.9433	0.0256
40	1	3	45	1546.866	3.659643	54.3109	29.2702	0.9431	0.0252
10	0.4	1	46	1577.197	1.525221	45.3989	26.9337	0.8276	0.0683
10	0.4	2	47	1607.528	1.564357	44.8093	26.6422	0.8318	0.0717
10	0.4	3	48	1637.858	1.519693	48.6575	28.3567	0.8315	0.0718
10	0.55	1	49	1679.563	1.778971	50.9847	26.245	0.88	0.0498
10	0.55	2	50	1721.268	1.78155	45.0981	25.7877	0.8759	0.0543
10	0.55	3	51	1762.972	1.716043	48.5902	26.9661	0.8632	0.0565
10	0.7	1	52	1816.051	1.902929	52.3737	26.1536	0.8964	0.0442
10	0.7	2	53	1869.13	1.889071	55.0306	29.0283	0.8917	0.0487
10	0.7	3	54	1922.209	1.91365	55.2284	28.9121	0.891	0.046
10	0.85	1	55	1986.661	2.104971	53.2896	36.4084	0.9117	0.038
10	0.85	2	56	2051.114	2.1586	54.2392	27.1513	0.912	0.0382
10	0.85	3	57	2115.567	2.098914	52.8082	25.88	0.9059	0.0394
10	1	1	58	2191.394	2.315486	56.5722	26.3641	0.923	0.033
10	1	2	59	2267.22	2.287979	52.437	25.3322	0.9196	0.0343
10	1	3	60	2343.047	2.293014	56.1862	27.8662	0.9216	0.0327

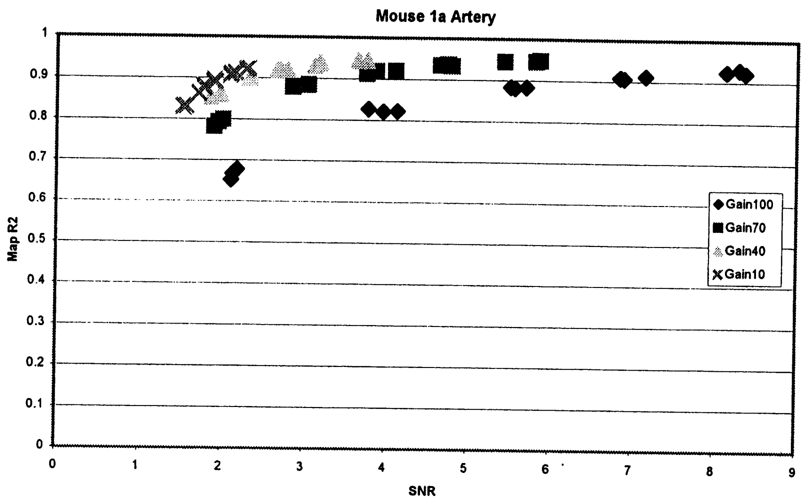
Mouse 1a Artery
Map R2
SNR
Gain100
Gain70
Gain40
Gain10
0
0.1
0.2
0.3
0.4
0.5
0.6
0.7
0.8
0.9
1
0
1
2
3
4
5
6
7
8
9

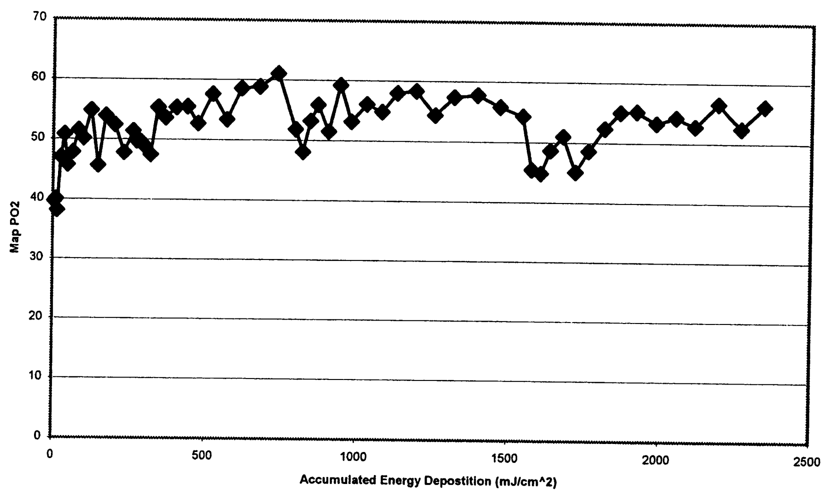
Map PO2
Accumulated Energy Depostition (mJ/cm^2)
0
10
20
30
40
50
60
70
0
500
1000
1500
2000
2500

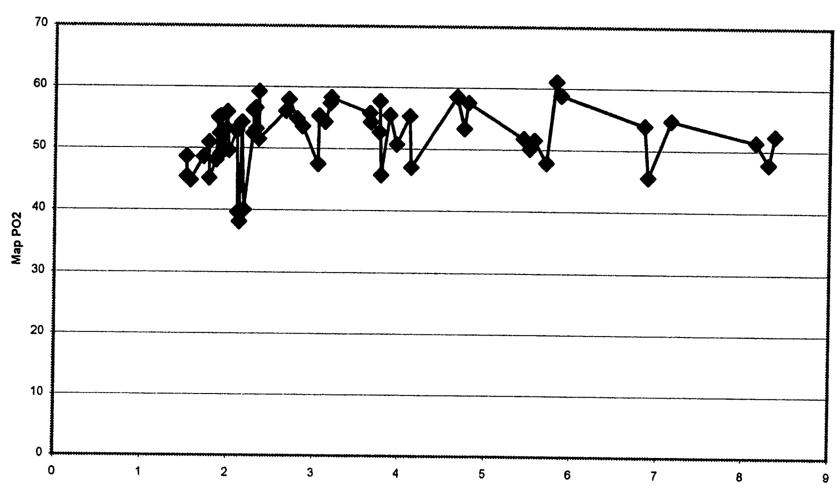
Map PO2
SNR
0
10
20
30
40
50
60
70
0
1
2
3
4
5
6
7
8
9

Gain	Exposure T	Relative Ir	Cumulative	Accumulat	SNR	PO2 Mean	PO2 St. De	R2 Mean	R2 St. Dev
100	0.06	1	1	4.549606	1.543421	40.7296	32.7735	0.5973	0.1516
100	0.06	2	2	9.099213	1.662514	37.6693	29.7527	0.6174	0.1511
100	0.06	3	3	13.64882	1.627964	41.0929	31.8999	0.608	0.1545
100	0.145	1	4	24.6437	2.570714	54.8134	30.8204	0.7835	0.0935
100	0.145	2	5	35.63858	2.604886	53.5213	29.5981	0.7761	0.0881
100	0.145	3	6	46.63346	2.6328	49.7479	30.9323	0.7937	0.0862
100	0.23	1	7	64.07362	3.561721	53.1262	28.7827	0.8444	0.069
100	0.23	2	8	81.51378	3.633271	57.9677	30.3869	0.8496	0.0662
100	0.23	3	9	98.95394	3.544707	59.0769	32.1188	0.851	0.0628
100	0.315	1	10	122.8394	4.515664	58.0034	29.9211	0.888	0.052
100	0.315	2	11	146.7248	4.442821	58.5357	30.2162	0.8795	0.049
100	0.315	3	12	170.6102	4.487464	60.8815	28.4017	0.8809	0.0531
100	0.4	1	13	200.9409	5.443357	60.3867	29.2909	0.9023	0.0411
100	0.4	2	14	231.2717	5.309457	61.9574	28.766	0.9032	0.0427
100	0.4	3	15	261.6024	4.96845	65.4685	29.9226	0.8998	0.0439
70	0.15	1	16	272.9764	1.587336	52.0365	30.546	0.7576	0.1023
70	0.15	2	17	284.3504	1.568971	52.5013	34.5642	0.7532	0.0995
70	0.15	3	18	295.7244	1.606071	45.6005	29.0918	0.7527	0.1016
70	0.31	1	19	319.2307	2.223664	54.2106	30.5602	0.8551	0.0608
70	0.31	2	20	342.737	2.26285	62.4493	33.3083	0.8468	0.064
70	0.31	3	21	366.2433	2.201386	60.29	31.7032	0.8442	0.0645
70	0.47	1	22	401.8819	2.880686	65.3519	30.0085	0.9028	0.0396
70	0.47	2	23	437.5205	2.77385	62.2263	30.2084	0.8926	0.0479
70	0.47	3	24	473.1591	2.717093	58.6863	30.1501	0.889	0.0499
70	0.63	1	25	520.9299	3.460143	61.9075	30.1302	0.9176	0.0351
70	0.63	2	26	568.7008	3.444807	63.4104	29.7229	0.9127	0.0368
70	0.63	3	27	616.4717	3.457171	65.4113	31.0919	0.9157	0.0398
70	0.79	1	28	676.3748	4.215021	68.0487	28.6898	0.9333	0.0293
70	0.79	2	29	736.278	4.029407	59.1901	28.651	0.9304	0.0291
70	0.79	3	30	796.1811	3.995114	61.517	27.6931	0.9338	0.0283
40	0.32	1	31	820.4457	1.570479	52.3609	32.2871	0.8108	0.0787
40	0.32	2	32	844.7102	1.650093	54.7581	31.4585	0.8286	0.0743
40	0.32	3	33	868.9748	1.6226	56.8063	31.2912	0.8141	0.0797
40	0.49	1	34	906.1299	1.858329	56.5369	28.9186	0.8616	0.0585
40	0.49	2	35	943.285	1.845286	59.1537	31.1602	0.8631	0.0578
40	0.49	3	36	980.4402	1.850293	64.1368	34.0511	0.8749	0.0543
40	0.66	1	37	1030.486	2.184379	57.325	28.899	0.8946	0.0491
40	0.66	2	38	1080.531	2.1062	61.5237	29.8273	0.8943	0.0453
40	0.66	3	39	1130.577	2.13385	62.4736	29.4271	0.8974	0.0447
40	0.83	1	40	1193.513	2.341079	64.2323	29.4555	0.9131	0.0376
40	0.83	2	41	1256.45	2.350821	62.1063	29.1446	0.9124	0.038
40	0.83	3	42	1319.386	2.375679	63.8288	29.727	0.9133	0.0364
40	1	1	43	1395.213	2.732914	63.4927	28.0271	0.9285	0.0305
40	1	2	44	1471.039	2.685343	62.8859	28.4713	0.927	0.032
40	1	3	45	1546.866	2.671571	64.0949	28.9529	0.926	0.0324
10	0.4	1	46	1577.197	1.334821	46.6725	29.0297	0.7481	0.1081
10	0.4	2	47	1607.528	1.347264	49.6254	31.4275	0.7758	0.0894
10	0.4	3	48	1637.858	1.355986	53.3671	31.4607	0.7611	0.1009
10	0.55	1	49	1679.563	1.471607	55.9165	32.442	0.8148	0.0753
10	0.55	2	50	1721.268	1.474186	56.8763	31.7184	0.8143	0.0785
10	0.55	3	51	1762.972	1.453136	53.0637	30.3818	0.8081	0.081
10	0.7	1	52	1816.051	1.574557	56.8056	31.7091	0.8441	0.0659
10	0.7	2	53	1869.13	1.569671	59.5999	33.0134	0.853	0.0636
10	0.7	3	54	1922.209	1.570557	55.8152	30.5754	0.8441	0.0663
10	0.85	1	55	1986.661	1.680764	60.2966	32.5642	0.8739	0.0526
10	0.85	2	56	2051.114	1.738907	59.0788	31.2603	0.8758	0.0534
10	0.85	3	57	2115.567	1.687836	65.1215	32.3143	0.8713	0.0565
10	1	1	58	2191.394	1.832129	58.8416	31.6698	0.8893	0.0477
10	1	2	59	2267.22	1.797793	64.9821	32.1015	0.8885	0.0492
10	1	3	60	2343.047	1.839357	60.7875	30.033	0.8919	0.0466

Mouse 1a Tissue

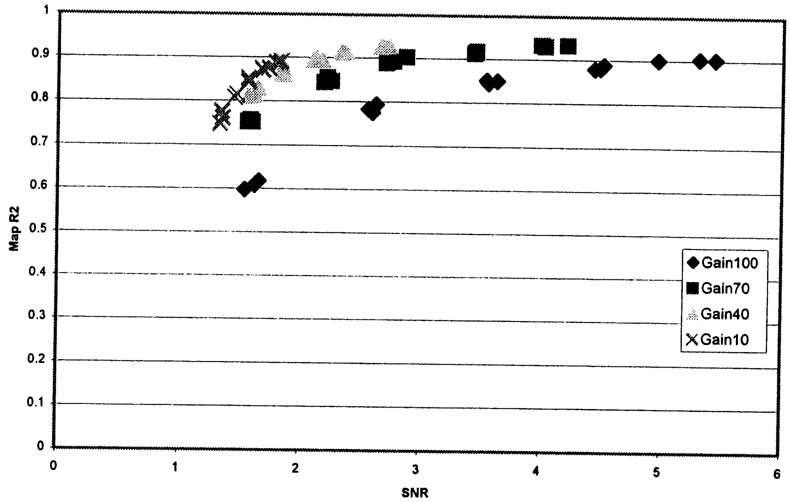

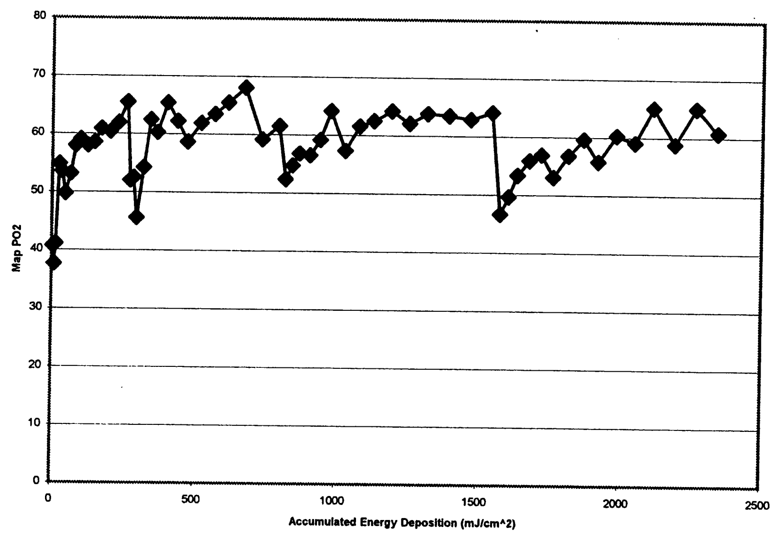

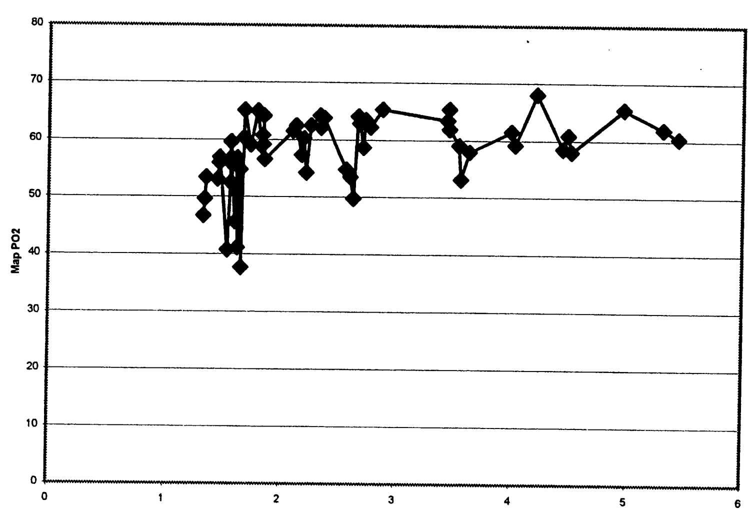

Gain	Exposure T	Relative Im	Cumulative	Accumulat	SNR	PO2 Mean	PO2 St. De	R2 Mean	R2 St. Dev
10	1	1	1	76.65354	2.565329	56.9668	24.9118	0.9447	0.0243
10	1	2	2	153.3071	2.622014	53.4213	23.5368	0.95	0.0218
10	1	3	3	229.9606	2.590086	55.6758	22.9388	0.945	0.0235
10	0.85	1	4	295.1161	2.376264	56.7692	25.3674	0.938	0.0276
10	0.85	2	5	360.2717	2.363529	55.7959	25.8445	0.9358	0.0279
10	0.85	3	6	425.4272	2.358593	55.0178	25.472	0.9351	0.0274
10	0.7	1	7	479.0846	2.24505	39.2874	20.6761	0.9064	0.0397
10	0.7	2	8	532.7421	2.746029	92.0398	29.2817	0.9585	0.018
10	0.7	3	9	586.3996	2.2328	67.2148	28.7629	0.9326	0.0286
10	0.55	1	10	628.5591	2.042814	30.059	22.1446	0.7523	0.0931
10	0.55	2	11	670.7185	2.0484	57.4077	24.3672	0.9279	0.0305
10	0.55	3	12	712.878	1.891586	77.4367	31.5587	0.9144	0.0374
10	0.4	1	13	743.5394	1.645614	61.6264	30.6959	0.8999	0.0441
10	0.4	2	14	774.2008	1.620443	57.0768	30.1289	0.855	0.0619
10	0.4	3	15	804.8622	1.912464	95.5203	30.0823	0.9257	0.032
40	1	1	16	881.5157	3.214429	63.9841	26.6199	0.9475	0.0234
40	1	2	17	958.1693	3.45935	32.5992	20.3859	0.8099	0.0851
40	1	3	18	1034.823	3.412014	73.3564	28.6087	0.9513	0.0209
40	0.83	1	19	1098.445	2.8844	19.1281	6.4826	0.9011	0.0376
40	0.83	2	20	1162.068	2.887443	64.6346	29.1275	0.9263	0.0313
40	0.83	3	21	1225.69	2.870486	35.0474	20.3473	0.8429	0.0602
40	0.66	1	22	1276.281	2.651079	61.856	28.3074	0.9312	0.0313
40	0.66	2	23	1326.873	2.839107	57.4792	30.4785	0.8298	0.069
40	0.66	3	24	1377.464	2.785543	42.3912	26.1678	0.8109	0.0773
40	0.49	1	25	1415.024	2.163493	56.1517	28.2674	0.9009	0.0429
40	0.49	2	26	1452.585	2.111593	51.7288	28.3655	0.89	0.0468
40	0.49	3	27	1490.145	2.295193	23.1599	8.9142	0.8924	0.0369
40	0.32	1	28	1514.674	1.75465	55.9479	31.176	0.8513	0.0649
40	0.32	2	29	1539.203	1.783964	53.4429	30.3767	0.8514	0.0646
40	0.32	3	30	1563.732	1.745214	53.3338	30.6464	0.8398	0.0682
70	0.79	1	31	1624.289	6.506057	77.0831	29.6504	0.9282	0.0283
70	0.79	2	32	1684.845	5.0259	49.4505	20.1898	0.9477	0.0242
70	0.79	3	33	1745.401	6.536979	97.367	27.0013	0.9225	0.0348
70	0.63	1	34	1793.693	5.04235	75.6431	31.7865	0.908	0.0406
70	0.63	2	35	1841.985	5.0521	74.589	32.8444	0.8976	0.0434
70	0.63	3	36	1890.276	4.505064	46.0104	21.0133	0.9333	0.0295
70	0.47	1	37	1926.304	3.751429	81.8249	30.4107	0.9306	0.0293
70	0.47	2	38	1962.331	3.547986	47.2302	27.093	0.835	0.0722
70	0.47	3	39	1998.358	3.389336	58.1711	28.1642	0.9146	0.0351
70	0.31	1	40	2022.12	3.027236	43.4873	28.8962	0.7554	0.1014
70	0.31	2	41	2045.883	2.573493	62.3756	30.7723	0.8782	0.0545
70	0.31	3	42	2069.646	2.681643	58.4532	30.3622	0.8737	0.0558
70	0.15	1	43	2081.144	1.758207	48.6087	31.8396	0.7462	0.0987
70	0.15	2	44	2092.642	1.692293	48.6453	31.4387	0.7737	0.0954
70	0.15	3	45	2104.14	1.83745	39.4355	29.1474	0.6785	0.1289
100	0.4	1	46	2134.801	6.696186	26.3566	17.8298	0.7967	0.0794
100	0.4	2	47	2165.463	6.508757	58.8378	31.5043	0.8644	0.0625
100	0.4	3	48	2196.124	6.120893	52.869	26.7578	0.9158	0.0384
100	0.315	1	49	2220.27	5.011457	55.1505	28.8766	0.8759	0.0542
100	0.315	2	50	2244.416	5.743014	53.4063	28.1759	0.8827	0.0525
100	0.315	3	51	2268.562	5.225079	62.1295	30.7703	0.8792	0.0549
100	0.23	1	52	2286.192	4.013893	46.8359	25.9023	0.8547	0.0613
100	0.23	2	53	2303.822	4.424657	52.9312	27.955	0.8644	0.0623
100	0.23	3	54	2321.453	4.059786	42.847	25.2951	0.8506	0.0644
100	0.145	1	55	2332.567	3.009921	38.769	28.2024	0.6833	0.1238
100	0.145	2	56	2343.682	3.129836	58.433	33.2484	0.8073	0.0815
100	0.145	3	57	2354.797	2.723236	30.3368	24.683	0.74	0.1022
100	0.06	1	58	2359.396	1.739021	42.4631	31.2443	0.6594	0.1363
100	0.06	2	59	2363.995	1.699414	42.0059	29.2385	0.6642	0.1333
100	0.06	3	60	2368.594	1.658679	43.2512	30.8114	0.6386	0.1328

Mouse 2a Vein

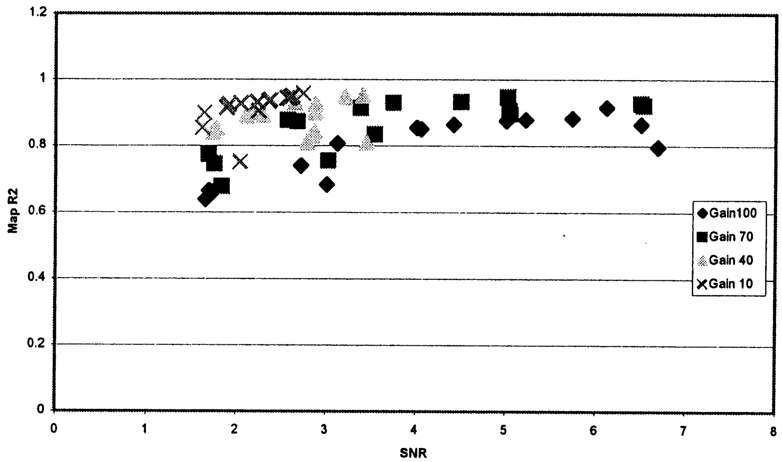

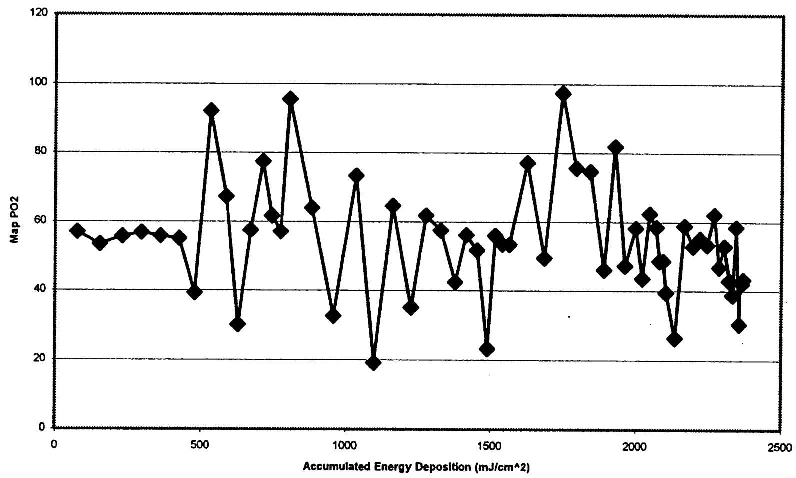

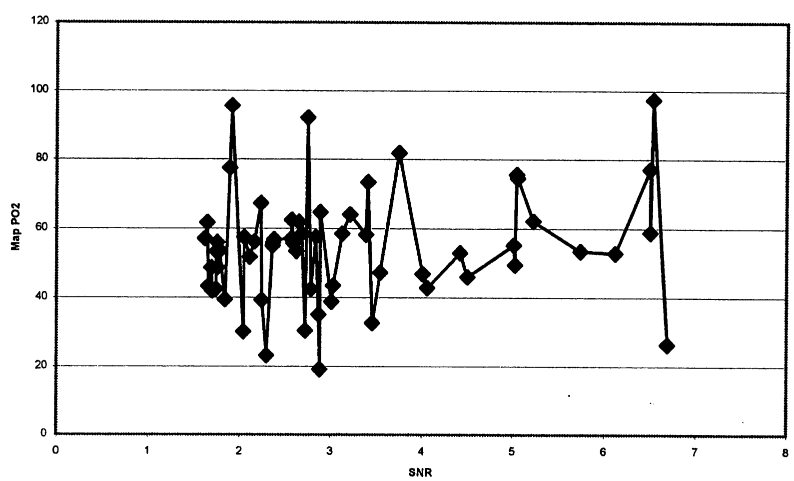

Gain	Exposure T	Relative Im	Cumulative	Accumulat	SNR	PO2 Mean	PO2 St. De	R2 Mean	R2 St. Dev
10	1	1	1	76.65354	1.963171	63.843	29.4655	0.9319	0.0334
10	1	2	2	153.3071	1.970014	61.5025	28.009	0.9319	0.0294
10	1	3	3	229.9606	1.980893	64.4603	28.7177	0.9297	0.0301
10	0.85	1	4	295.1161	1.826357	61.2324	28.6511	0.9138	0.0395
10	0.85	2	5	360.2717	1.757036	64.7109	31.0928	0.9145	0.0391
10	0.85	3	6	425.4272	1.749129	57.5263	28.2588	0.9024	0.042
10	0.7	1	7	479.0846	1.736929	47.6373	27.9232	0.8744	0.0516
10	0.7	2	8	532.7421	1.971564	75.9263	30.7795	0.926	0.0305
10	0.7	3	9	586.3996	1.8108	69.1917	30.4249	0.9097	0.0376
10	0.55	1	10	628.5591	1.656264	27.2656	18.3756	0.7847	0.0887
10	0.55	2	11	670.7185	1.727229	73.8256	29.2442	0.9187	0.0346
10	0.55	3	12	712.878	1.616386	72.7801	34.0154	0.8799	0.0496
10	0.4	1	13	743.5394	1.438093	61.8509	32.7413	0.8674	0.0558
10	0.4	2	14	774.2008	1.418757	52.8608	31.4433	0.8061	0.0821
10	0.4	3	15	804.8622	1.574	79.0714	30.4531	0.8867	0.047
40	1	1	16	881.5157	2.970529	72.7498	28.3305	0.9479	0.0251
40	1	2	17	958.1693	3.31735	38.8248	20.5448	0.8827	0.046
40	1	3	18	1034.823	3.251086	78.7902	28.1636	0.9528	0.0214
40	0.83	1	19	1098.445	2.882536	32.1917	11.8859	0.922	0.0301
40	0.83	2	20	1162.068	2.758043	73.5797	30.5994	0.9323	0.029
40	0.83	3	21	1225.69	2.793179	31.0872	13.675	0.8948	0.0421
40	0.66	1	22	1276.281	2.476057	72.8878	28.9564	0.9313	0.0293
40	0.66	2	23	1326.873	2.701136	60.6739	31.9878	0.8571	0.0593
40	0.66	3	24	1377.464	2.559514	41.5109	23.7744	0.8534	0.0597
40	0.49	1	25	1415.024	2.049921	67.8125	31.2995	0.9015	0.0413
40	0.49	2	26	1452.585	2.005021	58.3659	28.9462	0.8979	0.0445
40	0.49	3	27	1490.145	2.285964	54.8258	26.417	0.9069	0.0379
40	0.32	1	28	1514.674	1.694479	60.0485	30.9162	0.8642	0.0575
40	0.32	2	29	1539.203	1.694564	56.4628	30.6658	0.8574	0.0563
40	0.32	3	30	1563.732	1.689943	59.1837	31.2848	0.8521	0.0619
70	0.79	1	31	1624.289	5.278986	49.3071	21.111	0.9478	0.0222
70	0.79	2	32	1684.845	4.63985	59.0976	25.6647	0.9487	0.0223
70	0.79	3	33	1745.401	5.590479	99.3124	29.9255	0.9209	0.0336
70	0.63	1	34	1793.693	4.368914	77.0465	30.174	0.9046	0.0406
70	0.63	2	35	1841.985	4.506579	80.8483	28.67	0.909	0.0376
70	0.63	3	36	1890.276	4.006829	55.9467	25.4203	0.9319	0.0305
70	0.47	1	37	1926.304	3.316593	79.7966	30.2494	0.9221	0.0347
70	0.47	2	38	1962.331	3.213107	52.5233	28.9354	0.8488	0.0645
70	0.47	3	39	1998.358	3.17635	68.4994	31.7135	0.9181	0.0341
70	0.31	1	40	2022.12	2.529514	47.124	29.2947	0.803	0.0815
70	0.31	2	41	2045.883	2.369407	61.8032	29.3746	0.8747	0.0538
70	0.31	3	42	2069.646	2.376586	65.2965	32.5831	0.8657	0.0531
70	0.15	1	43	2081.144	1.650186	49.8913	31.4153	0.7378	0.1028
70	0.15	2	44	2092.642	1.613364	51.4848	31.0505	0.769	0.0927
70	0.15	3	45	2104.14	1.696336	43.5997	29.3534	0.6996	0.1236
100	0.4	1	46	2134.801	5.40435	28.3451	17.7348	0.8587	0.0608
100	0.4	2	47	2165.463	5.701907	60.764	30.1634	0.8687	0.0562
100	0.4	3	48	2196.124	5.4807	60.1958	29.8244	0.9133	0.0391
100	0.315	1	49	2220.27	4.58965	62.6501	29.3963	0.8648	0.0601
100	0.315	2	50	2244.416	4.936957	55.0361	2930209	0.8781	0.0504
100	0.315	3	51	2268.562	4.734857	62.9092	32.8323	0.8807	0.0518
100	0.23	1	52	2286.192	3.632279	53.7823	28.3964	0.8548	0.0645
100	0.23	2	53	2303.822	4.102021	65.5374	32.4188	0.8657	0.0587
100	0.23	3	54	2321.453	3.645779	48.3405	27.1014	0.8537	0.0637
100	0.145	1	55	2332.567	2.694007	42.7271	30.2718	0.7046	0.121
100	0.145	2	56	2343.682	2.780236	58.3201	32.3686	0.8011	0.0831
100	0.145	3	57	2354.797	2.507897	34.3168	23.7818	0.7796	0.0878
100	0.06	1	58	2359.396	1.62135	44.0424	32.2331	0.6346	0.1314
100	0.06	2	59	2363.995	1.6164	47.7245	33.0723	0.6695	0.1414
100	0.06	3	60	2368.594	1.578414	44.4237	31.7052	0.6199	0.1388

Mouse 2a Artery

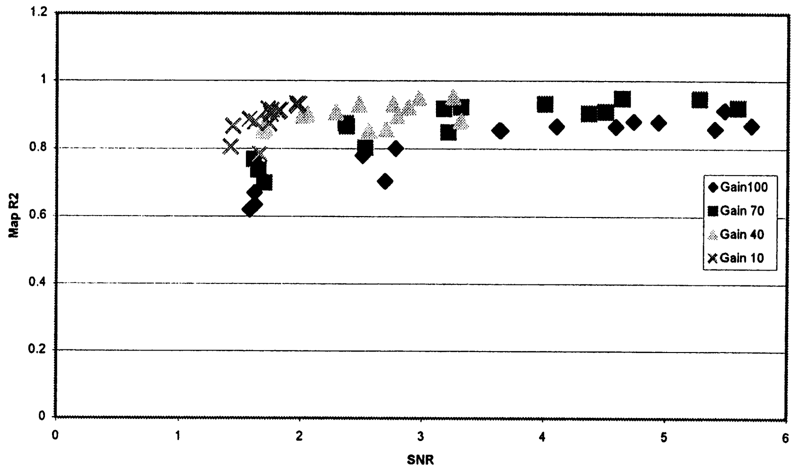

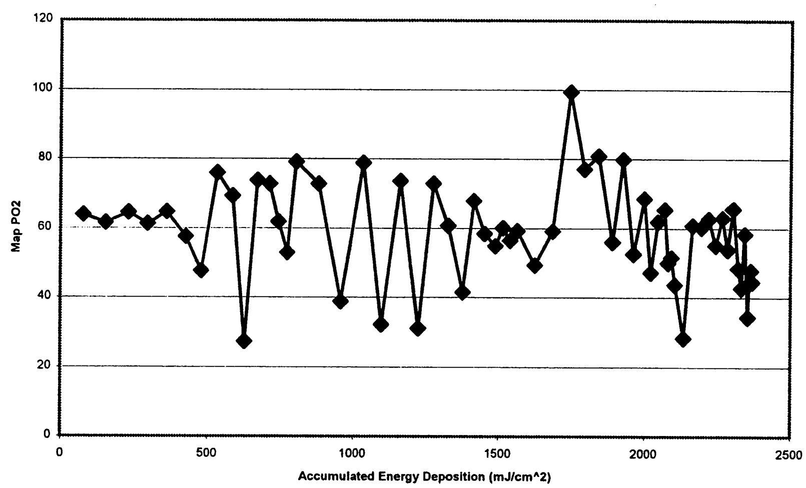

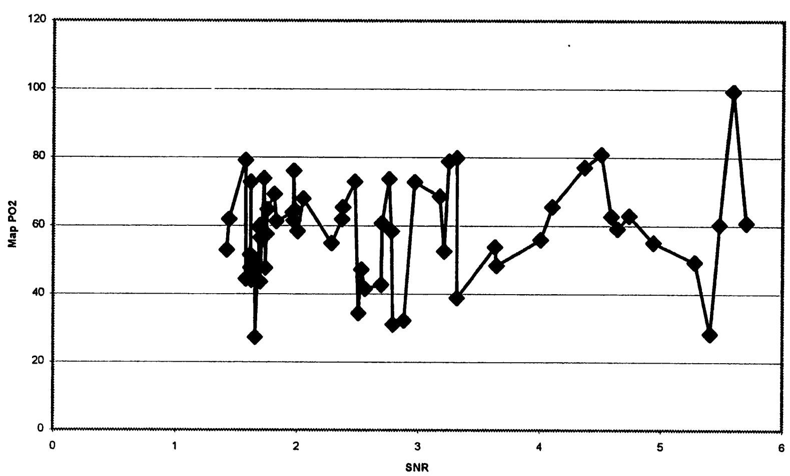

Gain	Exposure T	Relative In	Cumulative	Accumulat	SNR	PO2 Mean	PO2 St. De	R2 Mean	R2 St. Dev
10	1	1	1	76.65354	1.458314	76.3928	30.9213	0.8919	0.00473
10	1	2	2	153.3071	1.528507	72.135	30.5176	0.9012	0.0432
10	1	3	3	229.9606	1.4857	73.9111	30.829	0.8955	0.0461
10	0.85	1	4	295.1161	1.425407	72.9266	31.6653	0.8771	0.0541
10	0.85	2	5	360.2717	1.432193	73.0667	32.1045	0.8766	0.0542
10	0.85	3	6	425.4272	1.418893	74.2351	32.7031	0.8701	0.0516
10	0.7	1	7	479.0846	1.385064	65.1099	32.3446	0.8306	0.0722
10	0.7	2	8	532.7421	1.4625	80.9474	32.5748	0.8851	0.0501
10	0.7	3	9	586.3996	1.408657	69.6301	31.3032	0.8632	0.055
10	0.55	1	10	628.5591	1.342364	53.9505	32.1208	0.768	0.0982
10	0.55	2	11	670.7185	1.341036	66.7429	32.5805	0.8476	0.0625
10	0.55	3	12	712.878	1.338143	70.899	33.1039	0.8324	0.0706
10	0.4	1	13	743.5394	1.2339	59.7068	33.1784	0.7763	0.0936
10	0.4	2	14	774.2008	1.233364	59.2788	35.4172	0.7465	0.1072
10	0.4	3	15	804.8622	1.260157	68.7388	35.0929	0.788	0.0875
40	1	1	16	881.5157	1.973564	73.4267	31.1712	0.9035	0.0414
40	1	2	17	958.1693	2.041386	57.9837	29.3012	0.8502	0.063
40	1	3	18	1034.823	2.030379	73.7586	33.0437	0.9045	0.0408
40	0.83	1	19	1098.445	1.871243	47.8317	26.6129	0.8726	0.0511
40	0.83	2	20	1162.068	1.813829	67.9583	32.4025	0.876	0.0549
40	0.83	3	21	1225.69	1.8553	55.6266	31.0701	0.8505	0.0635
40	0.66	1	22	1276.281	1.704507	63.7792	32.1048	0.8665	0.0602
40	0.66	2	23	1326.873	1.744179	58.1461	33.0262	0.8035	0.0797
40	0.66	3	24	1377.464	1.743043	52.1219	30.1629	0.8087	0.079
40	0.49	1	25	1415.024	1.527579	55.7974	30.0914	0.8285	0.0722
40	0.49	2	26	1452.585	1.515957	56.6199	31.4221	0.8242	0.0715
40	0.49	3	27	1490.145	1.552579	53.8295	30.9495	0.837	0.0671
40	0.32	1	28	1514.674	1.3469	54.9296	32.7953	0.741	0.1092
40	0.32	2	29	1539.203	1.343586	51.4345	32.2577	0.7337	0.1009
40	0.32	3	30	1563.732	1.341079	53.6587	30.4489	0.736	0.1046
70	0.79	1	31	1624.289	3.025286	67.0569	30.7179	0.9028	0.0422
70	0.79	2	32	1684.845	2.907457	66.2741	31.2845	0.9138	0.0381
70	0.79	3	33	1745.401	3.0976	79.9557	32.3169	0.8809	0.0527
70	0.63	1	34	1793.693	2.528907	68.7506	32.7587	0.8599	0.059
70	0.63	2	35	1841.985	2.55015	65.4942	31.425	0.8523	0.0628
70	0.63	3	36	1890.276	2.532071	60.7547	30.0403	0.8806	0.0507
70	0.47	1	37	1926.304	2.212671	71.8664	32.8475	0.8668	0.0585
70	0.47	2	38	1962.331	2.115721	56.0456	31.7302	0.8301	0.0809
70	0.47	3	39	1998.358	2.142029	62.2864	32.1192	0.8487	0.0663
70	0.31	1	40	2022.12	1.754457	50.5175	31.5392	0.7311	0.1123
70	0.31	2	41	2045.883	1.691764	60.5259	33.6843	0.7869	0.0893
70	0.31	3	42	2069.646	1.761607	57.801	34.1796	0.7924	0.083
70	0.15	1	43	2081.144	1.372336	45.7276	31.9532	0.6251	0.1445
70	0.15	2	44	2092.642	1.356721	47.9529	32.5211	0.6658	0.1317
70	0.15	3	45	2104.14	1.3727	39.705	29.694	0.5985	0.1459
100	0.4	1	46	2134.801	3.364136	50.3808	31.2987	0.8062	0.0806
100	0.4	2	47	2165.463	3.642829	59.9986	31.8627	0.8117	0.0779
100	0.4	3	48	2196.124	3.486771	57.308	31.9603	0.8542	0.0648
100	0.315	1	49	2220.27	3.088614	63.5282	33.3704	0.8213	0.077
100	0.315	2	50	2244.416	3.073864	56.2492	31.0567	0.8118	0.0764
100	0.315	3	51	2268.562	2.944579	59.8996	33.8895	0.8104	0.0853
100	0.23	1	52	2286.192	2.46305	52.3167	30.5387	0.783	0.0926
100	0.23	2	53	2303.822	2.66165	59.384	31.3286	0.7951	0.086
100	0.23	3	54	2321.453	2.466729	53.065	33.5954	0.7645	0.0954
100	0.145	1	55	2332.567	1.982157	44.0428	32.8061	0.6381	0.141
100	0.145	2	56	2343.682	2.014993	53.622	34.9182	0.7178	0.1083
100	0.145	3	57	2354.797	1.903579	37.0593	26.1343	0.6766	0.1272
100	0.06	1	58	2359.396	1.350243	38.4301	31.0432	0.5496	0.1516
100	0.06	2	59	2363.995	1.360879	41.3349	32.6684	0.5525	0.1582
100	0.06	3	60	2368.594	1.350971	43.8024	32.0532	0.5309	0.1724

Mouse 2a Tissue

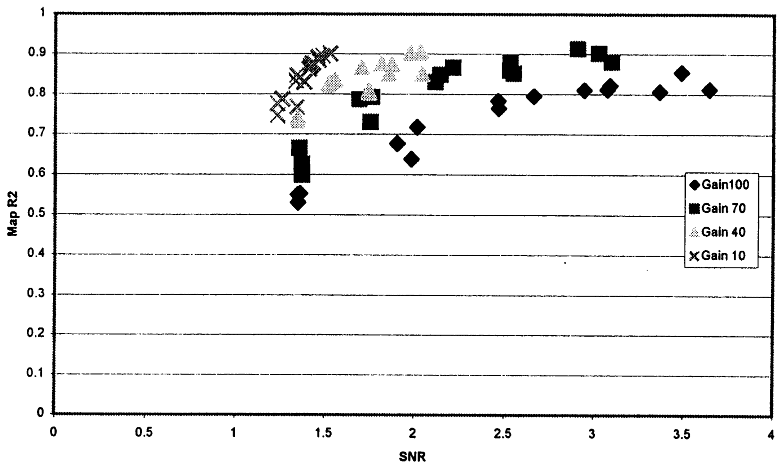

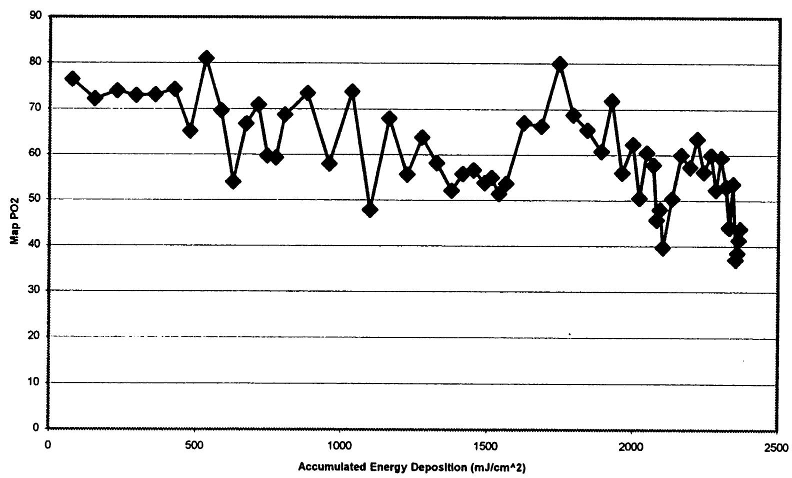

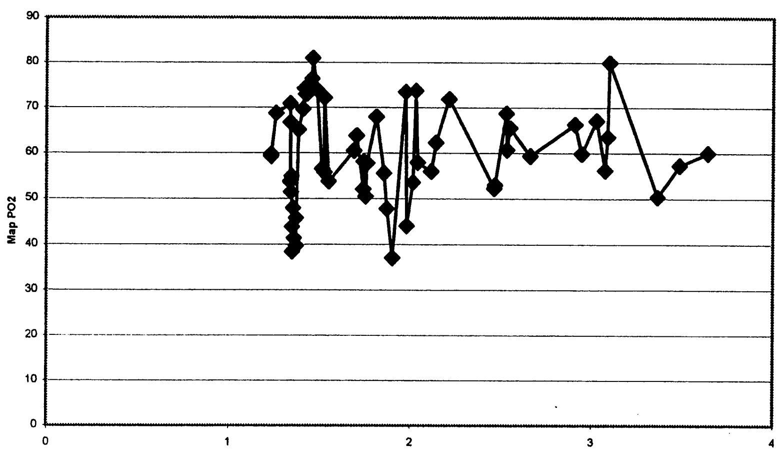

Gain	Exposure T	Relative Im	Cumulative	Accumulat	SNR	PO2 Mean	PO2 St. De	R2 Mean	R2 St. Dev
70	0.15	1	1	11.85236	2.185829	47.9307	28.7675	0.8441	0.0675
70	0.15	2	2	23.70472	2.203107	50.3199	29.1613	0.8485	0.0655
70	0.15	3	3	35.55709	2.183993	51.9934	29.5881	0.8393	0.0679
70	0.31	1	4	60.05197	3.522743	51.2359	23.7558	0.9156	0.0361
70	0.31	2	5	84.54685	3.504614	54.5836	27.2998	0.9149	0.0355
70	0.31	3	6	109.0417	3.442257	55.2661	28.412	0.9112	0.0388
70	0.47	1	7	146.1791	4.821871	55.5287	25.3589	0.9424	0.025
70	0.47	2	8	183.3165	4.770214	55.8252	25.549	0.937	0.028
70	0.47	3	9	220.4539	4.634579	54.9351	25.2639	0.9387	0.0272
70	0.63	1	10	270.2339	5.851957	52.6345	22.5959	0.951	0.0211
70	0.63	2	11	320.0138	5.812757	58.4187	24.7065	0.9509	0.0222
70	0.63	3	12	369.7937	5.872314	54.5329	23.8966	0.9528	0.0207
70	0.79	1	13	432.2161	6.919107	54.0441	20.5884	0.9616	0.0163
70	0.79	2	14	494.6386	6.919114	55.192	22.6778	0.9623	0.0166
70	0.79	3	15	557.061	6.717521	58.7159	22.7817	0.9606	0.0172
10	0.4	1	16	588.6673	1.706557	51.3835	27.1548	0.8885	0.0478
10	0.4	2	17	620.2736	1.680679	57.3794	30.7194	0.889	0.0459
10	0.4	3	18	651.8799	1.664493	53.279	29.6827	0.8823	0.0509
10	0.55	1	19	695.3386	1.92815	56.0958	28.1527	0.9089	0.0403
10	0.55	2	20	738.7972	1.899471	57.1476	28.0226	0.9081	0.0394
10	0.55	3	21	782.2559	1.873829	56.9709	27.4311	0.909	0.0407
10	0.7	1	22	837.5669	2.088164	59.828	28.8603	0.9246	0.0325
10	0.7	2	23	892.878	2.122993	56.3792	25.677	0.9267	0.0318
10	0.7	3	24	948.189	2.067364	56.3792	26.0962	0.9254	0.0325
10	0.85	1	25	1015.352	2.277836	60.9353	26.1129	0.9359	0.0279
10	0.85	2	26	1082.516	2.234364	57.9947	25.8706	0.9339	0.0276
10	0.85	3	27	1149.679	2.245657	59.9621	28.2941	0.9355	0.0282
10	1	1	28	1228.695	2.467307	59.5544	24.8666	0.9458	0.0242
10	1	2	29	1307.711	2.499221	62.7205	27.5507	0.9435	0.0251
10	1	3	30	1386.726	2.452829	61.9379	28.1479	0.9442	0.0249
100	0.06	1	31	1391.467	1.819057	43.8867	27.9793	0.6734	0.1241
100	0.06	2	32	1396.208	1.795079	44.7178	31.1779	0.6854	0.1178
100	0.06	3	33	1400.949	1.743571	41.9367	31.4977	0.6821	0.1249
100	0.145	1	34	1412.406	3.050093	55.7372	31.0853	0.8224	0.0743
100	0.145	2	35	1423.864	3.024393	52.9883	31.7841	0.8181	0.0785
100	0.145	3	36	1435.321	2.984279	55.9265	32.2057	0.8166	0.0796
100	0.23	1	37	1453.495	4.213486	59.1371	30.6578	0.8732	0.0526
100	0.23	2	38	1471.668	4.210864	55.058	28.6067	0.8693	0.0568
100	0.23	3	39	1489.842	4.143693	58.0294	29.7669	0.8655	0.0595
100	0.4	1	40	1521.448	6.467607	60.2619	28.5224	0.9195	0.0339
100	0.4	2	41	1553.055	6.645643	59.8131	29.5968	0.9224	0.0315
100	0.4	3	42	1584.661	6.408	61.0283	28.4155	0.9192	0.0343
40	0.32	1	43	1609.946	1.810236	59.0438	30.6342	0.8695	0.0546
40	0.32	2	44	1635.231	1.779579	55.081	30.8622	0.8646	0.0564
40	0.32	3	45	1660.516	1.805307	58.2978	29.7072	0.8596	0.0584
40	0.49	1	46	1699.234	2.197093	59.7527	29.3753	0.8972	0.0443
40	0.49	2	47	1737.951	2.191464	58.2904	30.1162	0.8955	0.0455
40	0.49	3	48	1776.669	2.348507	52.6866	27.7137	0.8911	0.047
40	0.66	1	49	1828.819	2.736057	58.9415	25.6724	0.9429	0.0245
40	0.66	2	50	1880.97	2.530343	63.2393	29.452	0.9229	0.0335
40	0.66	3	51	1933.12	2.504579	63.169	29.4751	0.9198	0.0347
40	0.83	1	52	1998.703	2.964393	61.4156	27.2456	0.9353	0.0281
40	0.83	2	53	2064.286	2.998536	60.5353	26.5314	0.9323	0.0299
40	0.83	3	54	2129.869	2.974129	57.8912	26.9543	0.9355	0.0283
40	1	1	55	2208.885	3.334679	59.3173	26.1898	0.9434	0.0243
40	1	2	56	2287.901	3.379264	66.2786	27.7106	0.9447	0.0247
40	1	3	57	2366.917	3.382593	60.0479	26.8645	0.9429	0.0254

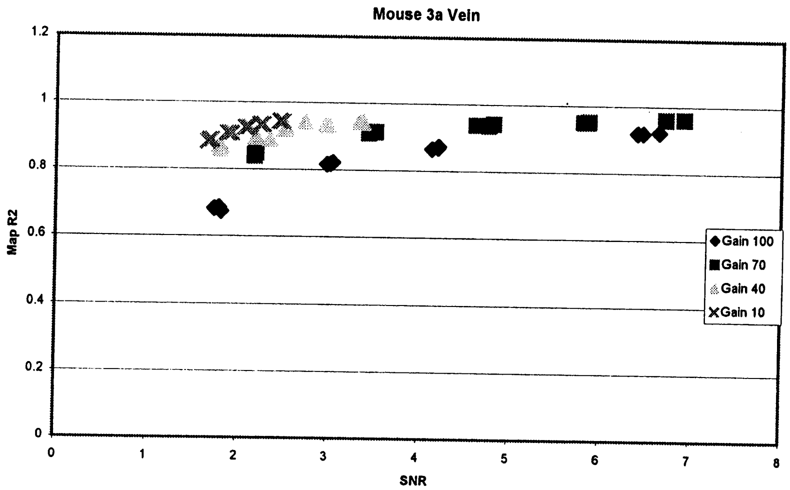
Mouse 3a Vein
Map R2
SNR
Gain 100
Gain 70
Gain 40
Gain 10
1.2
1
0.8
0.6
0.4
0.2
0
0
1
2
3
4
5
6
7
8

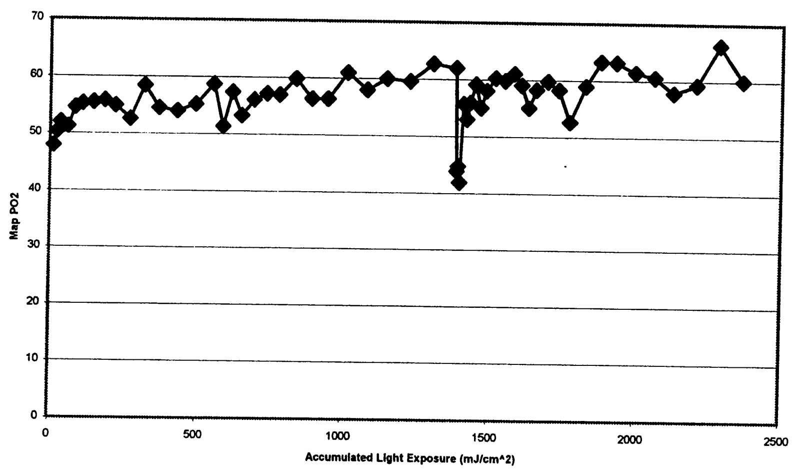
Map PO2
Accumulated Light Exposure (mJ/cm^2)
70
60
50
40
30
20
10
0
0
500
1000
1500
2000
2500

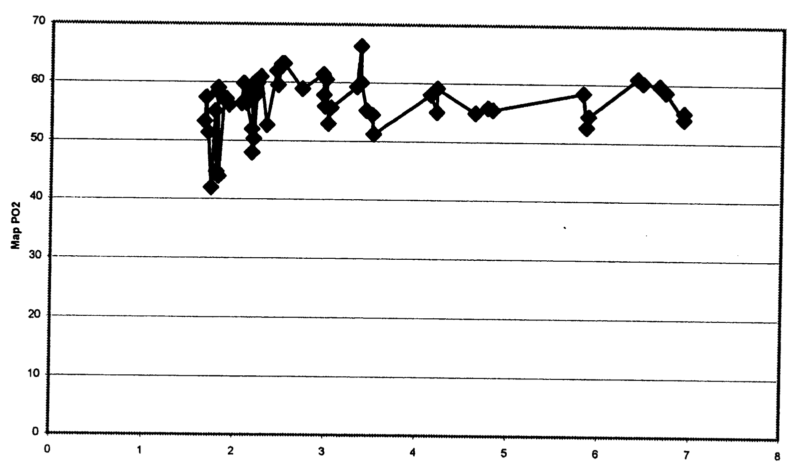
Map PO2
SNR
70
60
50
40
30
20
10
0
0
1
2
3
4
5
6
7
8

Gain	Exposure T	Relative Im	Cumulative	Accumulat	SNR	PO2 Mean	PO2 St. De	R2 Mean	R2 St. Dev
70	0.15	1	1	11.85236	1.603657	53.1055	31.2113	0.7796	0.0958
70	0.15	2	2	23.70472	1.595314	50.7682	31.4954	0.7855	0.0855
70	0.15	3	3	35.55709	1.596586	51.7846	31.5816	0.7755	0.0926
70	0.31	1	4	60.05197	2.254757	58.2223	30.8665	0.8733	0.0533
70	0.31	2	5	84.54685	2.304921	56.7583	31.9849	0.8764	0.0506
70	0.31	3	6	109.0417	2.263214	60.7205	32.3248	0.8716	0.0539
70	0.47	1	7	146.1791	2.948257	62.5186	28.8582	0.9135	0.0357
70	0.47	2	8	183.3165	2.997514	63.8171	28.6885	0.9109	0.0378
70	0.47	3	9	220.4539	2.959307	58.8974	27.8418	0.9704	0.0394
70	0.63	1	10	270.2339	3.504579	65.4751	27.5211	0.9207	0.0336
70	0.63	2	11	320.0138	3.58575	64.0734	29.6804	0.9274	0.031
70	0.63	3	12	369.7937	3.476564	64.9139	28.3856	0.9236	0.035
70	0.79	1	13	432.2161	4.185393	65.2427	26.7321	0.9431	0.0242
70	0.79	2	14	494.6386	4.155964	71.8692	29.7798	0.9411	0.0255
70	0.79	3	15	557.061	4.1066	68.9786	28.9941	0.9386	0.0264
10	0.4	1	16	588.6673	1.405007	56.9862	30.383	0.8439	0.0667
10	0.4	2	17	620.2736	1.404493	63.1363	33.5966	0.8376	0.0703
10	0.4	3	18	651.8799	1.384143	58.1358	32.4402	0.8272	0.0752
10	0.55	1	19	695.3386	1.550057	56.6854	28.6073	0.8759	0.0512
10	0.55	2	20	738.7972	1.531629	60.6583	30.9949	0.8671	0.0597
10	0.55	3	21	782.2559	1.538971	59.6844	30.2792	0.8735	0.0544
10	0.7	1	22	837.5669	1.643686	59.6811	29.8847	0.89	0.0483
10	0.7	2	23	892.878	1.665157	65.9298	30.6777	0.8948	0.0455
10	0.7	3	24	948.189	1.662371	61.7208	28.3624	0.8953	0.0462
10	0.85	1	25	1015.352	1.848643	68.5813	31.0531	0.9189	0.0346
10	0.85	2	26	1082.516	1.782129	62.3568	28.7479	0.9066	0.0421
10	0.85	3	27	1149.679	1.729321	64.6265	30.2779	0.9024	0.0443
10	1	1	28	1228.695	1.859807	67.7337	30.3843	0.9136	0.0379
10	1	2	29	1307.711	1.92155	65.8236	29.9062	0.9166	0.0363
10	1	3	30	1386.726	1.9013	69.2661	30.9281	0.9178	0.0364
100	0.06	1	31	1391.467	1.5174	43.5161	33.4359	0.6218	0.142
100	0.06	2	32	1396.208	1.462521	42.4348	32.1801	0.6088	0.152
100	0.06	3	33	1400.949	1.516171	46.245	30.5128	0.6297	0.1435
100	0.145	1	34	1412.406	2.273757	54.7378	32.7368	0.7662	0.1007
100	0.145	2	35	1423.864	2.257286	50.1788	30.7761	0.762	0.0972
100	0.145	3	36	1435.321	2.236279	53.8048	33.1385	0.7456	0.1092
100	0.23	1	37	1453.495	3.01475	55.2714	31.0975	0.8242	0.0734
100	0.23	2	38	1471.668	2.9164	57.8654	32.2111	0.8114	0.0806
100	0.23	3	39	1489.842	3.1197	60.2691	33.0445	0.8338	0.0721
100	0.4	1	40	1521.448	4.712071	61.2496	29.8165	0.8912	0.0443
100	0.4	2	41	1553.055	4.688257	61.2809	28.1974	0.8961	0.0454
100	0.4	3	42	1584.661	4.473707	63.6176	31.8991	0.8852	0.0487
40	0.32	1	43	1609.946	1.5368	55.4042	29.0272	0.8246	0.0734
40	0.32	2	44	1635.231	1.517071	53.8511	31.9076	0.8132	0.0785
40	0.32	3	45	1660.516	1.516057	54.6924	32.7898	0.8088	0.0804
40	0.49	1	46	1699.234	1.842079	59.6334	31.9336	0.8737	0.0535
40	0.49	2	47	1737.951	1.819757	56.709	30.7449	0.8594	0.0594
40	0.49	3	48	1776.669	1.851507	57.1019	30.4113	0.8525	0.0635
40	0.66	1	49	1828.819	2.104943	64.9133	30.0657	0.9138	0.037
40	0.66	2	50	1880.97	1.967729	64.18	31.5324	0.8841	0.0487
40	0.66	3	51	1933.12	1.986479	63.6933	29.7067	0.8922	0.046
40	0.83	1	52	1998.703	2.272907	64.8441	31.9518	0.9041	0.0425
40	0.83	2	53	2064.286	2.276714	62.4749	29.1944	0.9025	0.0439
40	0.83	3	54	2129.869	2.2759	62.9329	29.8147	0.9051	0.0418
40	1	1	55	2208.885	2.541343	66.0281	30.1749	0.9158	0.0359
40	1	2	56	2287.901	2.591857	67.9619	30.1246	0.9169	0.0369
40	1	3	57	2366.917	2.536957	61.9198	29.6126	0.9075	0.0394

Mouse 3a Artery

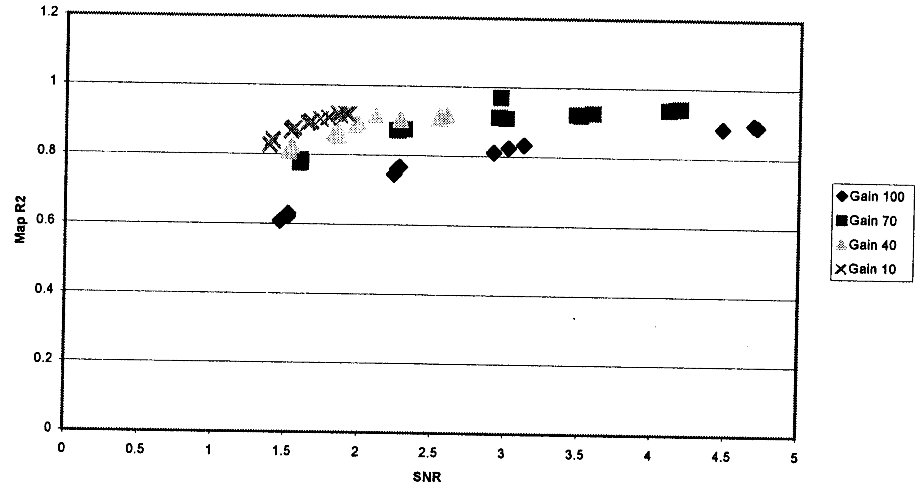

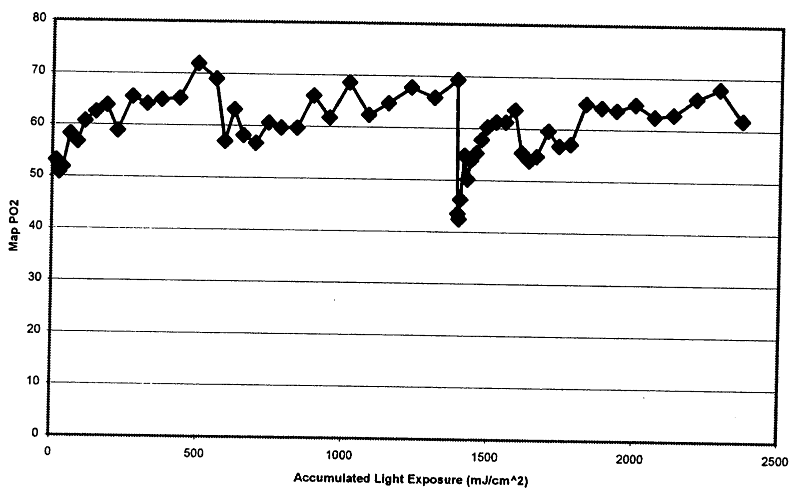

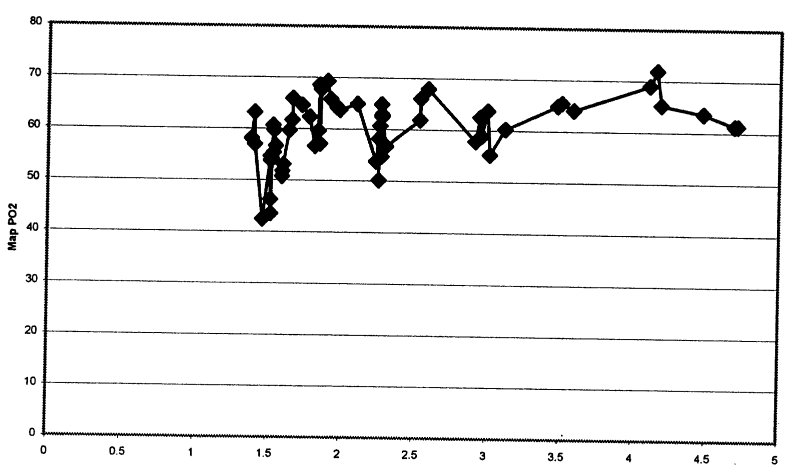

Gain	Exposure T	Relative Im	Cumulative	Accumulate	SNR	PO2 Mean	PO2 St. De	R2 Mean	R2 St. Dev
70	0.15	1	1	11.85236	1.310557	52.903	32.7733	0.7325	0.1041
70	0.15	2	2	23.70472	1.324557	55.8798	33.4164	0.7383	0.1113
70	0.15	3	3	35.55709	1.320429	60.6626	35.1454	0.7451	0.1041
70	0.31	1	4	60.05197	1.643371	64.7687	31.651	0.8305	0.0709
70	0.31	2	5	84.54685	1.698507	63.0644	32.4378	0.8325	0.0693
70	0.31	3	6	109.0417	1.743021	66.3737	32.445	0.8339	0.0721
70	0.47	1	7	146.1791	2.102364	68.5863	31.1614	0.8761	0.0053
70	0.47	2	8	183.3165	2.100821	72.3793	33.37	0.8765	0.053
70	0.47	3	9	220.4539	2.101557	68.7853	32.0801	0.8714	0.0561
70	0.63	1	10	270.2339	2.458307	74.2449	33.1039	0.8971	0.0459
70	0.63	2	11	320.0138	2.445171	73.4923	31.9805	0.926	0.0455
70	0.63	3	12	369.7937	2.480829	71.4642	31.3944	0.8985	0.0429
70	0.79	1	13	432.2161	2.866643	74.2537	30.2499	0.9163	0.0358
70	0.79	2	14	494.6386	2.979636	73.9385	30.8788	0.9173	0.0347
70	0.79	3	15	557.061	2.962064	72.0386	31.386	0.9186	0.0364
10	0.4	1	16	588.6673	1.2354	54.6041	33.4098	0.761	0.0981
10	0.4	2	17	620.2736	1.255164	57.0198	32.832	0.7526	0.101
10	0.4	3	18	651.8799	1.253093	55.4233	31.7813	0.7566	0.1024
10	0.55	1	19	695.3386	1.325571	59.1534	31.5551	0.8139	0.0768
10	0.55	2	20	738.7972	1.351636	60.8962	31.6401	0.8194	0.0778
10	0.55	3	21	782.2559	1.341893	58.8365	31.8688	0.8158	0.0784
10	0.7	1	22	837.5669	1.407286	64.6885	32.5044	0.8465	0.0683
10	0.7	2	23	892.878	1.425021	63.0371	31.3605	0.8538	0.0644
10	0.7	3	24	948.189	1.43875	65.7123	32.9903	0.8542	0.0602
10	0.85	1	25	1015.352	1.562129	67.5597	31.6752	0.8808	0.0505
10	0.85	2	26	1082.516	1.560307	66.0256	32.2798	0.8818	0.0505
10	0.85	3	27	1149.679	1.526779	64.5031	32.0364	0.8777	0.0518
10	1	1	28	1228.695	1.638779	69.8933	31.6102	0.8929	0.0466
10	1	2	29	1307.711	1.620521	68.056	32.4237	0.8904	0.0461
10	1	3	30	1386.726	1.658779	70.8272	31.4441	0.8964	0.0466
100	0.06	1	31	1391.467	1.365521	42.9322	32.6854	0.5683	0.153
100	0.06	2	32	1396.208	1.370479	46.0459	33.9414	0.5821	0.1439
100	0.06	3	33	1400.949	1.362493	43.235	31.5879	0.5802	0.1514
100	0.145	1	34	1412.406	1.947371	49.2172	31.9046	0.7268	0.1141
100	0.145	2	35	1423.864	1.9242	51.8969	32.2806	0.7089	0.1152
100	0.145	3	36	1435.321	1.915043	52.0852	35.4292	0.707	0.119
100	0.23	1	37	1453.495	2.527536	60.3997	34.5744	0.7999	0.0849
100	0.23	2	38	1471.668	2.501343	59.5653	32.4009	0.7986	0.0858
100	0.23	3	39	1489.842	2.583586	55.7673	31.8721	0.7961	0.0854
100	0.4	1	40	1521.448	3.634471	66.2506	33.1174	0.8635	0.0569
100	0.4	2	41	1553.055	3.749493	65.1519	32.4157	0.8652	0.0586
100	0.4	3	42	1584.661	3.613557	68.0268	32.1029	0.8637	0.0585
40	0.32	1	43	1609.946	1.011307	58.0296	32.3314	0.7945	0.0873
40	0.32	2	44	1635.231	1.441707	57.2084	31.2016	0.8001	0.0813
40	0.32	3	45	1660.516	1.3989	60.5947	34.1484	0.7843	0.0896
40	0.49	1	46	1699.234	1.5879	60.3772	30.8028	0.8415	0.068
40	0.49	2	47	1737.951	1.6362	62.6073	32.5153	0.8356	0.0701
40	0.49	3	48	1776.669	1.605014	56.3085	32.3405	0.8229	0.0779
40	0.66	1	49	1828.819	1.829336	67.8949	31.4686	0.8824	0.0516
40	0.66	2	50	1880.97	1.801843	63.456	33.6456	0.8671	0.0551
40	0.66	3	51	1933.12	1.762843	64.4078	31.5356	0.8596	0.0608
40	0.83	1	52	1998.703	1.753671	65.5881	30.644	0.8888	0.0471
40	0.83	2	53	2064.286	1.9844	64.5773	30.0431	0.8877	0.0484
40	0.83	3	54	2129.869	1.97485	63.604	30.9199	0.8802	0.0508
40	1	1	55	2208.885	2.114571	64.4976	30.0008	0.8899	0.0459
40	1	2	56	2287.901	2.177929	68.3007	32.2907	0.8966	0.0443
40	1	3	57	2366.917	2.23995	64.4078	30.7988	0.8945	0.0461

Mouse 3a Tissue

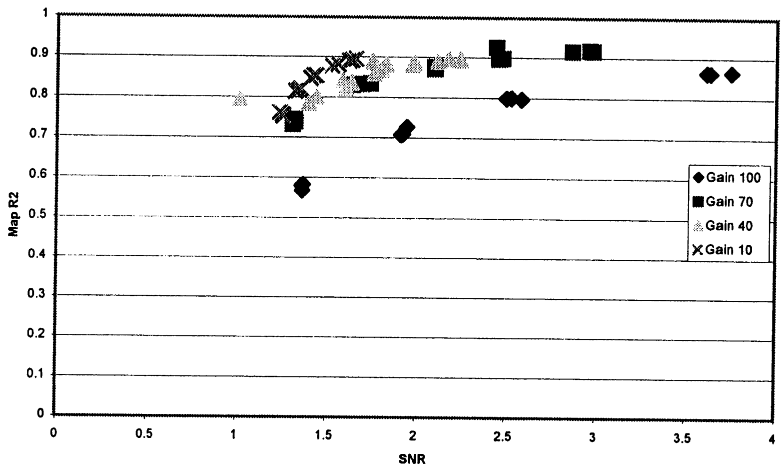

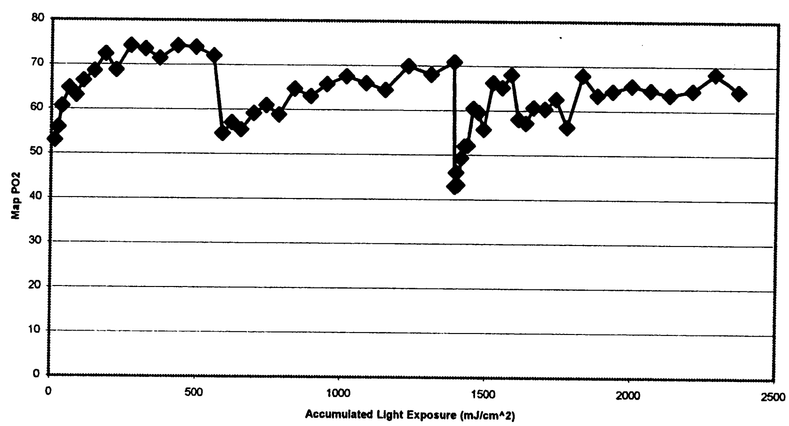

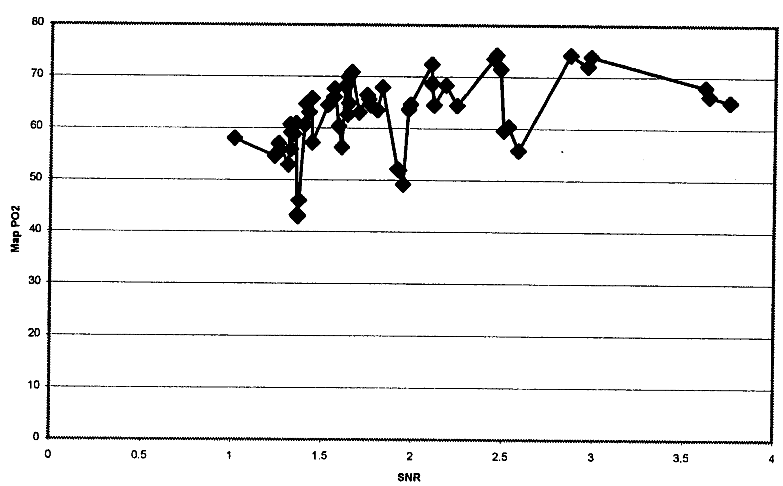

Gain	Exposure T	Relative Ir	Cumulative	Accumulat	SNR	PO2 Mean	PO2 St. De	R2 Mean	R2 St. Dev
10	0.4	1	1	29.83465	1.248415	54.2929	31.954	0.7545	0.1028
10	0.4	2	2	59.66929	1.258496	59.3012	32.9182	0.755	0.1012
10	0.4	3	3	89.50394	1.266393	61.4194	33.1379	0.768	0.0946
10	0.55	1	4	130.5266	1.349896	64.5087	32.7688	0.8357	0.0656
10	0.55	2	5	171.5492	1.338126	61.4447	31.6342	0.8213	0.0756
10	0.55	3	6	212.5719	1.353993	65.0657	31.7011	0.8316	0.0697
10	0.7	1	7	264.7825	1.428726	67.2662	33.2668	0.8621	0.059
10	0.7	2	8	316.9931	1.4462	67.5801	27.97	0.8697	0.058
10	0.7	3	9	369.2037	1.446259	70.3787	32.3974	0.8699	0.0542
10	0.85	1	10	432.6024	1.531704	70.1708	33.1687	0.8846	0.0498
10	0.85	2	11	496.001	1.522459	71.0868	32.7576	0.8849	0.0503
10	0.85	3	12	559.3996	1.550452	73.073	31.784	0.8865	0.051
10	1	1	13	633.9862	1.645319	76.4273	31.1483	0.9068	0.0409
10	1	2	14	708.5728	1.664059	78.4581	31.0013	0.9106	0.038
10	1	3	15	783.1594	1.674585	74.9484	31.3675	0.9122	0.0368
40	0.32	1	16	807.0272	1.422963	65.6925	32.1986	0.8232	0.0734
40	0.32	2	17	830.8949	1.416637	62.6822	32.652	0.8156	0.0768
40	0.32	3	18	854.7626	1.439726	67.3019	34.8399	0.8275	0.0726
40	0.49	1	19	891.31	1.639674	72.368	32.241	0.8789	0.0518
40	0.49	2	20	927.8575	1.626193	69.3753	31.945	0.8736	0.0531
40	0.49	3	21	964.4049	1.653133	75.0447	32.765	0.8821	0.0497
40	0.66	1	22	1013.632	1.837407	75.0644	30.7912	0.8997	0.044
40	0.66	2	23	1062.859	1.833711	72.127	31.1546	0.8985	0.0436
40	0.66	3	24	1112.086	1.831637	73.4233	31.4555	0.8977	0.0437
40	0.83	1	25	1173.993	2.069674	76.7009	30.8673	0.9166	0.0358
40	0.83	2	26	1235.9	2.056133	76.2951	31.5576	0.9187	0.0363
40	0.83	3	27	1297.807	2.079252	80.3291	30.7684	0.9197	0.0358
40	1	1	28	1372.394	2.259015	81.4934	30.4663	0.9327	0.0299
40	1	2	29	1446.98	2.267148	85.0689	29.602	0.9303	0.0309
40	1	3	30	1521.567	2.2616	82.2324	31.2938	0.9283	0.0314
70	0.15	1	31	1532.755	1.406711	59.3934	34.1476	0.7505	0.1029
70	0.15	2	32	1543.943	1.409481	59.3854	33.4786	0.7586	0.0997
70	0.15	3	33	1555.131	1.399504	54.8251	33.0757	0.7461	0.1022
70	0.31	1	34	1578.253	1.776459	67.2759	31.9246	0.842	0.0668
70	0.31	2	35	1601.375	1.815815	66.481	33.2796	0.8452	0.0651
70	0.31	3	36	1624.496	1.774333	66.2977	33.0188	0.8412	0.0665
70	0.47	1	37	1659.552	2.200267	74.4833	32.3745	0.8887	0.0473
70	0.47	2	38	1694.608	2.193904	76.6953	31.0294	0.8874	0.0499
70	0.47	3	39	1729.664	2.231926	73.1161	31.1217	0.889	0.0493
70	0.63	1	40	1776.653	2.571089	78.9465	31.3773	0.9108	0.0402
70	0.63	2	41	1823.643	2.580985	77.8667	31.2049	0.9085	0.0406
70	0.63	3	42	1870.632	2.549941	75.5965	32.2913	0.9104	0.0403
70	0.79	1	43	1929.556	2.973481	80.4637	29.3631	0.9284	0.0316
70	0.79	2	44	1988.479	2.963556	80.6906	31.025	0.9243	0.033
70	0.79	3	45	2047.403	3.025459	77.736	31.1334	0.9247	0.0325
100	0.06	1	46	2051.878	1.408807	46.6626	34.0599	0.6187	0.1413
100	0.06	2	47	2056.353	1.390311	41.8608	32.3684	0.6085	0.1512
100	0.06	3	48	2060.828	1.379985	41.6882	30.5675	0.61	0.1423
100	0.145	1	49	2071.643	1.964756	53.7948	32.2564	0.7638	0.0919
100	0.145	2	50	2082.458	1.967252	53.1316	33.4414	0.7543	0.107
100	0.145	3	51	2093.273	1.948896	54.8458	32.6001	0.7522	0.1026
100	0.23	1	52	2110.428	2.58243	65.9946	32.8156	0.8348	0.0714
100	0.23	2	53	2127.583	2.557644	64.0963	31.8675	0.8242	0.0717
100	0.23	3	54	2144.738	2.52437	67.9531	34.086	0.8266	0.0746
100	0.315	1	55	2168.233	3.149911	69.8047	32.5501	0.8642	0.0576
100	0.315	2	56	2191.728	3.119511	68.7328	32.0417	0.8667	0.0579
100	0.315	3	57	2215.222	3.152356	67.4219	31.3275	0.861	0.0624
100	0.4	1	58	2245.057	3.712978	74.0834	32.5521	0.8822	0.0505
100	0.4	2	59	2274.892	3.815556	75.3829	30.4895	0.8957	0.0465
100	0.4	3	60	2304.726	3.716726	72.5043	31.6959	0.8879	0.0492

Mouse 4a Vein

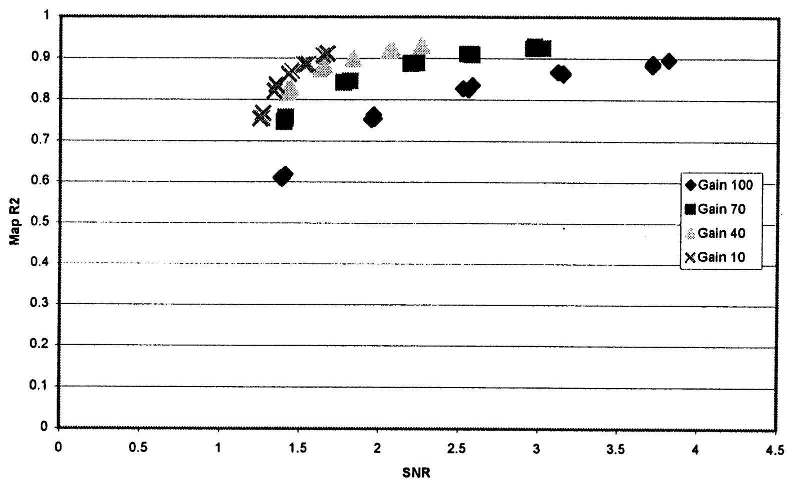

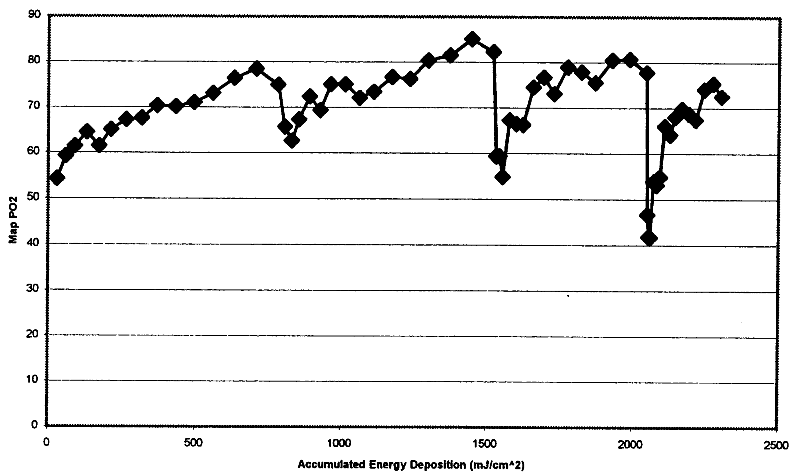

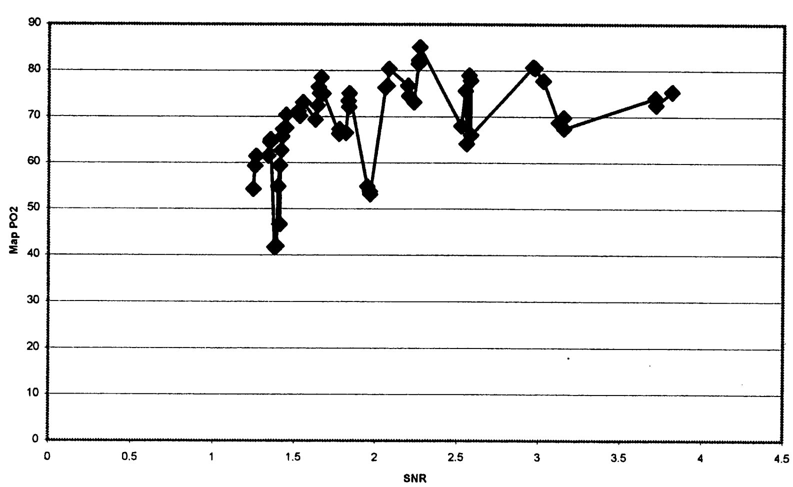

Gain	Exposure T	Relative Ir	Cumulative	Accumulat	SNR	PO2 Mean	PO2 St. De	R2 Mean	R2 St. Dev
10	0.4	1	1	29.83465	1.251659	68.3765	34.4412	0.7832	0.0918
10	0.4	2	2	59.66929	1.248578	60.3828	32.6263	0.7729	0.0938
10	0.4	3	3	89.50394	1.246104	61.2621	33.7001	0.7728	0.0947
10	0.55	1	4	130.5266	1.331163	72.8594	34.2186	0.8349	0.0681
10	0.55	2	5	171.5492	1.328911	68.5709	32.8407	0.8408	0.0673
10	0.55	3	6	212.5719	1.346163	72.869	32.4855	0.8396	0.0687
10	0.7	1	7	264.7825	1.412007	75.8372	32.2745	0.8683	0.0554
10	0.7	2	8	316.9931	1.433696	78.1534	33.3046	0.8785	0.0523
10	0.7	3	9	369.2037	1.416948	70.0845	33.5629	0.8751	0.0534
10	0.85	1	10	432.6024	1.523022	80.3243	34.2184	0.9	0.0458
10	0.85	2	11	496.001	1.517052	77.6035	32.1845	0.8952	0.0449
10	0.85	3	12	559.3996	1.533756	81.6392	33.856	0.9016	0.0448
10	1	1	13	633.9862	1.629644	79.9942	31.6674	0.9141	0.0366
10	1	2	14	708.5728	1.634059	82.098	31.8275	0.9141	0.0373
10	1	3	15	783.1594	1.623126	80.5158	32.7948	0.9152	0.0371
40	0.32	1	16	807.0272	1.405096	69.4751	31.8162	0.8238	0.0694
40	0.32	2	17	830.8949	1.414037	66.4904	35.4277	0.8396	0.0698
40	0.32	3	18	854.7626	1.417296	66.39	34.6509	0.8427	0.0663
40	0.49	1	19	891.31	1.637533	82.8177	30.4323	0.8915	0.0486
40	0.49	2	20	927.8575	1.614259	74.7071	32.9349	0.8881	0.0488
40	0.49	3	21	964.4049	1.6254	78.5523	32.4108	0.884	0.0521
40	0.66	1	22	1013.632	1.797348	82.2476	30.7741	0.9064	0.0405
40	0.66	2	23	1062.859	1.804652	82.0325	31.7717	0.905	0.0411
40	0.66	3	24	1112.086	1.798496	79.8511	31.6799	0.9042	0.0422
40	0.83	1	25	1173.993	1.992704	85.6966	28.6201	0.9214	0.0372
40	0.83	2	26	1235.9	2.029622	84.1408	33.4947	0.9255	0.0335
40	0.83	3	27	1297.807	2.012222	84.2075	31.5339	0.9276	0.0324
40	1	1	28	1372.394	2.197237	88.688	29.8057	0.9365	0.026
40	1	2	29	1446.98	2.212548	90.8213	30.4399	0.9367	0.034
40	1	3	30	1521.567	2.22037	91.3635	31.5302	0.934	0.0298
70	0.15	1	31	1532.755	1.370807	62.2085	33.6107	0.7621	0.0944
70	0.15	2	32	1543.943	1.367296	57.8711	32.4899	0.7715	0.0967
70	0.15	3	33	1555.131	1.395667	61.6869	32.7905	0.7686	0.0946
70	0.31	1	34	1578.253	1.760333	73.2865	31.2572	0.8592	0.0621
70	0.31	2	35	1601.375	1.792837	75.73	32.8233	0.8635	0.0577
70	0.31	3	36	1624.496	1.758459	71.6082	31.7988	0.8596	0.0601
70	0.47	1	37	1659.552	2.202963	83.6044	32.2228	0.8987	0.0445
70	0.47	2	38	1694.608	2.200126	75.4555	31.5909	0.8997	0.045
70	0.47	3	39	1729.664	2.171941	80.185	31.2833	0.9002	0.0445
70	0.63	1	40	1776.653	2.530963	85.9763	32.0092	0.9206	0.0337
70	0.63	2	41	1823.643	2.57697	87.1368	29.5879	0.9173	0.0362
70	0.63	3	42	1870.632	2.531178	77.7445	30.5814	0.9192	0.0358
70	0.79	1	43	1929.556	2.926904	91.541	29.4474	0.935	0.0271
70	0.79	2	44	1988.479	2.946548	86.1446	30.7619	0.9314	0.0294
70	0.79	3	45	2047.403	2.98623	85.0351	30.2432	0.9345	0.0301
100	0.06	1	46	2051.878	1.402022	49.8785	34.4963	0.6461	0.1402
100	0.06	2	47	2056.353	1.39563	49.51	31.9089	0.6124	0.1358
100	0.06	3	48	2060.828	1.402822	51.9903	32.1192	0.6332	0.1354
100	0.145	1	49	2071.643	1.949859	60.0672	33.4627	0.7852	0.0927
100	0.145	2	50	2082.458	1.932756	60.5336	33.4991	0.7826	0.0902
100	0.145	3	51	2093.273	1.932696	61.9497	36.0968	0.7751	0.0965
100	0.23	1	52	2110.428	2.4996	69.8069	32.4041	0.8384	0.0723
100	0.23	2	53	2127.583	2.499607	68.9733	33.1368	0.8379	0.0677
100	0.23	3	54	2144.738	2.508378	67.2756	31.9931	0.845	0.0692
100	0.315	1	55	2168.233	3.075081	75.7456	33.4292	0.8688	0.0553
100	0.315	2	56	2191.728	3.071356	73.8262	33.4248	0.8722	0.0557
100	0.315	3	57	2215.222	3.123289	79.8329	34.1004	0.875	0.0545
100	0.4	1	58	2245.057	3.610207	73.1357	30.0954	0.8916	0.0478
100	0.4	2	59	2274.892	3.636733	77.8711	32.1963	0.898	0.0446
100	0.4	3	60	2304.726	3.688763	78.6768	31.9384	0.8994	0.043

Mouse 4a Artery

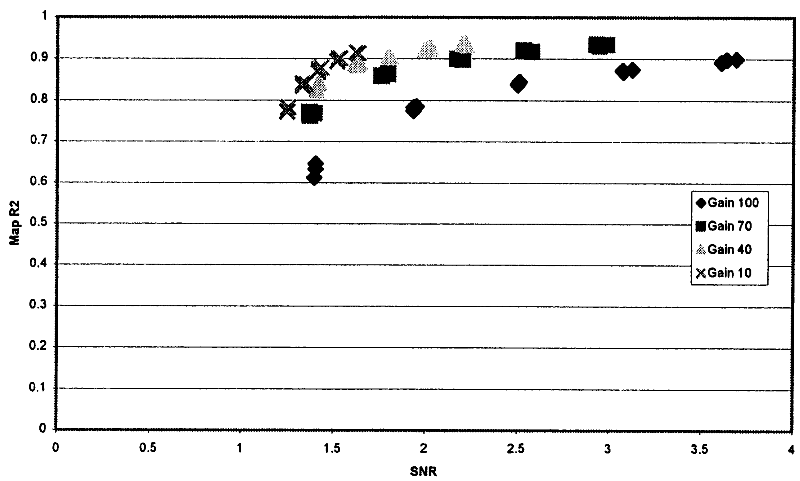

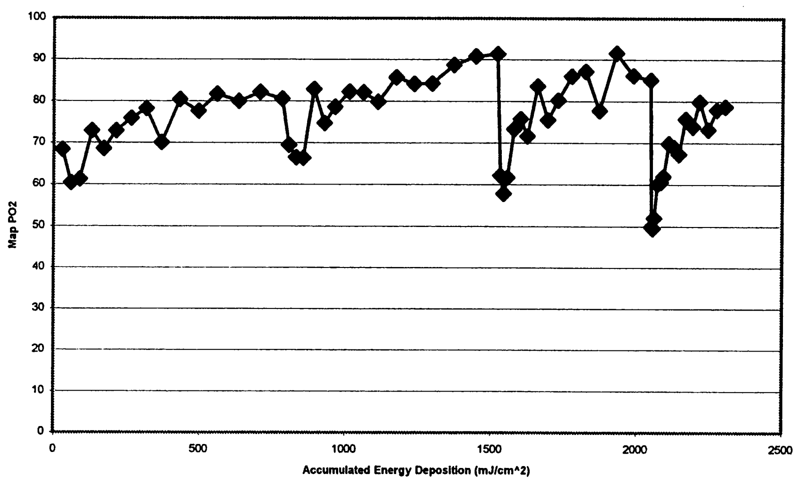

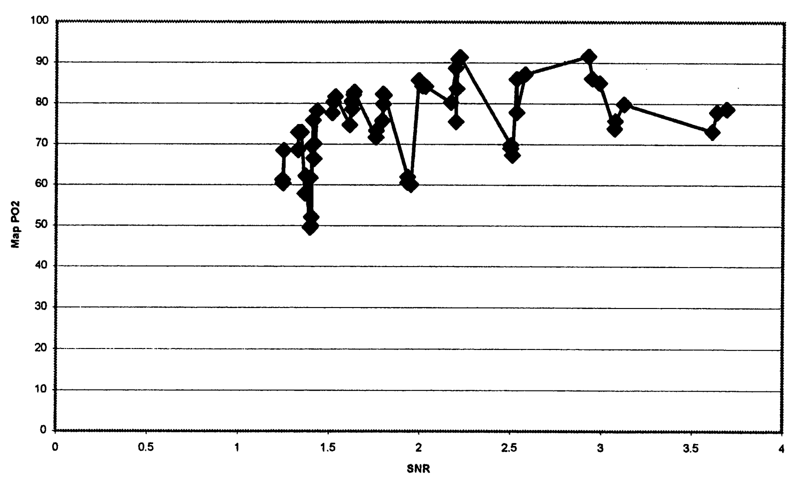

Gain	Exposure T	Relative Im	Cumulative	Accumulat	SNR	PO2 Mean	PO2 St. De	R2 Mean	R2 St. Dev
10	0.4	1	1	29.83465	1.232741	64.9766	32.5012	0.7795	0.0953
10	0.4	2	2	59.66929	1.233511	60.8096	33.4929	0.7645	0.095
10	0.4	3	3	89.50394	1.232089	57.3027	32.8772	0.7655	0.102
10	0.55	1	4	130.5266	1.303856	72.8217	33.3182	0.837	0.0674
10	0.55	2	5	171.5492	1.306815	69.7979	34.3218	0.8333	0.0705
10	0.55	3	6	212.5719	1.319326	77.0928	33.4159	0.841	0.0674
10	0.7	1	7	264.7825	1.394281	77.3774	32.1369	0.8741	0.0522
10	0.7	2	8	316.9931	1.403778	77.0324	33.0576	0.8769	0.0524
10	0.7	3	9	369.2037	1.398948	76.1231	32.8144	0.8767	0.0513
10	0.85	1	10	432.6024	1.484267	82.0979	31.2087	0.9014	0.043
10	0.85	2	11	496.001	1.49623	81.0378	32.8806	0.898	0.0455
10	0.85	3	12	559.3996	1.493163	82.1098	32.9046	0.9403	0.0422
10	1	1	13	633.9862	1.585807	88.0422	30.0346	0.9169	0.036
10	1	2	14	708.5728	1.585652	90.0391	30.5681	0.9202	0.0345
10	1	3	15	783.1594	1.580681	85.4821	31.6587	0.9173	0.0351
40	0.32	1	16	807.0272	1.371222	70.9834	30.8444	0.8332	0.0739
40	0.32	2	17	830.8949	1.390733	73.388	33.1665	0.8395	0.0693
40	0.32	3	18	854.7626	1.3834	69.123	31.7289	0.84	0.0674
40	0.49	1	19	891.31	1.572852	84.8061	34.425	0.8929	0.0472
40	0.49	2	20	927.8575	1.5584	75.3968	31.6618	0.8873	0.0505
40	0.49	3	21	964.4049	1.567067	78.9192	30.2684	0.886	0.0477
40	0.66	1	22	1013.632	1.745378	87.4987	32.4787	0.9131	0.037
40	0.66	2	23	1062.859	1.748489	85.2175	31.2961	0.911	0.0397
40	0.66	3	24	1112.086	1.767378	84.6003	31.7427	0.9116	0.0372
40	0.83	1	25	1173.993	1.945311	88.0657	28.8299	0.9286	0.0355
40	0.83	2	26	1235.9	1.949741	95.1213	30.8064	0.92831	0.032
40	0.83	3	27	1297.807	1.933481	85.696	31.6265	0.9256	0.0328
40	1	1	28	1372.394	2.125163	93.9374	29.5682	0.942	0.0261
40	1	2	29	1446.98	2.151667	96.8605	29.6409	0.9398	0.0274
40	1	3	30	1521.567	2.144533	95.49	30.6758	0.9394	0.0274
70	0.15	1	31	1532.755	1.355563	63.3009	34.7719	0.7575	0.1008
70	0.15	2	32	1543.943	1.347422	63.4385	33.5787	0.768	0.0929
70	0.15	3	33	1555.131	1.358393	61.052	32.647	0.7653	0.0925
70	0.31	1	34	1578.253	1.711	75.6701	32.4843	0.8668	0.0571
70	0.31	2	35	1601.375	1.696948	73.1317	34.4582	0.8632	0.0593
70	0.31	3	36	1624.496	1.701533	77.3596	32.0273	0.8586	0.0627
70	0.47	1	37	1659.552	2.083719	84.1888	31.3915	0.9047	0.0405
70	0.47	2	38	1694.608	2.076444	86.7617	32.1311	0.904	0.0414
70	0.47	3	39	1729.664	2.063815	84.763	30.1723	0.901	0.0454
70	0.63	1	40	1776.653	2.408141	89.0282	30.974	0.9245	0.0327
70	0.63	2	41	1823.643	2.426363	83.7486	31.6726	0.9217	0.0342
70	0.63	3	42	1870.632	2.407667	85.8464	30.0553	0.9208	0.0347
70	0.79	1	43	1929.556	2.747652	88.1612	30.9903	0.9348	0.0293
70	0.79	2	44	1988.479	2.778296	93.4185	28.9005	0.9348	0.029
70	0.79	3	45	2047.403	2.773304	91.5489	32.1736	0.939	0.0264
100	0.06	1	46	2051.878	1.373556	55.6798	35.5861	0.6254	0.146
100	0.06	2	47	2056.353	1.362904	55.1774	33.872	0.6471	0.1349
100	0.06	3	48	2060.828	1.354015	51.8807	33.1823	0.6507	0.1331
100	0.145	1	49	2071.643	1.850089	59.4823	30.7688	0.7867	0.092
100	0.145	2	50	2082.458	1.86057	63.7523	32.846	0.7874	0.0884
100	0.145	3	51	2093.273	1.882319	69.1437	36.7375	0.7919	0.0869
100	0.23	1	52	2110.428	2.39323	72.6975	34.2522	0.8486	0.0646
100	0.23	2	53	2127.583	2.389111	70.0519	33.1367	0.8401	0.0697
100	0.23	3	54	2144.738	2.371	71.6138	33.7361	0.8453	0.0669
100	0.315	1	55	2168.233	2.923511	80.7446	32.181	0.8864	0.0497
100	0.315	2	56	2191.728	2.874452	73.0974	32.1228	0.876	0.0529
100	0.315	3	57	2215.222	2.903193	78.1554	33.3231	0.8832	0.0528
100	0.4	1	58	2245.057	3.39423	81.6787	33.9078	0.8984	0.0461
100	0.4	2	59	2274.892	3.460215	82.1298	32.8302	0.9043	0.0414
100	0.4	3	60	2304.726	3.429778	82.9793	31.0943	0.9023	0.0438

Mouse 4a Tissue

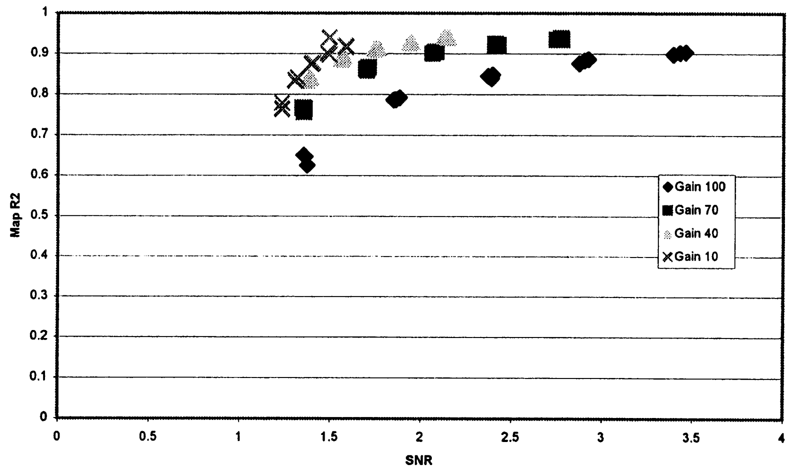

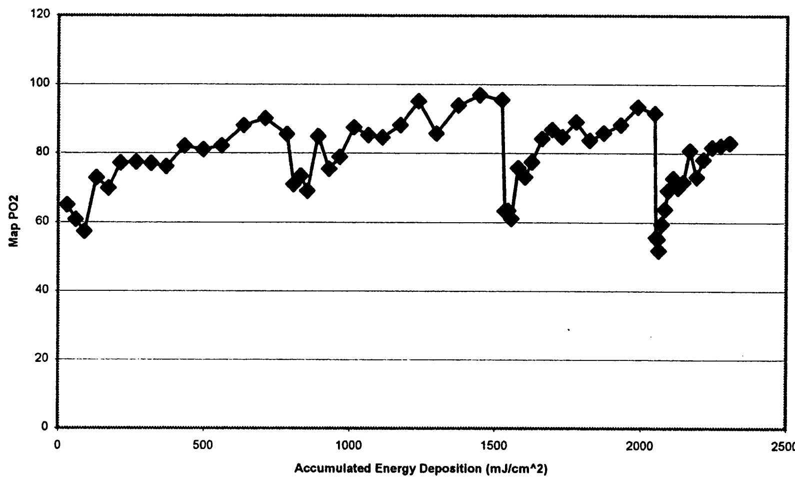

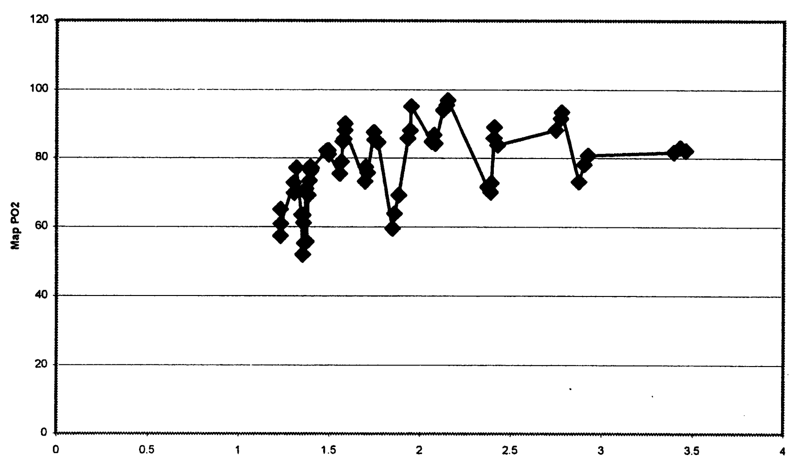

Gain	Exposure T	Relative Ir	Cumulative	Accumulat	SNR	PO2 Mean	PO2 St. De	R2 Mean	R2 St. Dev
100	0.06	1	1	4.443307	2.479533	46.2413	31.2319	0.7863	0.0904
100	0.06	2	2	8.886614	2.529274	51.0555	29.7192	0.7922	0.0838
100	0.06	3	3	13.32992	2.469422	49.412	30.5579	0.7936	0.0861
100	0.145	1	4	24.06791	4.774859	50.2866	26.4852	0.8989	0.0451
100	0.145	2	5	34.80591	4.92583	57.4998	29.7529	0.9034	0.0418
100	0.145	3	6	45.5439	4.965407	63.9757	30.3678	0.8897	0.0482
100	0.23	1	7	62.57657	7.118467	60.8788	28.8409	0.9333	0.0293
100	0.23	2	8	79.60925	7.277311	60.5036	27.4923	0.9317	0.0301
100	0.23	3	9	96.64193	7.343074	56.491	26.623	0.9285	0.0326
100	0.315	1	10	119.9693	9.189415	33.7939	11.3997	0.9417	0.0258
100	0.315	2	11	143.2967	9.575074	60.0648	26.1406	0.9488	0.0227
100	0.315	3	12	166.624	9.437111	57.8755	25.5156	0.9478	0.022
100	0.4	1	13	196.2461	11.95566	58.9466	24.3787	0.9578	0.0187
100	0.4	2	14	225.8681	12.33004	57.0861	23.1901	0.9584	0.0179
100	0.4	3	15	255.4902	12.36756	59.4674	22.9969	0.958	0.018
70	0.15	1	16	266.5984	2.609289	54.3219	30.4287	0.8877	0.0477
70	0.15	2	17	277.7067	2.475407	51.7616	27.7822	0.8816	0.0521
70	0.15	3	18	288.815	2.531274	52.8028	28.5423	0.8912	0.0466
70	0.31	1	19	311.772	4.200022	57.4241	26.6316	0.933	0.0289
70	0.31	2	20	334.7291	4.180252	55.8462	25.6705	0.9394	0.0265
70	0.31	3	21	357.6862	4.177326	58.301	25.6918	0.9367	0.0267
70	0.47	1	22	392.4921	5.99023	67.2376	27.6273	0.9571	0.0195
70	0.47	2	23	427.298	5.826548	64.8627	26.4966	0.9579	0.0187
70	0.47	3	24	462.1039	5.829711	57.2309	22.6513	0.955	0.0199
70	0.63	1	25	508.7587	7.567733	62.1207	22.5469	0.9686	0.0136
70	0.63	2	26	555.4134	7.680089	61.808	23.5587	0.9666	0.0147
70	0.63	3	27	602.0681	7.562593	61.6279	23.9916	0.9654	0.0156
70	0.79	1	28	660.5717	9.008341	53.7316	18.512	0.9717	0.0124
70	0.79	2	29	719.0752	9.256215	62.6192	21.4068	0.9725	0.0128
70	0.79	3	30	777.5787	9.252622	53.8831	19.1024	0.9712	0.0128
40	0.32	1	31	801.2764	2.624637	57.4538	27.3035	0.9219	0.0345
40	0.32	2	32	824.974	2.656207	52.3714	25.6035	0.9194	0.0352
40	0.32	3	33	848.6717	2.644719	51.6799	24.5364	0.9217	0.0338
40	0.49	1	34	884.9587	3.465193	54.3578	23.7446	0.9464	0.0233
40	0.49	2	35	921.2457	3.466926	55.6265	25.266	0.9458	0.0234
40	0.49	3	36	957.5327	3.474719	55.2153	24.3636	0.9465	0.023
40	0.66	1	37	1006.409	4.402711	56.3453	22.5382	0.9565	0.0198
40	0.66	2	38	1055.285	4.354867	55.5135	23.4137	0.9588	0.0183
40	0.66	3	39	1104.162	4.350637	53.4804	21.4382	0.9582	0.0187
40	0.83	1	40	1165.628	5.2354	54.276	21.1731	0.9632	0.0162
40	0.83	2	41	1227.093	5.107556	54.5259	21.9059	0.9644	0.0162
40	0.83	3	42	1288.559	5.162919	58.0108	23.145	0.9646	0.0154
40	1	1	43	1362.614	6.130444	55.4217	19.6536	0.9712	0.0121
40	1	2	44	1436.669	5.833956	52.6632	19.5386	0.9692	0.0133
40	1	3	45	1510.724	5.881252	59.3984	21.9245	0.97	0.0129
10	0.4	1	46	1540.346	2.047067	44.9983	23.2808	0.9064	0.0398
10	0.4	2	47	1569.969	2.051593	53.0802	26.854	0.9066	0.0398
10	0.4	3	48	1599.591	1.9928	54.0821	28.6099	0.8991	0.0422
10	0.55	1	49	1640.321	2.381311	49.8412	24.262	0.9292	0.0312
10	0.55	2	50	1681.051	2.278837	52.1385	25.517	0.9276	0.0319
10	0.55	3	51	1721.781	2.310526	53.3384	25.2274	0.9299	0.0301
10	0.7	1	52	1773.62	2.601807	56.0286	24.3599	0.9427	0.0253
10	0.7	2	53	1825.459	2.622178	55.3013	24.5241	0.9412	0.0252
10	0.7	3	54	1877.297	2.569689	55.4751	26.2194	0.9425	0.0247
10	0.85	1	55	1940.244	2.926919	53.0072	22.1237	0.9514	0.0212
10	0.85	2	56	2003.191	2.919859	56.872	23.3162	0.9527	0.0202
10	0.85	3	57	2066.138	2.875778	63.6572	26.796	0.9483	0.0231
10	1	1	58	2140.193	3.280837	52.4587	21.0436	0.9562	0.019
10	1	2	59	2214.248	3.280237	55.5089	22.9946	0.9549	0.0193
10	1	3	60	2288.303	3.256844	56.0607	22.9189	0.9544	0.0204

Mouse 5a Vein

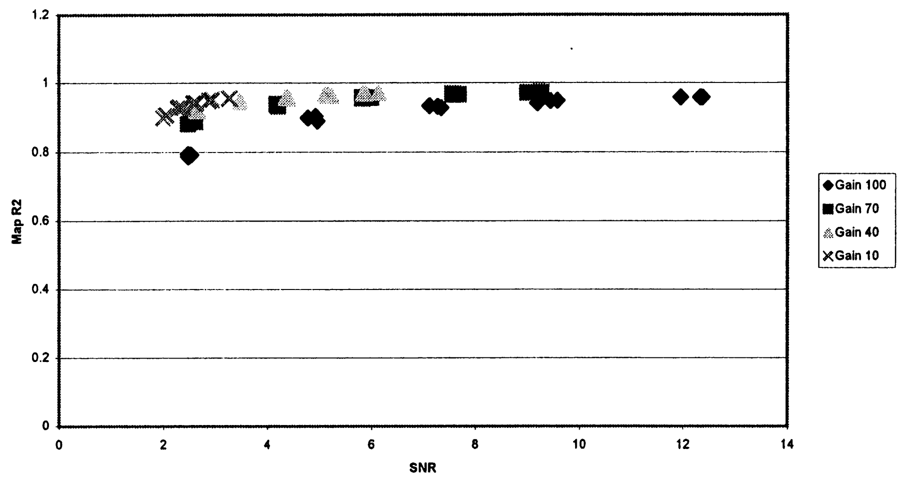

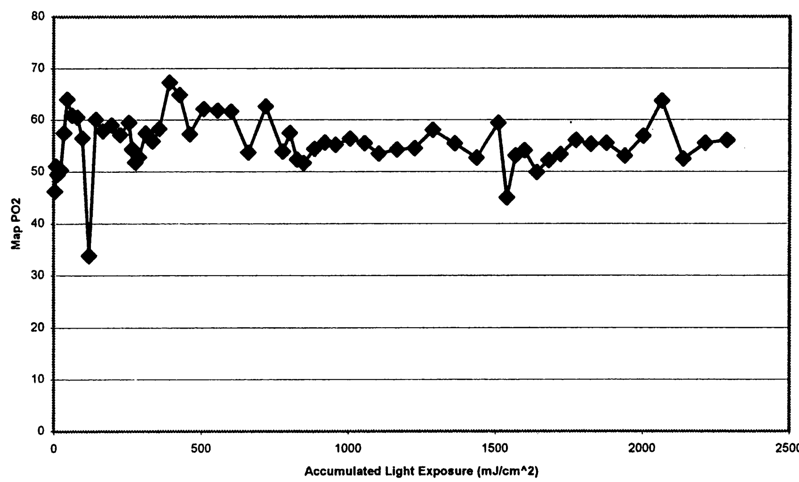

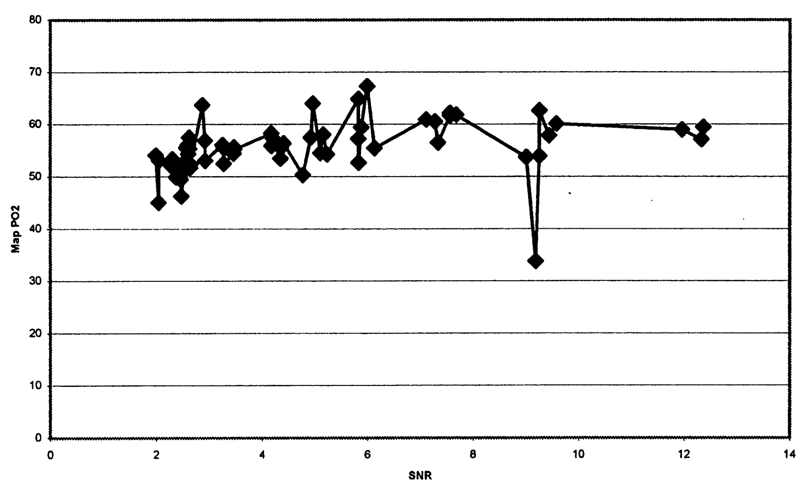

Gain	Exposure T	Relative Im	Cumulative	Accumulat	SNR	PO2 Mean	PO2 St. De	R2 Mean	R2 St. Dev
100	0.06	1	1	4.443307	1.878733	47.7652	34.0497	0.7541	0.1085
100	0.06	2	2	8.886614	1.848711	53.1851	32.2245	0.7416	0.107
100	0.06	3	3	13.32992	1.878156	55.1511	32.3214	0.762	0.0989
100	0.145	1	4	24.06791	3.212674	60.9515	31.4961	0.8634	0.0593
100	0.145	2	5	34.80591	3.104563	63.6236	31.56	0.8669	0.0575
100	0.145	3	6	45.5439	3.254993	62.8875	31.0666	0.866	0.0606
100	0.23	1	7	62.57657	4.701	71.1771	32.7502	0.9113	0.037
100	0.23	2	8	79.60925	4.648919	69.3285	29.9091	0.9121	0.0366
100	0.23	3	9	96.64193	4.674126	69.0837	32.0626	0.9074	0.00418
100	0.315	1	10	119.9693	6.076074	63.9224	27.2446	0.9317	0.0271
100	0.315	2	11	143.2967	5.858985	71.7915	29.1064	0.9334	0.0294
100	0.315	3	12	166.624	5.801637	72.796	31.3634	0.9334	0.0283
100	0.4	1	13	196.2461	7.050156	73.4951	29.44	0.9442	0.0249
100	0.4	2	14	225.8681	7.421222	77.5166	30.6204	0.9455	0.0244
100	0.4	3	15	255.4902	7.648237	79.055	29.7445	0.9475	0.0226
70	0.15	1	16	266.5984	1.891281	57.8994	30.4998	0.853	0.0612
70	0.15	2	17	277.7067	1.897696	63.3721	32.2227	0.8448	0.0651
70	0.15	3	18	288.815	1.894978	65.7333	33.7442	0.8609	0.0608
70	0.31	1	19	311.772	2.801504	69.8133	30.1597	0.9141	0.0379
70	0.31	2	20	334.7291	2.790333	70.0534	31.195	0.914	0.0389
70	0.31	3	21	357.6862	2.814096	72.5058	30.5953	0.9157	0.0374
70	0.47	1	22	392.4921	3.823978	80.7039	31.1622	0.9438	0.0245
70	0.47	2	23	427.298	3.826896	80.7321	28.9344	0.9441	0.0251
70	0.47	3	24	462.1039	3.82303	77.5781	28.6279	0.9452	0.0253
70	0.63	1	25	508.7587	4.750311	80.2946	29.5501	0.9552	0.0194
70	0.63	2	26	555.4134	4.784341	78.1494	28.1699	0.9531	0.0206
70	0.63	3	27	602.0681	4.7232	80.0924	28.942	0.9516	0.0212
70	0.79	1	28	660.5717	5.760593	80.6246	28.2649	0.9638	0.0167
70	0.79	2	29	719.0752	5.812978	83.8884	28.4426	0.9624	0.0175
70	0.79	3	30	777.5787	5.722548	79.2245	27.7121	0.9625	0.0164
40	0.32	1	31	801.2764	1.981281	67.8055	31.0842	0.8991	0.0415
40	0.32	2	32	824.974	1.925681	64.0778	31.2149	0.8906	0.0494
40	0.32	3	33	848.6717	1.940415	67.9342	31.0329	0.8964	0.0462
40	0.49	1	34	884.9587	2.448111	70.9768	29.592	0.9271	0.0317
40	0.49	2	35	921.2457	2.433785	70.0152	31.0149	0.926	0.0317
40	0.49	3	36	957.5327	2.401237	72.9757	30.6364	0.9245	0.0324
40	0.66	1	37	1006.409	2.926274	76.2121	30.0589	0.9422	0.0244
40	0.66	2	38	1055.285	2.922622	75.4443	29.5041	0.9414	0.0262
40	0.66	3	39	1104.162	2.892837	77.1184	30.596	0.9401	0.025
40	0.83	1	40	1165.628	3.421378	79.6789	28.6756	0.9505	0.0219
40	0.83	2	41	1227.093	3.38583	78.7134	28.226	0.9523	0.0213
40	0.83	3	42	1288.559	3.478748	78.2875	28.8438	0.9536	0.0204
40	1	1	43	1362.614	3.798889	77.8734	28.3193	0.9592	0.0189
40	1	2	44	1436.669	3.81663	77.6165	29.0069	0.958	0.018
40	1	3	45	1510.724	3.76597	80.4811	28.1495	0.9549	0.0202
10	0.4	1	46	1540.346	1.647711	55.3826	29.2869	0.8794	0.0488
10	0.4	2	47	1569.969	1.65937	63.0616	31.3006	0.8792	0.0494
10	0.4	3	48	1599.591	1.6552	65.3658	33.1906	0.8774	0.049
10	0.55	1	49	1640.321	1.866304	64.7691	30.5943	0.9061	0.0399
10	0.55	2	50	1681.051	1.831541	65.9882	30.0864	0.9081	0.0397
10	0.55	3	51	1721.781	1.831259	66.1458	32.8499	0.9025	0.0421
10	0.7	1	52	1773.62	2.059059	72.8709	31.3669	0.9265	0.0331
10	0.7	2	53	1825.459	2.0186	65.6895	29.4057	0.9238	0.0323
10	0.7	3	54	1877.297	2.029089	72.3919	32.5485	0.9189	0.0364
10	0.85	1	55	1940.244	2.207733	67.3396	29.4738	0.9337	0.0287
10	0.85	2	56	2003.191	2.188607	70.6172	30.8073	0.932	0.0314
10	0.85	3	57	2066.138	2.189674	72.7602	30.3415	0.9317	0.0307
10	1	1	58	2140.193	2.403896	67.5463	28.7448	0.9382	0.0272
10	1	2	59	2214.248	2.418711	74.3731	31.5861	0.9398	0.0253
10	1	3	60	2288.303	2.404259	70.9447	28.3395	0.9354	0.0285

Mouse 5a Artery

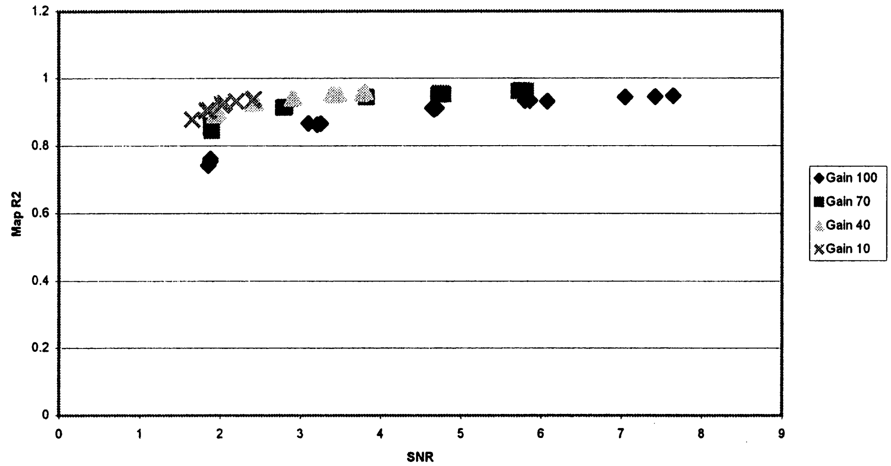

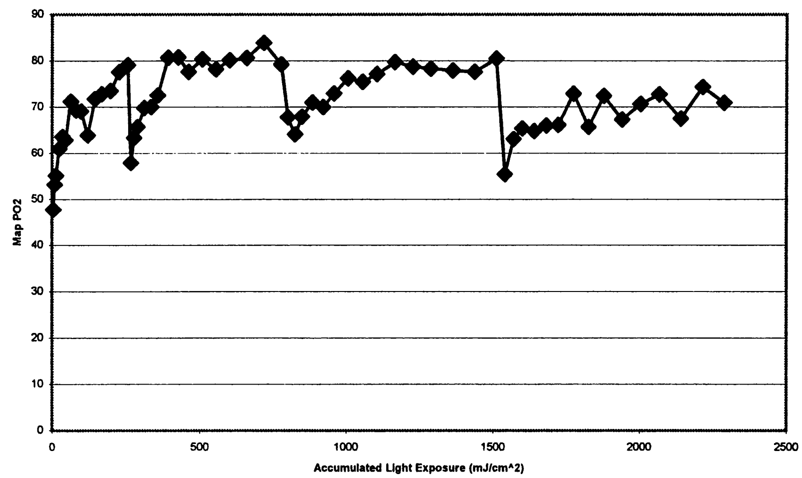

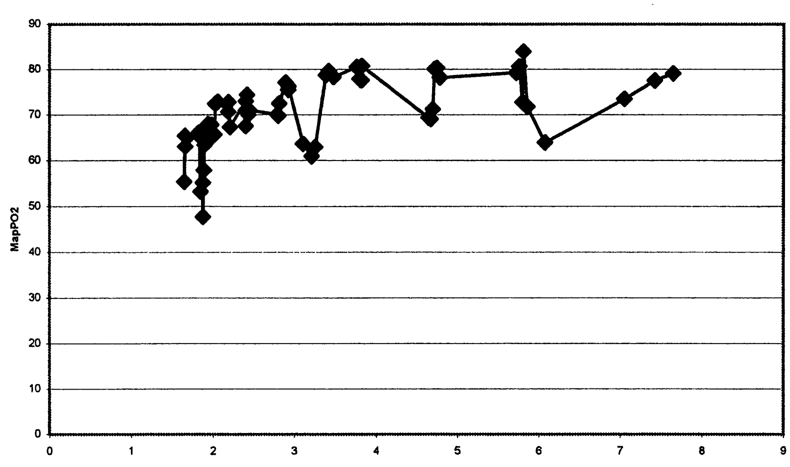

Gain	Exposure T	Relative Im	Cumulative	Accumulat	SNR	PO2 Mean	PO2 St. De	R2 Mean	R2 St. Dev
100	0.06	1	1	4.443307	1.467904	43.5548	32.2989	0.706	0.1219
100	0.06	2	2	8.886614	1.51377	57.1264	34.388	0.7258	0.1093
100	0.06	3	3	13.32992	1.5078	56.6324	32.0772	0.7178	0.1118
100	0.145	1	4	24.06791	2.287311	71.4797	33.2975	0.8417	0.072
100	0.145	2	5	34.80591	2.260341	67.5991	31.2017	0.8396	0.0666
100	0.145	3	6	45.5439	2.311615	69.9141	32.6131	0.8438	0.0705
100	0.23	1	7	62.57657	3.119822	78.4037	33.2322	0.8934	0.0455
100	0.23	2	8	79.60925	3.063385	76.1637	32.3134	0.8858	0.0494
100	0.23	3	9	96.64193	3.099259	77.637	32.486	0.8931	0.0467
100	0.315	1	10	119.9693	3.872133	78.5093	30.7984	0.9185	0.0351
100	0.315	2	11	143.2967	3.890489	85.2743	30.9947	0.9149	0.0372
100	0.315	3	12	166.624	3.827437	79.511	31.5683	0.9107	0.041
100	0.4	1	13	196.2461	4.61463	84.9656	30.6047	0.9259	0.0321
100	0.4	2	14	225.8681	4.697644	86.718	30.4836	0.9329	0.0301
100	0.4	3	15	255.4902	4.720844	86.1941	31.5897	0.9322	0.0307
70	0.15	1	16	266.5984	1.541726	64.5076	33.1464	0.8262	0.0752
70	0.15	2	17	277.7067	1.521889	63.6234	33.1206	0.8193	0.0745
70	0.15	3	18	288.815	1.526511	66.3763	33.3459	0.8268	0.0723
70	0.31	1	19	311.772	2.115244	78.5733	31.4295	0.8964	0.0462
70	0.31	2	20	334.7291	2.123341	79.0106	31.1489	0.8943	0.047
70	0.31	3	21	357.6862	2.092074	77.9216	32.1514	0.8943	0.0475
70	0.47	1	22	392.4921	2.683926	82.5698	30.1576	0.9255	0.0326
70	0.47	2	23	427.298	2.670141	87.848	31.2968	0.9264	0.0332
70	0.47	3	24	462.1039	2.679637	86.8616	31.0748	0.9248	0.034
70	0.63	1	25	508.7587	3.245519	87.0019	30.2508	0.9417	0.0264
70	0.63	2	26	555.4134	3.271785	89.5631	28.5702	0.9422	0.0265
70	0.63	3	27	602.0681	3.27723	88.8839	30.6957	0.9398	0.0264
70	0.79	1	28	660.5717	3.903874	96.2313	28.5921	0.9515	0.0224
70	0.79	2	29	719.0752	3.90563	93.8041	29.9284	0.9498	0.0212
70	0.79	3	30	777.5787	3.897378	88.9249	29.4781	0.9483	0.0237
40	0.32	1	31	801.2764	1.621156	72.8141	33.5044	0.8717	0.531
40	0.32	2	32	824.974	1.598259	70.0742	32.4769	0.8762	0.0547
40	0.32	3	33	848.6717	1.611	71.2131	32.2693	0.8693	0.056
40	0.49	1	34	884.9587	1.923459	78.9008	32.564	0.905	0.0412
40	0.49	2	35	921.2457	1.924267	76.9724	32.0939	0.9013	0.044
40	0.49	3	36	957.5327	1.936267	75.7244	31.9027	0.9059	0.0398
40	0.66	1	37	1006.409	2.256696	82.2923	30.8797	0.9252	0.033
40	0.66	2	38	1055.285	2.261296	81.8245	31.4522	0.9254	0.0333
40	0.66	3	39	1104.162	2.271215	82.8509	30.673	0.9247	0.0348
40	0.83	1	40	1165.628	2.595356	87.29	30.5153	0.9298	0.0268
40	0.83	2	41	1227.093	2.587807	82.3839	30.6405	0.9373	0.0272
40	0.83	3	42	1288.559	2.603385	83.2837	31.313	0.9288	0.0273
40	1	1	43	1362.614	2.953437	87.6259	30.0576	0.9457	0.0239
40	1	2	44	1436.669	2.93283	84.8932	29.4324	0.9443	0.0237
40	1	3	45	1510.724	2.968919	85.1262	30.8059	0.9456	0.0243
10	0.4	1	46	1540.346	1.402185	59.0896	32.02	0.8224	0.0741
10	0.4	2	47	1569.969	1.409141	63.479	32.5313	0.818	0.0782
10	0.4	3	48	1599.591	1.411148	64.1089	33.2134	0.826	0.0752
10	0.55	1	49	1640.321	1.538385	67.6241	32.4744	0.8703	0.0562
10	0.55	2	50	1681.051	1.52637	67.8957	32.9326	0.8602	0.0601
10	0.55	3	51	1721.781	1.535022	65.0922	32.0557	0.8654	0.0564
10	0.7	1	52	1773.62	1.673489	70.8176	31.9787	0.894	0.0451
10	0.7	2	53	1825.459	1.668659	71.3344	32.8242	0.8906	0.047
10	0.7	3	54	1877.297	1.664511	68.8153	30.9859	0.8878	0.0496
10	0.85	1	55	1940.244	1.802548	71.8552	31.2236	0.9084	0.0384
10	0.85	2	56	2003.191	1.803207	71.7543	30.8969	0.9075	0.0403
10	0.85	3	57	2066.138	1.802467	73.5595	31.2532	0.904	0.042
10	1	1	58	2140.193	1.969763	74.2993	31.1816	0.9169	0.0363
10	1	2	59	2214.248	2.001341	75.5048	30.5542	0.9141	0.0381
10	1	3	60	2288.303	2.031059	69.1801	30.7321	0.9023	0.0419

Mouse 5a Tissue

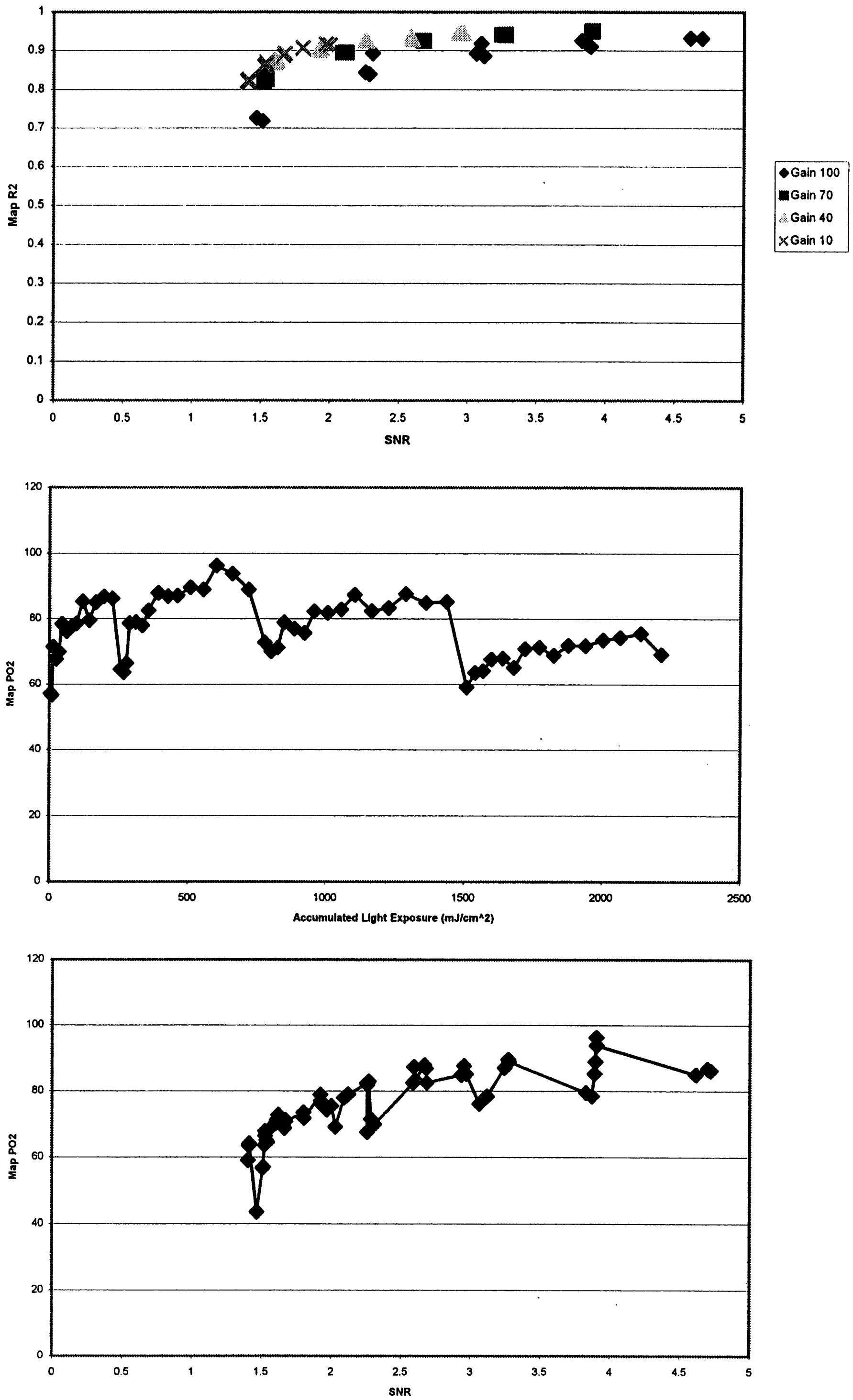

Gain	Exposure 1	Relative Ir	Cumulative	Accumulat	SNR	PO2 Mean	PO2 St. De	R2 Mean	R2 St. Dev
10	0.55	1	1	43.10138	2.395671	29.747	23.7742	0.6966	0.129
10	0.55	2	2	86.20276	2.401879	34.5	26.6582	0.7137	0.1173
10	0.55	3	3	129.3041	1.81845	84.5685	32.0814	0.857	0.0627
100	0.06	1	4	134.0061	4.682986	24.7623	26.018	0.4258	0.1792
100	0.06	2	5	138.7081	4.658593	23.5131	26.6065	0.405	0.1801
100	0.06	3	6	143.41	4.765929	22.7952	24.3599	0.384	0.1863
40	1	1	7	221.7762	13.38494	23.7151	11.8737	0.8749	0.0591
40	1	2	8	300.1423	12.56751	24.1796	11.357	0.8785	0.0559
40	1	3	9	378.5085	11.90782	24.8932	13.2223	0.08741	0.058
70	0.47	1	10	415.3406	11.61982	25.6125	17.6148	0.7872	0.0904
70	0.47	2	11	452.1726	10.94506	30.1621	22.6711	0.7988	0.0981
70	0.47	3	12	489.0047	10.63664	24.0272	16.7616	0.8049	0.0812
70	0.79	1	13	550.914	17.24391	28.5788	15.6978	0.8739	0.0585
70	0.79	2	14	612.8232	17.80051	24.8413	13.3198	0.8583	0.0614
70	0.79	3	15	674.7325	16.29986	32.1015	17.9156	0.8745	0.0546
40	0.32	1	16	699.8096	3.725086	31.5125	26.0308	0.6873	0.126
40	0.32	2	17	724.8868	3.689443	33.1512	24.9948	0.6922	0.1341
40	0.32	3	18	749.964	3.558114	29.8872	24.3217	0.7124	0.1188
10	0.85	1	19	816.5752	4.324079	31.8299	21.2095	0.8296	0.0793
10	0.85	2	20	883.1864	4.427536	30.2618	20.7714	0.8131	0.0804
10	0.85	3	21	949.7976	4.480621	30.3282	20.2491	0.8137	0.0786
100	0.4	1	22	981.1441	17.95599	29.9827	24.4624	0.7667	0.0972
100	0.4	2	23	1012.491	17.47234	34.4066	24.0839	0.7812	0.1028
100	0.4	3	24	1043.837	17.24619	32.2917	22.7189	0.8017	0.0838
10	0.4	1	25	1075.183	2.508929	28.1878	24.2145	0.6637	0.1323
10	0.4	2	26	1106.53	2.468714	33.5509	26.3254	0.6988	0.1246
10	0.4	3	27	1137.876	1.825029	87.677	32.6266	0.8563	0.0633
100	0.23	1	28	1155.901	10.65046	39.3371	24.4196	0.8033	0.1778
100	0.23	2	29	1173.925	4.579829	48.5458	32.0213	0.6916	0.1208
100	0.23	3	30	1191.949	4.020764	52.5716	30.8783	0.75	0.1065

Mouse 6a Vein

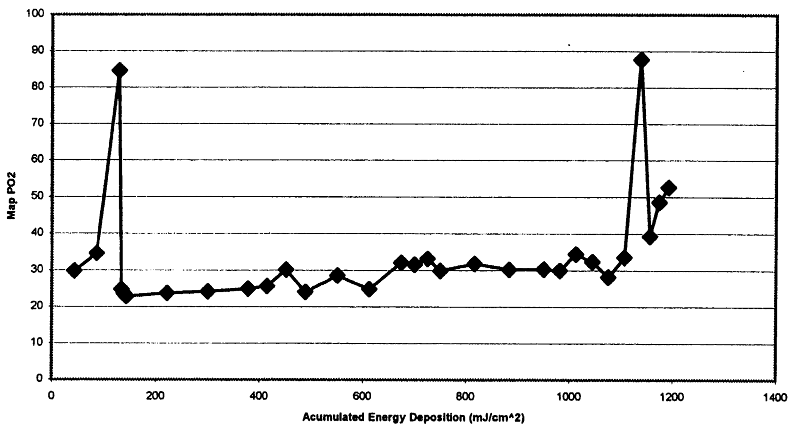

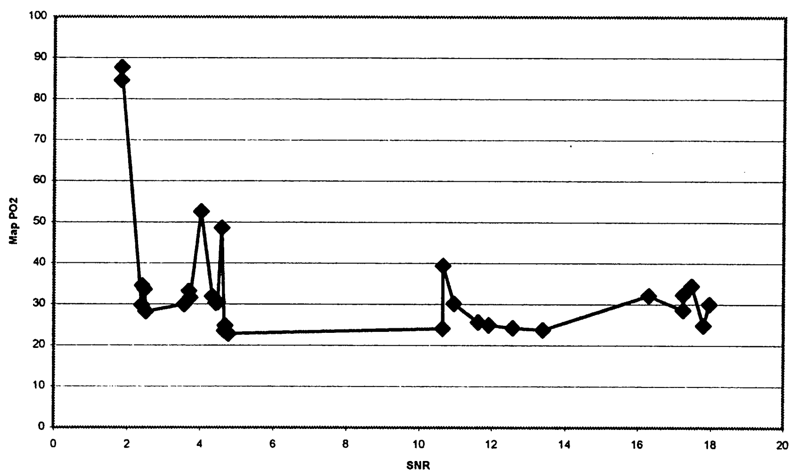

Gain	Exposure T	Relative Im	Cumulative	Accumulat	SNR	PO2 Mean	PO2 St. De	R2 Mean	R2 St. Dev
10	0.55	1	1	43.10138	1.6822	49.3075	30.992	0.7858	0.0913
10	0.55	2	2	86.20276	1.6965	53.9733	31.3614	0.7942	0.0832
10	0.55	3	3	129.3041	1.735943	63.2369	31.2701	0.5675	0.1594
100	0.06	1	4	134.0061	2.055271	50.8819	34.8957	0.6708	0.1244
100	0.06	2	5	138.7081	2.063707	47.2779	31.4022	0.6704	0.1258
100	0.06	3	6	143.41	2.067171	51.7946	35.5517	0.6739	0.1228
40	1	1	7	221.7762	4.362057	73.0184	28.3021	0.9464	0.0234
40	1	2	8	300.1423	4.249179	72.0658	27.9342	0.9518	0.022
40	1	3	9	378.5085	4.120564	57.8418	27.2207	0.9444	0.0238
70	0.47	1	10	415.3406	4.222421	68.0117	31.8056	0.8899	0.0475
70	0.47	2	11	452.1726	4.276243	55.8318	28.2183	0.9099	0.0373
70	0.47	3	12	489.0047	4.278157	63.7527	29.2946	0.9031	0.0393
70	0.79	1	13	550.914	6.58805	66.3317	28.4793	0.9351	0.0298
70	0.79	2	14	612.8232	6.551957	70.1753	29.356	0.933	0.0287
70	0.79	3	15	674.7325	6.764686	72.0691	29.7986	0.932	0.031
40	0.32	1	16	699.8096	2.113286	52.798	30.8152	0.8222	0.07808
40	0.32	2	17	724.8868	2.11605	55.6847	31.2029	0.8344	0.0701
40	0.32	3	18	749.964	2.062079	53.8808	30.6514	0.8285	0.0712
10	0.85	1	19	816.5752	2.495886	61.0584	32.456	0.8952	0.042
10	0.85	2	20	883.1864	2.520514	62.985	29.186	0.8977	0.0434
10	0.85	3	21	949.7976	2.505529	61.0581	29.8639	0.8956	0.0456
100	0.4	1	22	981.1441	8.709564	62.1457	29.551	0.8809	0.051
100	0.4	2	23	1012.491	8.804207	60.9789	31.6326	0.8811	0.0544
100	0.4	3	24	1043.837	8.610229	59.3866	31.1957	0.8812	0.0521
10	0.4	1	25	1075.183	1.690429	52.2744	31.7192	0.7962	0.084
10	0.4	2	26	1106.53	1.685571	52.9881	30.6631	0.7919	0.0855
10	0.4	3	27	1137.876	1.723443	59.5982	32.6467	0.5731	0.1565
100	0.23	1	28	1155.901	5.182893	53.3846	32.1763	0.8251	0.0706
100	0.23	2	29	1173.925	4.542164	42.7674	31.0102	0.6033	0.1334
100	0.23	3	30	1191.949	3.760886	61.7685	31.7414	0.8302	0.073

Mouse 6a Artery

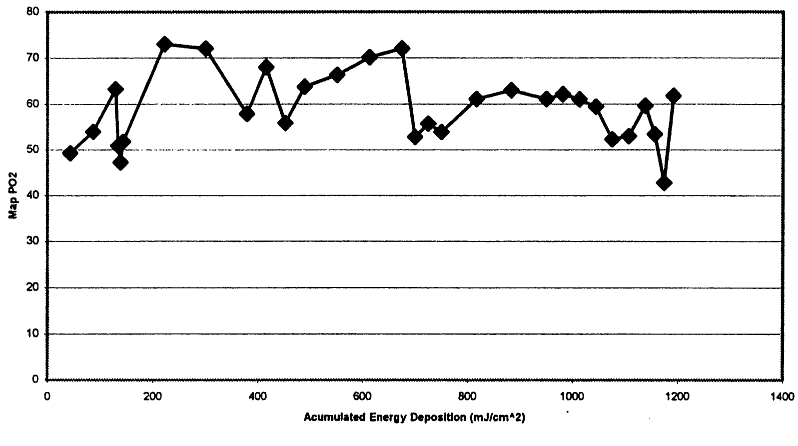

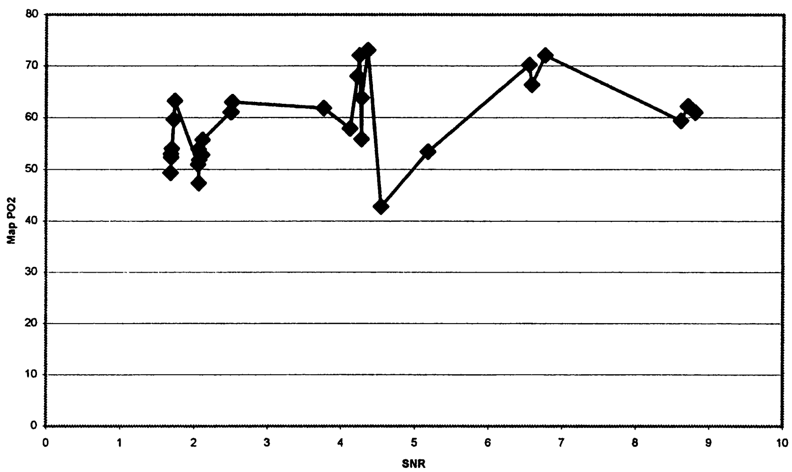

Gain	Exposure T	Relative Ir	Cumulative	Accumulat	SNR	PO2 Mean	PO2 St. De	R2 Mean	R2 St. Dev
10	0.55	1	1	43.10138	1.59845	45.0042	29.1851	0.7246	0.1119
10	0.55	2	2	86.20276	1.575086	51.6795	30.9596	0.7418	0.1035
10	0.55	3	3	129.3041	1.480793	65.2168	33.7728	0.7545	0.1029
100	0.06	1	4	134.0061	1.761621	42.2214	33.8521	0.5307	0.0168
100	0.06	2	5	138.7081	1.798329	38.8014	31.7598	0.4969	0.1708
100	0.06	3	6	143.41	1.77115	31.8993	27.8824	0.5065	0.1622
40	1	1	7	221.7762	3.737871	62.973	30.1596	0.8852	0.0512
40	1	2	8	300.1423	3.698029	62.1602	30.1193	0.9089	0.0396
40	1	3	9	378.5085	3.594121	57.3765	27.5421	0.9029	0.0443
70	0.47	1	10	415.3406	3.6734	65.3405	33.441	0.8398	0.0688
70	0.47	2	11	452.1726	3.74505	56.2466	31.1747	0.8457	0.0689
70	0.47	3	12	489.0047	3.669836	53.4364	30.1142	0.8416	0.0686
70	0.79	1	13	550.914	5.616071	63.4912	30.5935	0.8961	0.0454
70	0.79	2	14	612.8232	5.558986	65.3312	30.5295	0.8959	0.0436
70	0.79	3	15	674.7325	5.400007	68.5534	31.195	0.8979	0.0434
40	0.32	1	16	699.8096	1.866543	53.3638	33.2487	0.7561	0.0984
40	0.32	2	17	724.8868	1.875314	52.4893	32.6618	0.75	0.1013
40	0.32	3	18	749.964	1.861321	50.7679	32.6359	0.7472	0.1015
10	0.85	1	19	816.5752	2.172771	60.5152	32.4011	0.85	0.0736
10	0.85	2	20	883.1864	2.170229	62.1143	32.2467	0.8554	0.0596
10	0.85	3	21	949.7976	2.193186	59.9848	32.0708	0.8482	0.0662
100	0.4	1	22	981.1441	6.969193	57.3756	30.6339	0.837	0.0681
100	0.4	2	23	1012.491	6.822393	60.7537	31.5668	0.8489	0.0622
100	0.4	3	24	1043.837	6.97665	60.2811	31.8092	0.8377	0.0685
10	0.4	1	25	1075.183	1.584471	48.2846	30.6572	0.7309	0.1075
10	0.4	2	26	1106.53	1.533786	53.0867	32.2792	0.741	0.1042
10	0.4	3	27	1137.876	1.472107	65.0854	33.8918	0.7595	0.1016
100	0.23	1	28	1155.901	4.37225	53.9694	31.3088	0.7872	0.0858
100	0.23	2	29	1173.925	3.440464	53.8152	32.6526	0.726	0.1056
100	0.23	3	30	1191.949	3.291336	58.3846	32.8472	0.7777	0.0897

Mouse 6a Tissue

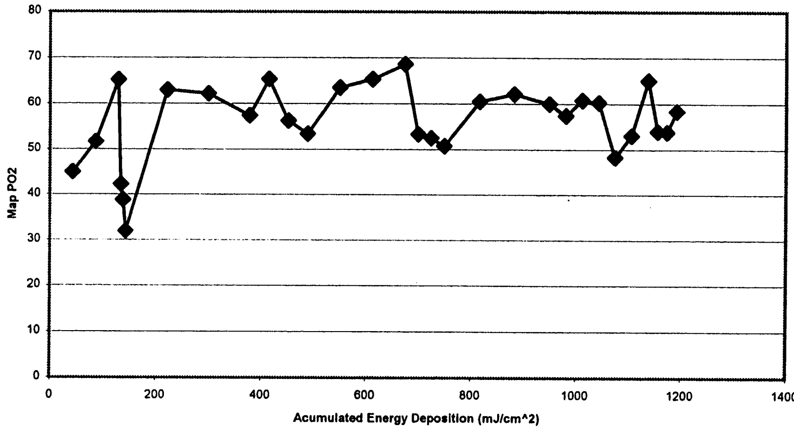

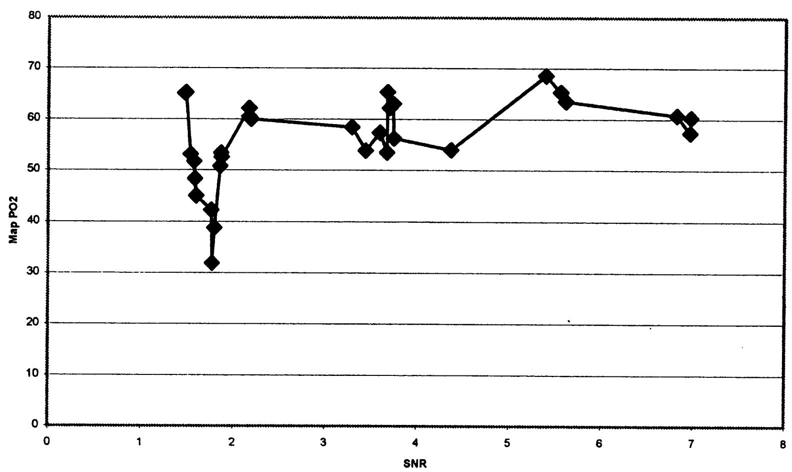

Gain	Exposure T	Relative Ir	Cumulative	Accumulate	SNR	PO2 Mean	PO2 St. De	R2 Mean	R2 St. Dev
40	0.32	1	1	4.606299	2.252593	68.8044	31.2106	0.916	0.0405
40	0.32	2	2	29.17323	2.912644	93.8139	22.9927	0.8931	0.0465
40	0.32	3	3	53.74016	2.362837	71.1036	31.2493	0.9292	0.0314
40	0.49	1	4	91.35827	3.313741	18.1823	8.0122	0.8052	0.0672
40	0.49	2	5	128.9764	2.9376	74.3462	29.6955	0.9386	0.0271
40	0.49	3	6	166.5945	3.087667	22.5538	7.59	0.8945	0.0417
40	0.66	1	7	217.2638	3.759141	31.5466	12.2421	0.8942	0.0387
40	0.66	2	8	267.9331	4.195222	110.3499	24.81	0.9695	0.0146
40	0.66	3	9	318.6024	4.097644	17.6724	9.503	0.8417	0.0682
40	0.83	1	10	382.3228	4.3604	35.4445	18.2562	0.8673	0.0472
40	0.83	2	11	446.0433	4.583022	71.9903	26.6711	0.8998	0.0329
40	0.83	3	12	509.7638	4.093296	88.2576	29.4925	0.9599	0.0185
40	1	1	13	586.5354	4.306659	16.1251	3.4174	0.8952	0.0357
40	1	2	14	663.3071	6.176689			0.9434	0.0197
40	1	3	15	740.0787	4.084481	16.8419	3.2154	0.9454	0.0225
100	0.06	1	16	744.685	2.246259	64.9049	32.8002	0.8072	0.0835
100	0.06	2	17	749.2913	2.219704	42.3699	26.7311	0.8079	0.0758
100	0.06	3	18	753.8976	2.238489	61.0427	32.2805	0.8101	0.0765
100	0.145	1	19	765.0295	3.746904	43.5304	24.0178	0.8875	0.0467
100	0.145	2	20	776.1614	3.935844	36.1372	20.3349	0.8912	0.0447
100	0.145	3	21	787.2933	3.687874	42.6731	23.6777	0.885	0.0474
100	0.23	1	22	804.9508	6.038437	87.2633	29.6702	0.9194	0.0361
100	0.23	2	23	822.6083	5.688748	70.2286	31.1108	0.8894	0.0461
100	0.23	3	24	840.2657	5.29257	68.2215	31.8766	0.8955	0.0461
100	0.315	1	25	864.4488	6.240437	51.9048	27.1945	0.8963	0.0429
100	0.315	2	26	888.6319	6.65763	39.9473	21.8943	0.894	0.0455
100	0.315	3	27	912.815	7.455037	59.0961	30.0235	0.8604	0.0563
100	0.4	1	28	943.5236	9.219007	94.2311	28.8572	0.835	0.0287
70	0.15	1	29	955.0394	2.046859	51.2416	31.2838	0.7728	0.0908
70	0.15	2	30	966.5551	2.103807	60.2566	30.4709	0.8473	0.0682
70	0.15	3	31	978.0709	2.057526	58.6069	31.2342	0.7996	0.0821
70	0.31	1	32	1001.87	3.057415	69.5822	31.6809	0.9031	0.0419
70	0.31	2	33	1025.669	3.031607	66.3983	29.546	0.9103	0.0378
70	0.31	3	34	1049.469	3.132519	52.9377	28.4965	0.8567	0.0581
70	0.47	1	35	1085.551	4.344667	87.2942	29.948	0.9464	0.0238
70	0.47	2	36	1121.634	4.756748	84.5099	30.4683	0.93	0.0312
70	0.47	3	37	1157.717	3.872119	33.8376	14.7263	0.9166	0.0342
70	0.63	1	38	1206.083	6.0336	93.6515	29.4582	0.9305	0.0293
70	0.63	2	39	1254.449	4.875333	85.1731	30.1613	0.9523	0.0215
70	0.63	3	40	1302.815	4.334222	29.5939	9.4831	0.9366	0.0253
70	0.79	1	41	1363.465	5.669956	34.4212	10.1276	0.9564	0.019
70	0.79	2	42	1424.114	6.588274	70.0455	26.2873	0.9267	0.0273
70	0.79	3	43	1484.764	6.216778	49.1708	21.5662	0.9311	0.0271
10	0.4	1	44	1515.472	1.733859	75.2444	32.2363	0.8833	0.0502
10	0.4	2	45	1546.181	1.6388	46.0037	25.2196	0.8889	0.0481
10	0.4	3	46	1576.89	1.7436	70.4221	34.0038	0.8644	0.0549
10	0.55	1	47	1619.114	1.907163	63.6227	29.8465	0.9001	0.0431
10	0.55	2	48	1661.339	1.9518	70.7966	31.3566	0.9186	0.0349
10	0.55	3	49	1703.563	1.873022	59.425	28.1104	0.9051	0.0413
10	0.7	1	50	1757.303	2.156059	85.6312	29.4138	0.9374	0.0273
10	0.7	2	51	1811.043	2.239696	68.6899	31.5558	0.8794	0.0509
10	0.7	3	52	1864.783	2.457726	64.1286	31.8605	0.7605	0.0918
10	0.85	1	53	1930.039	2.359963	70.6842	29.5201	0.9374	0.0276
10	0.85	2	54	1995.295	2.371037	73.0027	30.0614	0.9367	0.0278
10	0.85	3	55	2060.551	2.319556	58.2536	27.1059	0.9188	0.0347
10	1	1	56	2137.323	2.067259	11.1294	2.1751	0.894	0.0326
10	1	2	57	2214.094	2.626778	54.75	25.4091	0.9178	0.0338
10	1	3	58	2290.866	2.597156	64.1275	27.2512	0.9288	0.0275

Mouse 7a Vein

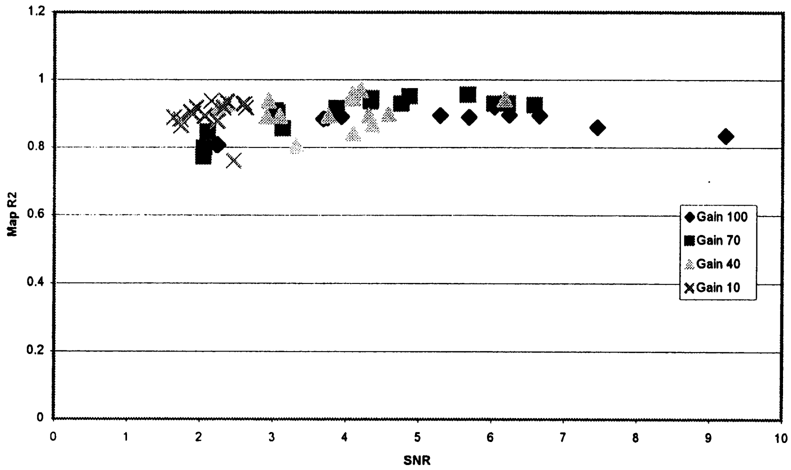

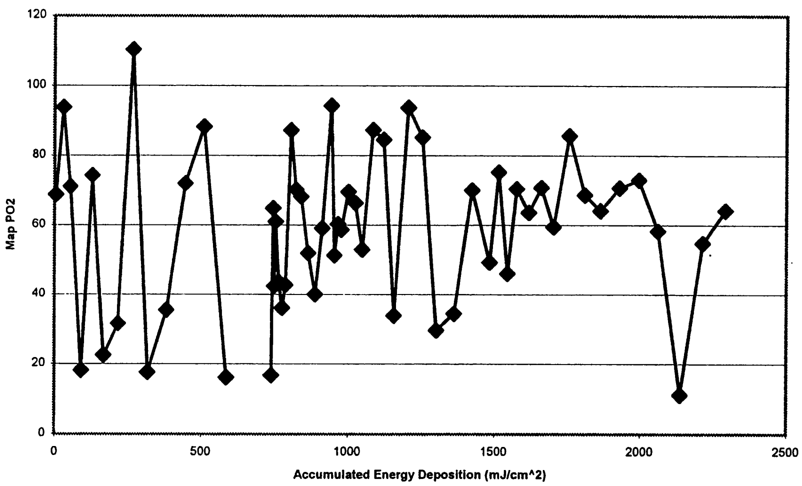

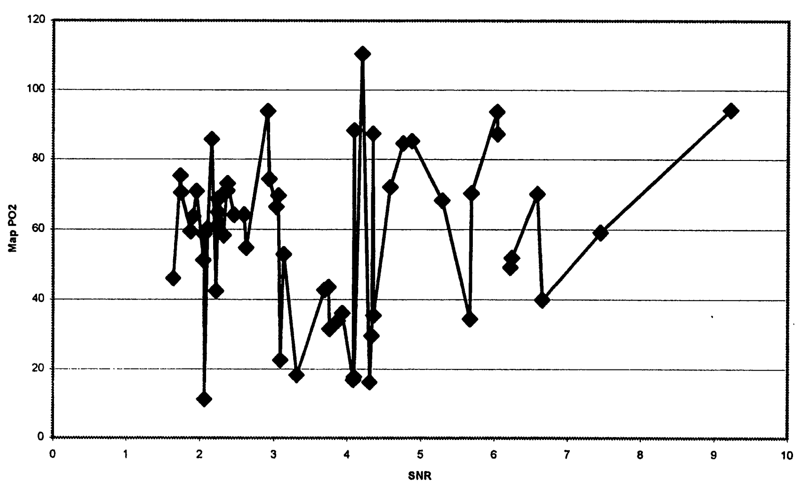

Mouse7a

Gain	Exposure T	Relative Im	Cumulative	Accumulat	SNR	PO2 Mean	PO2 St. De	R2 Mean	R2 St. Dev
40	0.32	1	1	4.606299	1.683548	70.8455	30.6055	0.8755	0.0567
40	0.32	2	2	29.17323	2.092867	109.2541	38.9873	0.8609	0.0577
40	0.32	3	3	53.74016	1.70603	65.4583	30.5117	0.9023	0.0436
40	0.49	1	4	91.35827	2.13297	29.8225	15.9387	0.8525	0.0565
40	0.49	2	5	128.9764	2.090467	80.8359	32.6677	0.9106	0.038
40	0.49	3	6	166.5945	2.123956	35.2091	18.5705	0.8542	0.0495
40	0.66	1	7	217.2638	2.288556	34.5426	17.6597	0.8929	0.045
40	0.66	2	8	267.9331	2.558867	102.0563	28.6738	0.9522	0.0222
40	0.66	3	9	318.6024	2.528215	25.5898	12.69	0.8706	0.0523
40	0.83	1	10	382.3228	2.713681	47.9954	24.9178	0.8683	0.051
40	0.83	2	11	446.0433	2.59	49.2206	22.6919	0.8982	0.0378
40	0.83	3	12	509.7638	2.617644	91.487	31.7326	0.9345	0.0305
40	1	1	13	586.5354	2.700844	23.0843	6.8782	0.9129	0.0317
40	1	2	14	663.3071	3.329741	113.1708	21.8803	0.9041	0.0339
40	1	3	15	740.0787	2.706133	26.42	7.7907	0.9232	0.0325
100	0.06	1	16	744.685	1.730644	69.7565	32.0596	0.751	0.1026
100	0.06	2	17	749.2913	1.699215	52.8509	31.8979	0.7383	0.1031
100	0.06	3	18	753.8976	1.737563	69.9195	32.8344	0.7611	0.1022
100	0.145	1	19	765.0295	2.649933	66.4552	30.6936	0.8489	0.0647
100	0.145	2	20	776.1614	2.678733	56.4394	29.1715	0.8523	0.0619
100	0.145	3	21	787.2933	2.516904	67.323	32.3404	0.8276	0.0752
100	0.23	1	22	804.9508	3.2918	62.1198	30.8858	0.8616	0.0615
100	0.23	2	23	822.6083	3.403215	64.044	34.0146	0.82	0.0772
100	0.23	3	24	840.2657	3.348533	69.9095	33.634	0.8372	0.0727
100	0.315	1	25	864.4488	3.112889	48.6219	27.658	0.8539	0.0569
100	0.315	2	26	888.6319	3.726667	38.4066	22.0276	0.8561	0.0596
100	0.315	3	27	912.815	4.166615	52.0204	29.6071	0.8271	0.0683
100	0.4	1	28	943.5236	5.740933	97.6957	25.6182	0.9102	0.0387
70	0.15	1	29	955.0394	1.550393	41.8279	27.4844	0.7219	0.1023
70	0.15	2	30	966.5551	1.559015	52.0781	31.1217	0.77	0.094
70	0.15	3	31	978.0709	1.589844	55.3086	31.3081	0.7057	0.1217
70	0.31	1	32	1001.87	2.189637	70.9532	34.4801	0.8472	0.0636
70	0.31	2	33	1025.669	2.104674	62.4106	30.1482	0.8676	0.0567
70	0.31	3	34	1049.469	2.087281	42.4885	25.2776	0.8108	0.0743
70	0.47	1	35	1085.551	2.784081	77.8774	31.3127	0.9147	0.038
70	0.47	2	36	1121.634	3.00583	80.8444	32.0801	0.889	0.0474
70	0.47	3	37	1157.717	2.722074	49.8552	24.7003	0.8827	0.0473
70	0.63	1	38	1206.083	3.826711	81.2233	29.8977	0.9007	0.0457
70	0.63	2	39	1254.449	3.255156	83.2558	29.6647	0.9241	0.0335
70	0.63	3	40	1302.815	2.968852	38.5874	17.805	0.9089	0.0359
70	0.79	1	41	1363.465	3.773815	53.7616	21.4293	0.9377	0.0261
70	0.79	2	42	1424.114	4.106644	79.8841	31.1844	0.9123	0.0363
70	0.79	3	43	1484.764	3.972096	59.8501	27.487	0.9091	0.0357
10	0.4	1	44	1515.472	1.424985	61.8534	31.6675	0.7936	0.0833
10	0.4	2	45	1546.181	1.405481	59.5395	31.7441	0.8325	0.0685
10	0.4	3	46	1576.89	1.428341	57.2696	30.5162	0.778	0.0948
10	0.55	1	47	1619.114	1.543726	66.0749	34.059	0.8492	0.0651
10	0.55	2	48	1661.339	1.545652	66.5736	34.1983	0.8652	0.0552
10	0.55	3	49	1703.563	1.486637	54.8662	29.4067	0.8387	0.0719
10	0.7	1	50	1757.303	1.687356	80.1336	34.1151	0.8963	0.0459
10	0.7	2	51	1811.043	1.765274	67.9196	34.4058	0.8382	0.0659
10	0.7	3	52	1864.783	1.847481	56.4528	31.6574	0.7742	0.0955
10	0.85	1	53	1930.039	1.802681	67.5455	31.3095	0.9001	0.0432
10	0.85	2	54	1995.295	1.845844	70.3832	31.0639	0.8983	0.0445
10	0.85	3	55	2060.551	1.851563	61.9221	31.323	0.8894	0.0494
10	1	1	56	2137.323	1.762511	19.3637	5.7828	0.8948	0.0379
10	1	2	57	2214.094	2.028289	59.6783	28.4991	0.892	0.0437
10	1	3	58	2290.866	2.023119	63.3193	29.3132	0.9056	0.0399

Artery (2)

Mouse 7a Artery

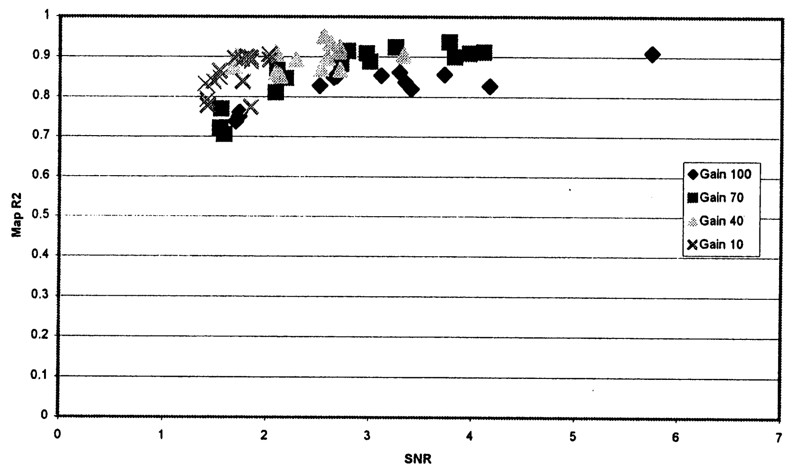

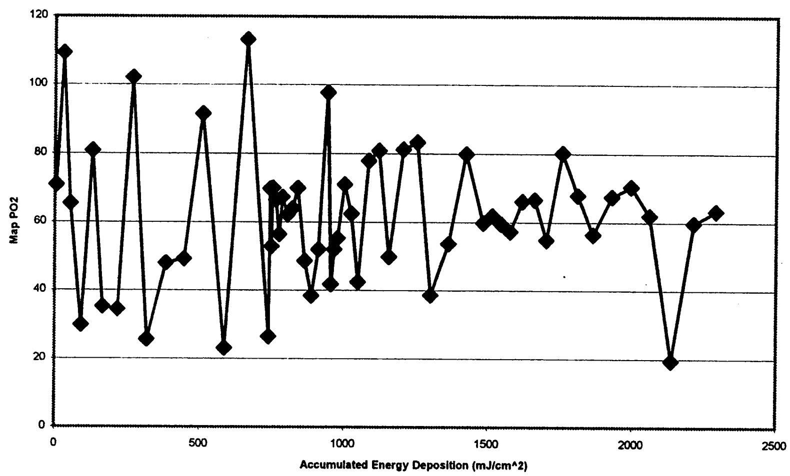

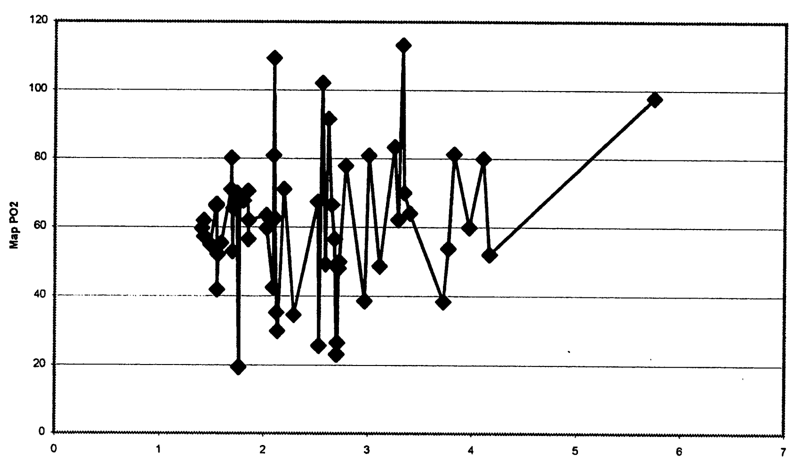

Gain	Exposure 1	Relative Ir	Cumulative	Accumulat	SNR	PO2 Mean	PO2 St. De	R2 Mean	R2 St. Dev
40	0.32	1	1	4.606299	1.38543	66.0312	34.0154	0.8019	0.0801
40	0.32	2	2	29.17323	1.544096	77.784	33.3576	0.7984	0.0865
40	0.32	3	3	53.74016	1.416889	62.688	31.9904	0.823	0.0719
40	0.49	1	4	91.35827	1.660963	47.4943	28.0336	0.8263	0.0673
40	0.49	2	5	128.9764	1.642496	71.4634	31.565	0.8724	0.0566
40	0.49	3	6	166.5945	1.634148	55.2751	30.2666	0.8556	0.0587
40	0.66	1	7	217.2638	1.82417	58.1615	29.6712	0.8791	0.0518
40	0.66	2	8	267.9331	1.928259	90.7991	28.4605	0.9262	0.0312
40	0.66	3	9	318.6024	1.865067	51.7046	29.5919	0.8526	0.0621
40	0.83	1	10	382.3228	1.988756	67.5634	31.8492	0.8815	0.0488
40	0.83	2	11	446.0433	2.036185	75.6843	32.2844	0.9023	0.0413
40	0.83	3	12	509.7638	1.978185	86.6363	33.1054	0.9153	0.037
40	1	1	13	586.5354	2.062859	50.3835	27.2298	0.9076	0.0398
40	1	2	14	663.3071	2.318941	101.0003	27.5538	0.9217	0.0333
40	1	3	15	740.0787	2.136119	46.2956	23.7173	0.919	0.0358
100	0.06	1	16	744.685	1.423081	53.9747	34.1192	0.6485	0.1384
100	0.06	2	17	749.2913	1.419022	46.7842	32.3321	0.6581	0.1322
100	0.06	3	18	753.8976	1.457985	58.1187	35.4562	0.6711	0.1368
100	0.145	1	19	765.0295	1.943185	59.3999	32.5927	0.7741	0.0911
100	0.145	2	20	776.1614	1.999956	53.8148	31.4264	0.7854	0.0876
100	0.145	3	21	787.2933	1.986556	57.6375	31.4136	0.7769	0.091
100	0.23	1	22	804.9508	2.573422	63.691	33.1865	0.8236	0.0789
100	0.23	2	23	822.6083	2.591556	65.2326	33.3333	0.8036	0.0808
100	0.23	3	24	840.2657	2.569689	64.4844	32.7098	0.8132	0.0796
100	0.315	1	25	864.4488	2.987637	62.2819	33.5227	0.8393	0.0671
100	0.315	2	26	888.6319	2.958793	53.9284	32.0208	0.8356	0.0693
100	0.315	3	27	912.815	3.329785	57.3698	30.9929	0.8218	0.0713
100	0.4	1	28	943.5236	3.900837	80.4918	32.299	0.8865	0.0491
70	0.15	1	29	955.0394	1.389541	47.1028	31.6236	0.6685	0.1315
70	0.15	2	30	966.5551	1.391104	51.3252	33.1651	0.6993	0.121
70	0.15	3	31	978.0709	1.422733	53.9557	34.0287	0.673	0.1277
70	0.31	1	32	1001.87	1.880622	68.3289	33.6593	0.8284	0.0736
70	0.31	2	33	1025.669	1.812652	65.1475	33.7344	0.8275	0.0745
70	0.31	3	34	1049.469	1.809904	58.0019	33.8576	0.7819	0.0912
70	0.47	1	35	1085.551	2.259415	76.3864	32.7919	0.885	0.0515
70	0.47	2	36	1121.634	2.272785	71.3931	31.5558	0.8626	0.0582
70	0.47	3	37	1157.717	2.238052	57.2309	31.1347	0.8702	0.056
70	0.63	1	38	1206.083	2.8646	80.5134	32.2844	0.8855	0.0483
70	0.63	2	39	1254.449	2.664081	77.7624	31.2216	0.9051	0.0429
70	0.63	3	40	1302.815	2.443696	55.4961	29.5883	0.8942	0.0468
70	0.79	1	41	1363.465	2.969593	61.0717	27.5278	0.9228	0.0326
70	0.79	2	42	1424.114	3.354763	75.4166	31.4166	0.9113	0.0375
70	0.79	3	43	1484.764	3.187311	65.5874	29.784	0.907	0.0395
10	0.4	1	44	1515.472	1.322274	60.1128	34.4292	0.7419	0.104
10	0.4	2	45	1546.181	1.297756	55.1515	33.5696	0.7518	0.108
10	0.4	3	46	1576.89	1.322837	58.3417	33.2074	0.7267	0.1143
10	0.55	1	47	1619.114	1.401081	62.4011	33.4096	0.7972	0.0854
10	0.55	2	48	1661.339	1.405526	64.5927	31.8958	0.8138	0.0798
10	0.55	3	49	1703.563	1.382644	56.8192	33.579	0.8094	0.0792
10	0.7	1	50	1757.303	1.517896	72.3317	32.0207	0.8654	0.0602
10	0.7	2	51	1811.043	1.504911	63.9293	32.8963	0.8061	0.0822
10	0.7	3	52	1864.783	1.6104	57.8424	32.2302	0.7542	0.0989
10	0.85	1	53	1930.039	1.60317	64.5091	30.9498	0.8706	0.0561
10	0.85	2	54	1995.295	1.595178	64.1368	31.8819	0.8606	0.0588
10	0.85	3	55	2060.551	1.668993	62.107	32.464	0.8644	0.057
10	1	1	56	2137.323	1.622763	25.8606	13.2643	0.8809	0.0464
10	1	2	57	2214.094	1.730674	61.6675	30.8714	0.8689	0.0567
10	1	3	58	2290.866	1.725452	66.1538	32.1491	0.8773	0.0522

Mouse 7a Tissue

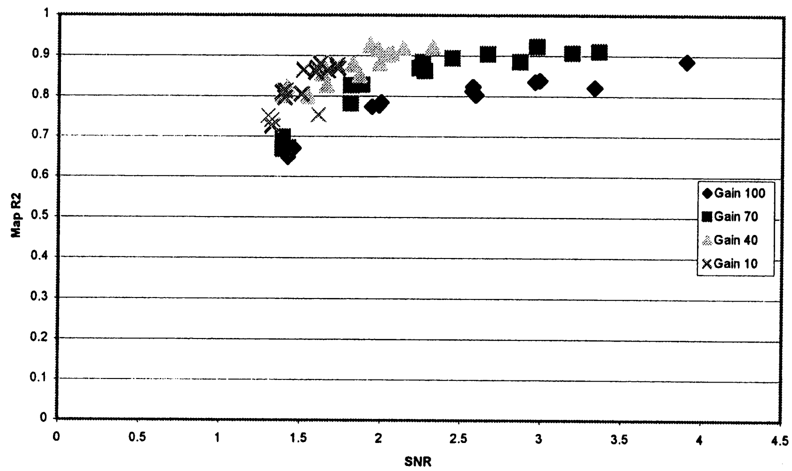

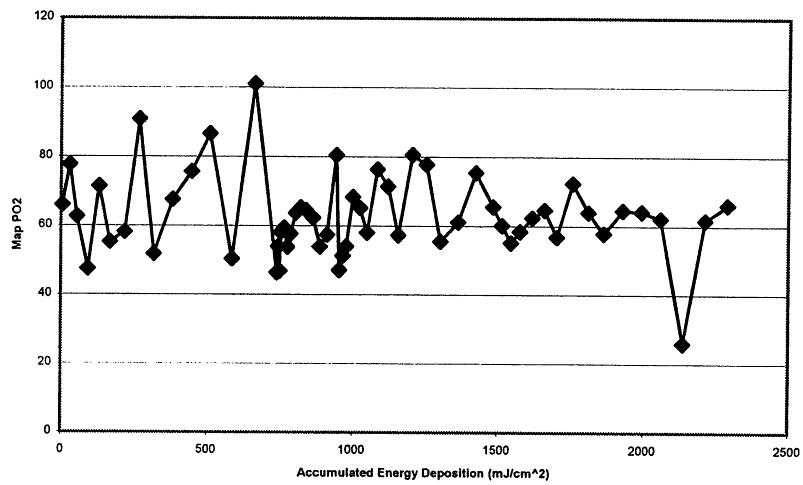

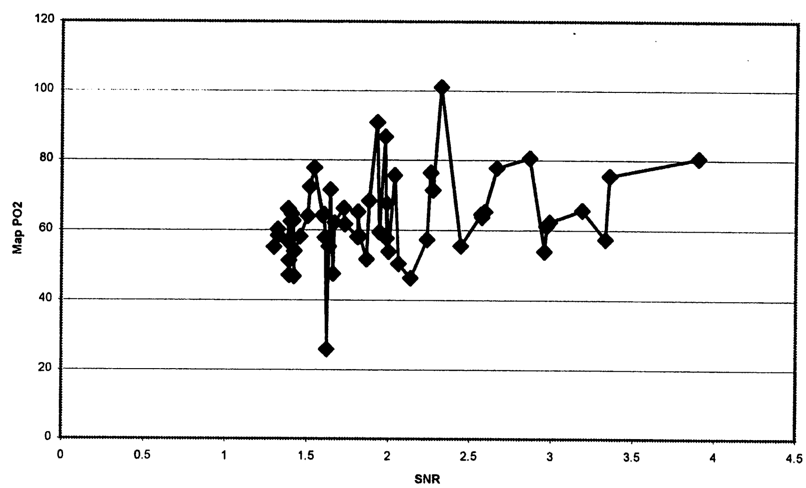

Gain	Exposure T	Relative Im	Cumulative	Accumulat	SNR	PO2 Mean	PO2 St. De	R2 Mean	R2 St. Dev
100	0.06	1	1	4.54252	2.043363	51.2522	32.5461	0.7657	0.0993
100	0.06	2	2	9.085039	2.060933	48.1868	31.5843	0.7313	0.1103
100	0.06	3	3	13.62756	2.054281	47.5757	31.4819	0.7309	0.1092
100	0.145	1	4	24.60531	3.756933	59.2386	31.5466	0.8593	0.0599
100	0.145	2	5	35.58307	3.577726	55.1357	30.7004	0.8557	0.0602
100	0.145	3	6	46.56083	3.558311	51.7116	29.1017	0.8449	0.0649
100	0.23	1	7	63.97382	5.109081	55.4518	29.0772	0.8961	0.046
100	0.23	2	8	81.38681	5.036807	56.982	30.9034	0.8872	0.0476
100	0.23	3	9	98.7998	5.018837	53.1879	27.7022	0.8901	0.0458
100	0.315	1	10	122.648	7.346926	49.7864	24.8386	0.9189	0.0347
100	0.315	2	11	146.4963	7.314015	52.3969	24.8752	0.9223	0.034
100	0.315	3	12	170.3445	7.181674	54.1517	26.7849	0.9161	0.0361
100	0.4	1	13	200.628	8.989585	52.9003	24.4024	0.9378	0.0273
100	0.4	2	14	230.9114	8.512652	46.0958	22.0689	0.9347	0.0293
100	0.4	3	15	261.1949	8.908911	52.0602	23.8576	0.9349	0.0279
70	0.15	1	16	272.5512	2.091956	47.7034	28.271	0.8326	0.0706
70	0.15	2	17	283.9075	2.101385	48.7137	28.187	0.8245	0.0719
70	0.15	3	18	295.2638	2.139459	48.9345	29.2114	0.832	0.0704
70	0.31	1	19	318.7335	3.31497	53.7492	27.7283	0.9057	0.0407
70	0.31	2	20	342.2031	3.311104	51.7378	26.8534	0.9081	0.0415
70	0.31	3	21	365.6728	3.18703	49.638	26.3136	0.9016	0.043
70	0.47	1	22	401.2559	4.495763	54.4591	25.8896	0.9321	0.0304
70	0.47	2	23	436.839	3.996444	61.1229	27.2159	0.9332	0.0279
70	0.47	3	24	472.422	3.949319	61.0035	28.2116	0.9323	0.0292
70	0.63	1	25	520.1185	4.727763	58.693	25.4072	0.9449	0.0237
70	0.63	2	26	567.815	4.782474	57.4444	25.6168	0.9432	0.0243
70	0.63	3	27	615.5114	4.746578	58.75	26.2106	0.9448	0.0243
70	0.79	1	28	675.3213	5.785104	64.7497	26.3841	0.9547	0.0194
70	0.79	2	29	735.1311	5.890881	60.0488	24.4148	0.9542	0.0205
70	0.79	3	30	794.9409	5.915519	61.4809	24.3235	0.9558	0.0189
40	0.32	1	31	819.1677	1.99837	58.3149	31.9065	0.8808	0.0514
40	0.32	2	32	843.3945	1.9532	53.2416	28.45	0.8767	0.0518
40	0.32	3	33	867.6213	1.935326	54.2847	28.6299	0.8758	0.0551
40	0.49	1	34	904.7185	2.452867	59.4933	30.2921	0.9107	0.0339
40	0.49	2	35	941.8157	2.395215	58.5932	28.9138	0.9103	0.0405
40	0.49	3	36	978.913	2.482926	59.7318	29.6266	0.9183	0.0359
40	0.66	1	37	1028.881	2.93803	56.9624	26.015	0.9336	0.0285
40	0.66	2	38	1078.848	2.959311	56.1154	26.2368	0.9336	0.0292
40	0.66	3	39	1128.816	2.962926	59.6643	27.3152	0.9312	0.0299
40	0.83	1	40	1191.654	3.324244	57.2343	24.2672	0.944	0.0246
40	0.83	2	41	1254.493	3.297748	60.4372	26.3299	0.9432	0.0248
40	0.83	3	42	1317.331	3.368489	58.6195	25.1595	0.9424	0.0249
40	1	1	43	1393.039	3.702393	58.2919	25.1145	0.9515	0.0208
40	1	2	44	1468.748	3.708593	65.2939	26.4707	0.9517	0.0218
40	1	3	45	1544.457	3.851319	55.7396	23.2156	0.9533	0.0203
10	0.4	1	46	1574.74	1.578615	52.3828	28.6463	0.8615	0.0566
10	0.4	2	47	1605.024	1.576244	52.8995	29.344	0.8632	0.0592
10	0.4	3	48	1635.307	1.583119	54.5037	29.6446	0.8599	0.059
10	0.55	1	49	1676.947	1.758985	58.0021	29.2707	0.8896	0.0479
10	0.55	2	50	1718.587	1.787104	55.8741	28.8495	0.8944	0.0451
10	0.55	3	51	1760.226	1.745015	53.9976	28.5266	0.8927	0.0471
10	0.7	1	52	1813.222	1.913481	56.4832	28.5009	0.9069	0.0408
10	0.7	2	53	1866.219	1.946533	57.1108	28.0541	0.9103	0.0397
10	0.7	3	54	1919.215	1.915956	54.4318	26.9905	0.909	0.0378
10	0.85	1	55	1983.567	2.141689	60.0487	28.0802	0.9245	0.0326
10	0.85	2	56	2047.919	2.075622	56.8497	26.839	0.9215	0.0328
10	0.85	3	57	2112.272	2.11877	57.8371	27.5946	0.9215	0.0359
10	1	1	58	2187.98	2.264356	59.345	27.4214	0.9323	0.0294
10	1	2	59	2263.689	2.264926	60.1358	26.505	0.9312	0.0286
10	1	3	60	2339.398	2.245711	57.9603	26.4987	0.9306	0.0302

Mouse 8a Vein

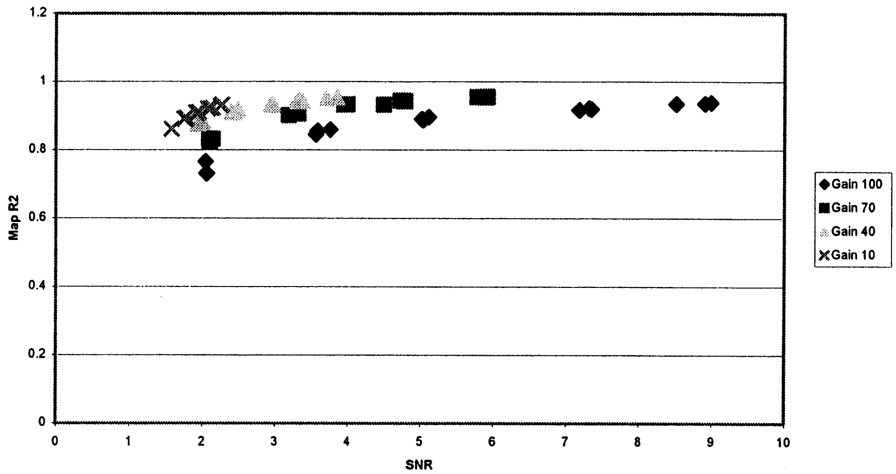

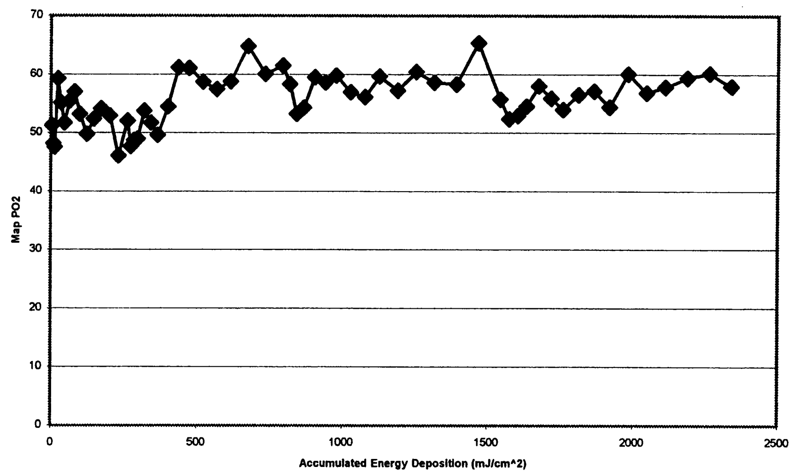

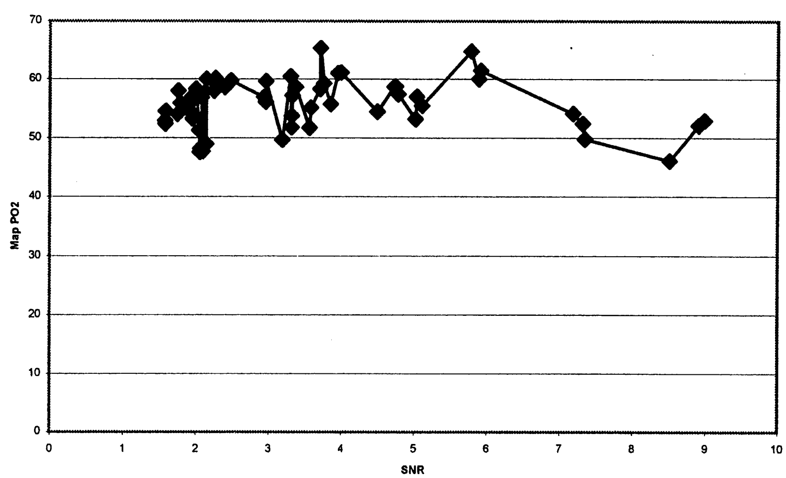

Gain	Exposure T	Relative Im	Cumulative	Accumulat	SNR	PO2 Mean	PO2 St. De	R2 Mean	R2 St. Dev
100	0.06	1	1	4.54252	1.689133	52.1644	32.5389	0.7251	0.1117
100	0.06	2	2	9.085039	1.7336	53.0021	33.1555	0.7375	0.1026
100	0.06	3	3	13.62756	1.742874	51.3431	30.5347	0.7306	0.1135
100	0.145	1	4	24.60531	2.808822	62.927	32.2955	0.8405	0.066
100	0.145	2	5	35.58307	2.774763	63.0811	32.674	0.841	0.0638
100	0.145	3	6	46.56083	2.737185	63.7751	32.9013	0.8402	0.0685
100	0.23	1	7	63.97382	3.770526	66.4799	31.2111	0.8904	0.0483
100	0.23	2	8	81.38681	3.755533	67.219	31.5977	0.8829	0.0504
100	0.23	3	9	98.7998	3.759215	70.2678	31.6941	0.8925	0.0483
100	0.315	1	10	122.648	4.630126	65.441	29.8351	0.9097	0.0389
100	0.315	2	11	146.4963	4.905785	67.4619	29.9911	0.9142	0.0364
100	0.315	3	12	170.3445	4.629519	67.0081	30.9477	0.9099	0.0392
100	0.4	1	13	200.628	5.705681	67.2509	29.7154	0.9265	0.033
100	0.4	2	14	230.9114	5.516719	68.0288	31.7979	0.9273	0.0307
100	0.4	3	15	261.1949	5.501074	67.7005	30.0347	0.9229	0.0348
70	0.15	1	16	272.5512	1.675822	59.8028	31.0707	0.8176	0.0745
70	0.15	2	17	283.9075	1.678763	56.065	30.516	0.8169	0.0743
70	0.15	3	18	295.2638	1.696193	61.169	32.6118	0.8234	0.0787
70	0.31	1	19	318.7335	2.41583	70.5662	32.7382	0.8985	0.0437
70	0.31	2	20	342.2031	2.378474	64.969	29.9347	0.8896	0.0476
70	0.31	3	21	365.6728	2.333822	65.8583	32.8095	0.8938	0.0454
70	0.47	1	22	401.2559	2.997615	65.7786	28.0036	0.9252	0.0333
70	0.47	2	23	436.839	3.017874	71.8051	29.6283	0.9216	0.0354
70	0.47	3	24	472.422	2.973022	72.5883	30.323	0.9163	0.0367
70	0.63	1	25	520.1185	3.592215	76.6084	31.32	0.9361	0.0284
70	0.63	2	26	567.815	3.619156	70.9096	29.8143	0.9345	0.0279
70	0.63	3	27	615.5114	3.606407	73.7711	30.7518	0.9304	0.03
70	0.79	1	28	675.3213	4.295281	75.7892	29.7497	0.9463	0.024
70	0.79	2	29	735.1311	4.256904	74.358	29.3394	0.9457	0.0241
70	0.79	3	30	794.9409	4.263778	75.2624	29.8057	0.944	0.0238
40	0.32	1	31	819.1677	1.719015	63.0575	31.2391	0.8677	0.055
40	0.32	2	32	843.3945	1.671622	65.743	32.5224	0.8653	0.0537
40	0.32	3	33	867.6213	1.677726	62.4427	30.9485	0.861	0.0594
40	0.49	1	34	904.7185	2.060993	66.0117	28.7913	0.9024	0.0381
40	0.49	2	35	941.8157	2.008822	67.8351	30.0332	0.9008	0.0435
40	0.49	3	36	978.913	2.030911	63.5411	30.131	0.8984	0.0421
40	0.66	1	37	1028.881	2.343044	73.0713	31.9102	0.9226	0.0347
40	0.66	2	38	1078.848	2.380163	67.6297	30.8956	0.9241	0.0327
40	0.66	3	39	1128.816	2.285726	70.2035	30.2747	0.9171	0.0345
40	0.83	1	40	1191.654	2.659096	73.2779	30.2291	0.9341	0.0287
40	0.83	2	41	1254.493	2.699689	71.7243	30.4414	0.9334	0.0297
40	0.83	3	42	1317.331	2.696096	70.5876	28.8809	0.9358	0.0293
40	1	1	43	1393.039	2.959156	73.3168	29.1648	0.9443	0.0233
40	1	2	44	1468.748	3.001519	69.9585	27.4935	0.9425	0.0248
40	1	3	45	1544.457	3.037867	76.9408	29.8755	0.9458	0.0226
10	0.4	1	46	1574.74	1.451067	59.5751	32.0203	0.8433	0.0659
10	0.4	2	47	1605.024	1.435281	59.121	31.8087	0.839	0.0663
10	0.4	3	48	1635.307	1.42597	54.2659	31.4928	0.8328	0.0718
10	0.55	1	49	1676.947	1.563756	64.1448	32.4539	0.8725	0.0522
10	0.55	2	50	1718.587	1.586489	62.9891	30.8988	0.8781	0.0515
10	0.55	3	51	1760.226	1.565719	65.3893	33.0551	0.8741	0.0544
10	0.7	1	52	1813.222	1.743089	66.5638	29.6604	0.8995	0.0417
10	0.7	2	53	1866.219	1.691289	67.5443	32.3446	0.8924	0.0457
10	0.7	3	54	1919.215	1.706126	67.2317	31.4161	0.8935	0.0476
10	0.85	1	55	1983.567	1.829096	65.4657	29.9242	0.9093	0.0395
10	0.85	2	56	2047.919	1.858007	66.3008	30.2654	0.9149	0.0358
10	0.85	3	57	2112.272	1.845096	68.2785	30.7638	0.9137	0.0367
10	1	1	58	2187.98	1.998415	72.8268	30.5513	0.9244	0.0351
10	1	2	59	2263.689	1.951222	69.7145	29.6427	0.9196	0.0357
10	1	3	60	2339.398	1.992756	72.2702	30.568	0.9246	0.0343

Mouse 8a Artery

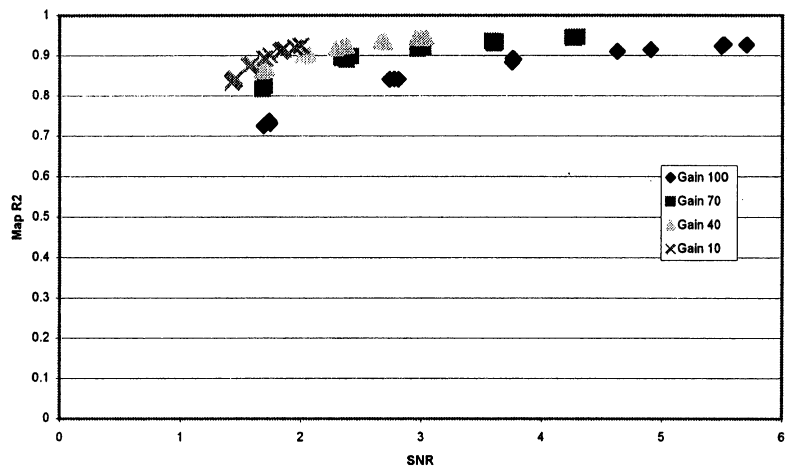

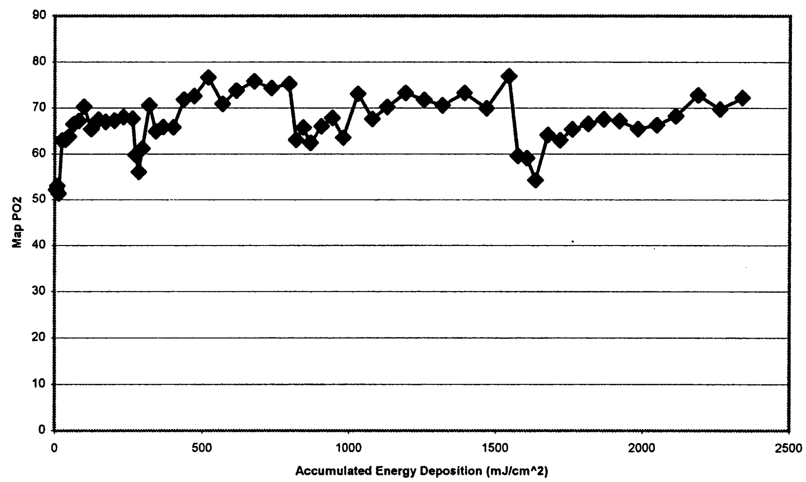

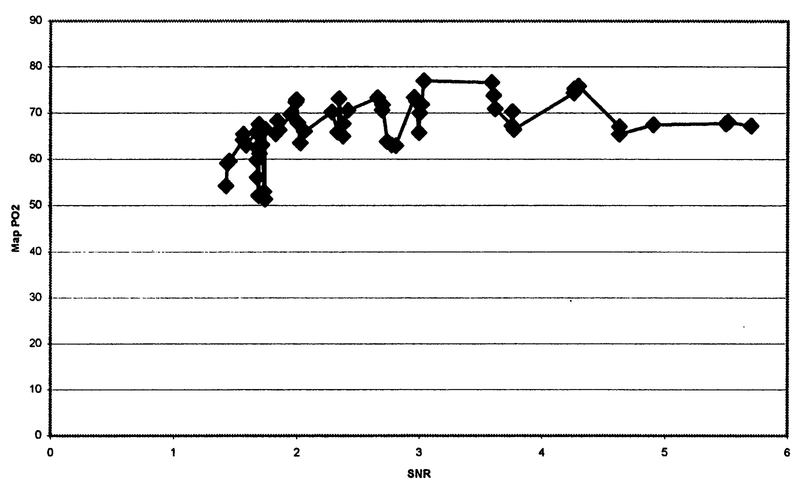

Gain	Exposure T	Relative Ir	Cumulative	Accumulat	SNR	PO2 Mean	PO2 St. De	R2 Mean	R2 St. Dev
100	0.06	1	1	4.54252	1.321148	48.438	34.3619	0.6361	0.1464
100	0.06	2	2	9.085039	1.332244	47.9535	31.4493	0.6369	0.1419
100	0.06	3	3	13.62756	1.37483	50.1646	32.5265	0.6702	0.1259
100	0.145	1	4	24.60531	1.890274	65.5605	35.3906	0.7903	0.0934
100	0.145	2	5	35.58307	1.832244	67.3054	34.6884	0.7907	0.0894
100	0.145	3	6	46.56083	1.902489	59.696	34.329	0.7925	0.0925
100	0.23	1	7	63.97382	2.491437	72.3287	32.8979	0.8615	0.0624
100	0.23	2	8	81.38681	2.376304	71.6752	32.7111	0.8499	0.0653
100	0.23	3	9	98.7998	2.438111	67.5771	34.8443	0.8498	0.0652
100	0.315	1	10	122.648	3.14897	73.2653	34.3795	0.8811	0.0535
100	0.315	2	11	146.4963	3.113667	75.2875	33.4604	0.8824	0.0524
100	0.315	3	12	170.3445	3.206	68.0415	31.3756	0.8774	0.0562
100	0.4	1	13	200.628	3.67043	73.6296	30.4495	0.8994	0.0441
100	0.4	2	14	230.9114	3.626941	74.0757	32.6875	0.9006	0.0443
100	0.4	3	15	261.1949	3.624259	73.9852	33.433	0.8978	0.0455
70	0.15	1	16	272.5512	1.377059	56.6847	34.2903	0.7433	0.1029
70	0.15	2	17	283.9075	1.397985	60.2896	33.4264	0.7605	0.0956
70	0.15	3	18	295.2638	1.41757	56.5688	31.8388	0.7762	0.0908
70	0.31	1	19	318.7335	1.821659	71.3911	32.744	0.8608	0.0568
70	0.31	2	20	342.2031	1.767993	67.5699	32.1551	0.8525	0.0624
70	0.31	3	21	365.6728	1.75863	61.8384	30.1394	0.8568	0.0635
70	0.47	1	22	401.2559	2.111378	72.6717	32.5205	0.8909	0.0473
70	0.47	2	23	436.839	2.249015	71.0113	31.5012	0.8849	0.0497
70	0.47	3	24	472.422	2.203193	70.927	30.7979	0.8844	0.05
70	0.63	1	25	520.1185	2.67983	70.6311	30.7937	0.9089	0.0397
70	0.63	2	26	567.815	2.614385	71.5783	30.3907	0.903	0.0414
70	0.63	3	27	615.5114	2.53843	73.3809	33.3957	0.8977	0.0435
70	0.79	1	28	675.3213	3.003511	77.1974	30.7505	0.9196	0.0345
70	0.79	2	29	735.1311	2.938096	75.5845	31.3405	0.9154	0.0379
70	0.79	3	30	794.9409	3.078059	75.796	32.0106	0.9194	0.0356
40	0.32	1	31	819.1677	1.454585	59.8533	30.0829	0.8189	0.0746
40	0.32	2	32	843.3945	1.48097	59.9443	32.3529	0.8102	0.0747
40	0.32	3	33	867.6213	1.442993	59.317	32.6905	0.7948	0.0868
40	0.49	1	34	904.7185	1.621904	65.2272	32.1569	0.8537	0.0614
40	0.49	2	35	941.8157	1.660319	64.3871	32.3502	0.8572	0.06
40	0.49	3	36	978.913	1.638289	65.6546	31.9243	0.8551	0.0643
40	0.66	1	37	1028.881	1.855067	70.6107	32.4583	0.8883	0.0504
40	0.66	2	38	1078.848	1.826452	68.8369	31.9053	0.8807	0.0516
40	0.66	3	39	1128.816	1.821756	69.5494	32.0716	0.877	0.0545
40	0.83	1	40	1191.654	2.019185	71.1695	31.7329	0.9027	0.0438
40	0.83	2	41	1254.493	2.019844	74.3629	31.7346	0.8869	0.0462
40	0.83	3	42	1317.331	2.012104	73.0265	31.0523	0.898	0.0467
40	1	1	43	1393.039	2.2052	73.7654	30.2036	0.9142	0.038
40	1	2	44	1468.748	2.225274	73.2246	31.0708	0.9136	0.0374
40	1	3	45	1544.457	2.300807	73.1487	31.4915	0.9188	0.0356
10	0.4	1	46	1574.74	1.285081	57.5078	34.6709	0.7454	0.1034
10	0.4	2	47	1605.024	1.269763	51.2285	30.7564	0.7204	0.1184
10	0.4	3	48	1635.307	1.282578	51.8962	31.6959	0.7254	0.1108
10	0.55	1	49	1676.947	1.373156	58.4486	31.6444	0.796	0.0839
10	0.55	2	50	1718.587	1.378104	60.3394	33.0291	0.8139	0.0789
10	0.55	3	51	1760.226	1.357978	60.2865	32.9742	0.7979	0.0839
10	0.7	1	52	1813.222	1.445452	64.2744	34.4958	0.8352	0.0688
10	0.7	2	53	1866.219	1.440244	65.4519	32.626	0.8303	0.072
10	0.7	3	54	1919.215	1.450059	67.8503	32.7177	0.8396	0.0644
10	0.85	1	55	1983.567	1.521156	65.3798	31.7728	0.8606	0.0591
10	0.85	2	56	2047.919	1.537496	66.4293	31.9935	0.8671	0.056
10	0.85	3	57	2112.272	1.524244	64.7581	32.2312	0.8599	0.061
10	1	1	58	2187.98	1.603081	71.4261	32.8702	0.8837	0.05
10	1	2	59	2263.689	1.592607	66.5228	32.3265	0.8765	0.0529
10	1	3	60	2339.398	1.620015	66.7075	31.7473	0.8825	0.0523

Mouse 8a Tissue

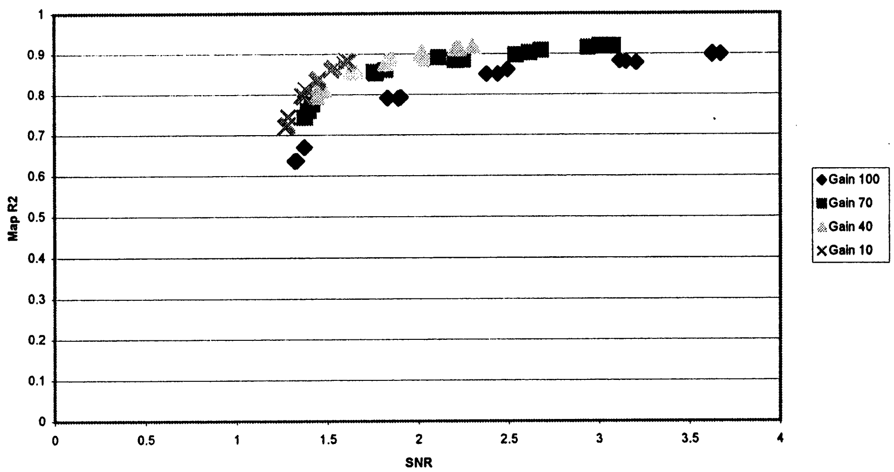

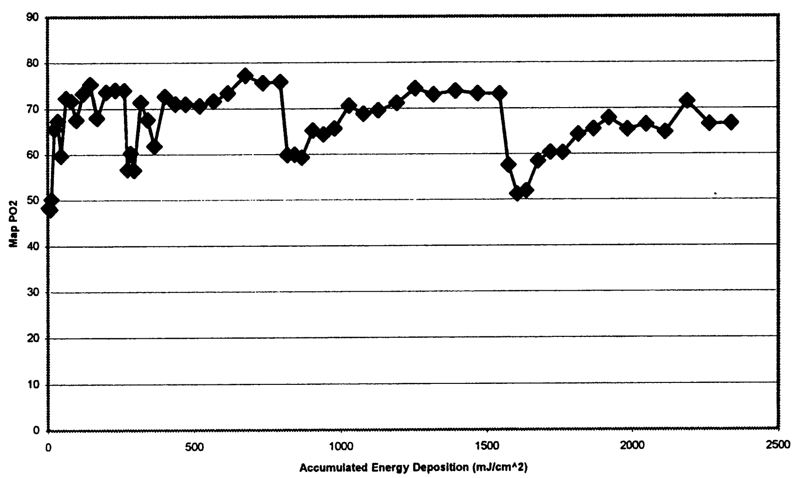

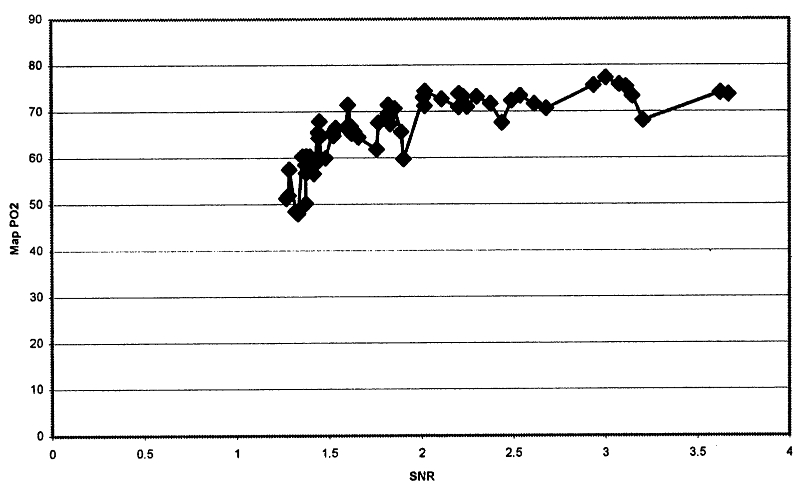

Appendix F: ARVO Abstract

The following abstract was submitted to the Association for Research in Vision and Ophthalmology, and accepted for poster presentation at the 2002 Annual Meeting, May 5-10. A travel grant was also awarded.

IMAGING OF OXYGEN TENSION IN THE MOUSE RETINA

PURPOSE

Retinal hypoxia and inadequate oxygen delivery have been implicated as causal for the development of several eye diseases, including diabetic retinopathy, glaucoma, and retinopathy of prematurity. The imaging of oxygen tension (PO_2) in the retina, generated from a measure of the phosphorescence lifetimes of bolus-injected palladium-porphyrin probes has been used successfully for nearly a decade to study retinal oxygen dynamics in the cat, miniature pig, and monkey; however, the specific parameters for applying this technique in the mouse have not been thoroughly investigated. As the number of transgenic and knockout mouse models displaying characteristics of human retinal diseases rapidly increases, an ability to image PO_2 in these very small eyes will likely be of great benefit. In this study, we investigate the refinement of a technique for generating PO_2 maps in the mouse retina using our recently constructed phosphorescence lifetime imaging system.

METHOD

To accurately measure retinal PO_2 in this animal, it was necessary to optimize a number of important acquisition parameters, including excitation power, intravascular probe concentration, camera exposure time, and camera intensifier gain settings. Measurements were made using both an in vitro calibration system and in vivo experiments in mice. Appropriate ranges for the stated parameters were determined using relationships between camera signal-to-noise values and the coefficient of determination (R^2) generated from the least-squares analysis used to produce the PO_2 maps.

RESULTS

R^2 decreased with increasing intensifier gain (at the same signal-to-noise ratio), with the highest gain setting for the camera (255) producing unacceptable fits. Intensifier gain settings of 10 and 100 yielded R^2 values above 0.90 with exposure times of 440 ms and 43 ms, respectively. Thus, moderate intensifier gain (near 100) reduced exposure time dramatically without significantly affecting the fits. The determined ranges for these parameters are currently being applied to the in vivo experiments, where excitation power and intravascular probe concentration will also be varied to study the effects of probe excitaiton on mouse retinal physiology.

CONCLUSION

Determination of these parameters will allow a more efficient and effective method for creating oxygen maps in the mouse retina. Investigation of how changes in retinal oxygen tension correlate with ocular disease progression in cases where abnormalities in the delivery and consumption of oxygen are thought to be contributing factors, such as diabetic retinopathy, will then be possible.

Appendix G: Sigma Xi MS Research Award Executive Summary

The following executive summary was submitted to the Worcester Polytechnic Institute Chapter of Sigma Xi, the Scientific Research Society, in nomination for their annual MS Research Award. The project was granted the award for 2002.

Introduction and Specific Aims

Retinal hypoxia has been recognized as a causal factor in the development of numerous eye diseases, including diabetic retinopathy, retinopathy of prematurity, and glaucoma. An ability to measure oxygen tension non-invasively in the eye would significantly advance our understanding of oxygen's role in these diseases. Recently, a phosphorescence lifetime imaging technique has been developed in the laboratory of Ross Shonat for measuring oxygen tension in the eye, and has important implications for the study of retinal oxygenation in mouse models of all of these serious diseases. It will be used specifically at WPI to study diabetic retinopathy.

While the phosphorescence lifetime imaging technique has become recognized in the literature, the specific parameters for data collection and analysis in the mouse eye have not been thoroughly investigated. This goal of this project was to examine these parameters in an effort to optimize the phosphorescence lifetime imaging technique for measuring oxygen tension in the mouse retina. The specific aims for achieving the goal of optimization were:

5. To calibrate the phosphorescence lifetime imaging system *in vitro* using known oxygen concentrations
6. To determine appropriate parameters for optimal excitation of the probe, including energy and power of the excitation light
7. To determine optimal procedures for image collection and analysis, including camera exposure time and intensifier gain

Background

Phosphorescence lifetime imaging is the marriage of techniques in physiology, pathology, imaging, and microscopy. Understanding its application to the diabetic mouse eye requires study of the pathogenesis of diabetic retinopathy and the basics of imaging and microscopy. The following sections provide background in these areas.

Diabetes and Diabetic Retinopathy

Diabetes is a disease characterized by the body's inability to produce insulin or utilize it efficiently. There exist two forms of diabetes: type-1, also known as juvenile-onset or insulin-dependent diabetes mellitus, and type-2, also known as adult-onset or non-insulin dependent diabetes mellitus. The greatest risk for complications, including diabetic retinopathy, exists in type-1 patients. Major risk factors in complications include abnormalities in blood glucose and/or levels of insulin, usually resulting from poor glycemic control.

Diabetic retinopathy is the most common microvascular complication of diabetes. Within 20 years of developing diabetes, more than 80% of type-1 patients have some degree of retinopathy. The disease is the leading cause of blindness among Americans of working age.

Diabetic retinopathy enters its earliest clinical stage when microaneurysms begin to form. These abnormalities manifest themselves as minute bulges or outpouchings on the retinal capillaries. Increased vascular permeability follows, reflecting an alteration in the blood-retinal barrier. Fluid begins to accumulate in the retina at this stage, accompanied by hard exudates (yellow-white discrete patches of lipid that occur in rings around leaking capillaries) and cotton wool spots (areas of dense, scar-like tissue), resulting in obscured vision. Ultimately, capillary nonperfusion, ischemia, and hypoxia result.

In the proliferative stages of the disease, new blood vessels begin to grow, possibly induced by the ischemic/hypoxic state of the retina. These new vessels are fenestrated capillaries and are thus extremely fragile and prone to hemorrhage. The new vessels grow out of the retina and into the vitreous, causing vitreal scarring and shrinkage. This traction pulls on the fragile new vessels, causing retinal traction, retinal tears, vitreous hemorrhage, and retinal detachment (which results in blindness).

The pathogenesis of diabetic retinopathy is thought to be related to hypoxia. It is not completely understood whether a change in oxygen consumption causes the alterations in vascular responses to compensate for changes in blood flow, or if the changes in blood flow cause alterations in oxygen consumption. However, it is understood that, by the time capillary closure and nonperfusion are clinically apparent, the retinal tissue is hypoxic, and the primary stimulus for neovascularization is hypoxia.

The two most common treatments for diabetic retinopathy are vitrectomy and panretinal photocoagulation. These are aimed at relieving hypoxia and slowing the neovascularization process, hopefully reducing the risk of visual loss. The treatments tend to improve oxygenation in the ischemic and hypoxic retina. Progression of diabetic retinopathy can often be prevented with good glycemic control of diabetic patients; the progress of the disease may be stopped in its very early stages if blood glucose is strictly regulated. For all forms of treatment, early detection of the disease is essential; once the cascade of prolifereative retinopathy has begun, little can be done to save the sight of the patient.

Numerous animal models, including dogs, cats, rats, and mice, have been developed for diabetic retinopathy. Mouse models for the disease have gained prominence due to the similarity between the human and mouse retinas, the relatively quick breeding time for mice, and the ease of working with these animals in a laboratory setting. The ability to study the changes in oxygen tension in these diabetic mouse eyes will likely be of great benefit to diabetic retinopathy research.

Phosphorescent Probe for Intravascular PO_2 Measurements

Light-emitting probes have received considerable attention in the literature as imaging aids. Chemicals that may be injected into the bloodstream, and that emit light when excited, have numerous implications for the study of blood vessels. Additionally, the phosphorescent probe used in this study, palladium meso-tetra porphrine, has the favorable quality of being sensitive to oxygen molecules in the bloodstream.

Phosphorescence is defined as the emission of light during a transition from an excited triplet state to the ground state. When a large number of phosphorescent molecules are excited simultaneously, the resultant total light emission can be represented by the function:

$$I(t) = I_0 \exp(-t/\tau)$$

where I(t) is the phosphorescence intensity as a function of time, I_0 is the initial, maximum intensity at t = 0, t is the time post-excitation, and τ is the lifetime of the decay.

When the phosphorescent probe is excited by light that has been sinusoidally modulated, the phosphorescence emitted will have the same frequency, but will have lower amplitude and be delayed in phase by an angle θ. θ is related to the probe lifetime by the following equation:

$$\tan \theta = \omega\tau$$

where ω is the excitation frequency.

A phosphorescent molecule that has been excited to the triplet state may transfer its energy to another molecule without light emission, a phenomenon termed *quenching*. Such interactions between phosphors and their environment are common; the spin-forbidden transition from the triplet state to the ground has a relatively long lifetime (on the order of ms), and increases the probability of contact between molecules. In blood, the only significant quenching agent is oxygen. The efficiency of phosphorescence quenching depends on the frequency of collision between the excited triplet state molecule and the quencher before the phosphor returns to the ground state, and is therefore dependent on the concentration of oxygen in the vicinity of the probe. This relationship is represented by the Stern-Volmer equation for an oxygen-quenched probe:

$$\tau_o / \tau = 1 + k_Q \tau_0 [PO_2]$$

where k_Q is the bimolecular rate constant (or quenching constant), and $[PO_2]$ is the oxygen concentration. In a zero oxygen environment, $\tau = \tau_o$ and the lifetime is at a maximum.

Phosphorescence Lifetime Imaging of Oxygen Tension

Phosphorescence lifetime imaging requires a unique microscopic instrument (Figure 1). An illuminating beam is emitted by a xenon arc lamp, sinusoidally modulated using an optical chopper, and filtered to 524±20 nm (the excitation wavelength of the phosphorescent probe used in this study) by a monochromator. The light is then reflected down into the objective by a dichromatic mirror. This light excites the phosphorescent molecules in the specimen to the triplet state, and phosphorescence is emitted during the decay of the molecules back to their ground states. This emitted light then passes straight through the dichromatic mirror to the CCD camera, which transmits the image to the PC-based image analysis system.

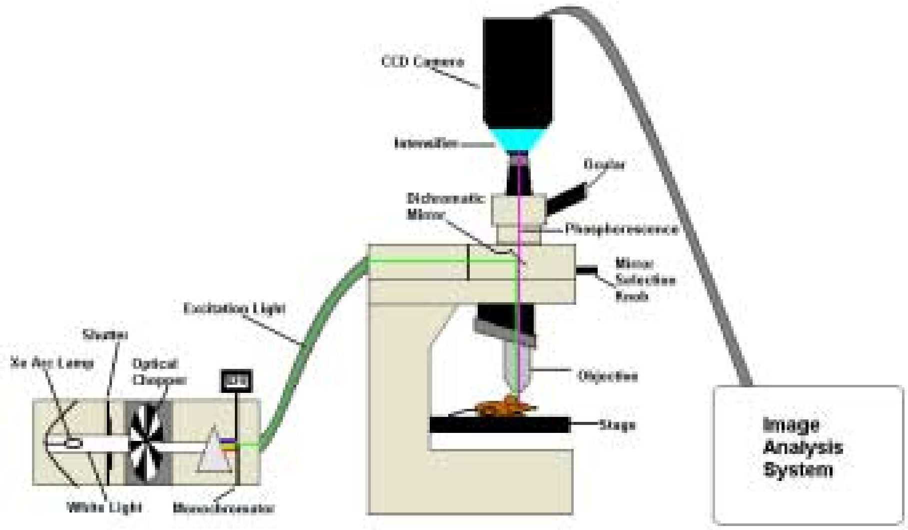

Figure 1—The phosphorescence lifetime imaging system

A phase-sensitive measure of the phosphorescence lifetime in the presence of oxygen is possible when the delivered excitation light and the sensitivity of the collection system (intensifier) are independently modulated and the phase relationship between these two elements is accurately varied. Intensity images (Figure 2) may then be taken with varying intensifier phase delays, and a graph of intensity versus phase delay may be constructed. This graph may be used in conjunction with the following equation to determine the phosphorescence phase delay, θ:

$$I(\theta_D) = k[Pd]\{1+ m_D m\cos(\theta-\theta_D)\}$$

where $I(\theta_D)$ is the intensity, k is a constant, [Pd] is the probe concentration, θ_D is the phase delay of the intensifier sensitivity, and m and m_D are parameters defined as:

$$(1 + \omega^2\tau^2)^{-1/2}$$

for the excitation/emission and intensifier sinusoids, respectively. A best-fit estimate for τ may then calculated using linear regression. This value of τ may be used in the Stern-Volmer equation to calculate PO_2 maps (Figure 2).

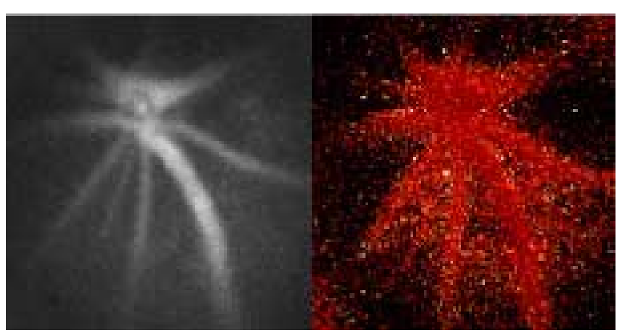

Figure 2—Phosphorescence intensity image and PO_2 map of the mouse retina

Methods and Results

In Vitro System

An *in vitro* system was designed and constructed to calibrate the probe prior to data collection and to determine approximate gain settings and exposure times required to produce acceptable oxygen maps (Figure 3). The system includes a length of Tygon® tubing, into which a solution consisting of albumin stock solution, NaCl, glucose, and probe is injected. A peristaltic pump is used to circulate the fluid through the system. The phosphorescent solution flows through an oxygenator used to apply gas mixtures with known oxygen concentrations. Upon leaving the oxygenator, the solution then flows through a glass capillary tube situated under a microscope equipped with the phosphorescence lifetime imaging system. The phosphorescence lifetime is then measured as previously described, and a PO_2 map is generated.

Signal-to-noise ratios (SNR) were used to determine appropriate gain settings and exposure times for subsequent *in vivo* experiments. A physiological oxygen concentration of 40 mm Hg (5% oxygen applied using the oxygenator) was applied to the probe solution. Exposure times were tested at random in an attempt to achieve a maximal range of SNR for camera intensifier gain settings 10, 100, and 255. Exposure times yielding SNR of approximately 2 and approximately 225 were noted for each gain.

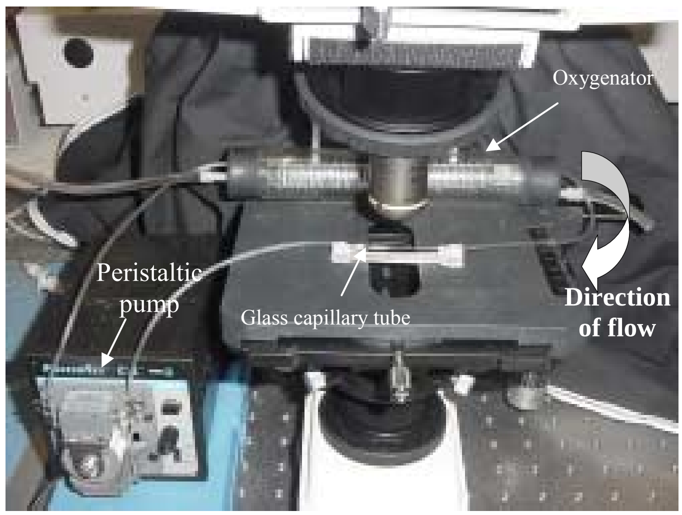

Figure 3—*In vitro* phosphorescence lifetime imaging system

Phosphoresce lifetime images were then taken at a range of ten exposure times equally spaced between the time yielding SNR ≈ 2 and the time yielding SNR ≈ 225. R^2 maps, which demonstrate the integrity of the fit between the phosphorescence intensity data and the equation $I(\theta_D) = k[Pd]\{1+ m_D m\cos(\theta-\theta_D)\}$, were then created. From these maps, the average R^2 value for the entire capillary tube was determined. These values were plotted versus SNR for each gain setting (Figure 4).

These data indicate that a gain setting of 255 does not produce images with acceptable R^2 values, regardless of the SNR. Conversely, R^2 values of greater than 0.9 were obtained with gain settings 10 and 100 for all SNR > 50. These results were verified in later experiments for a full range of physiological oxygen concentrations. As a result, all subsequent experiments were conducted at gain settings between 10 and 100. Since the data indicate that all SNR > 50 yield similarly high R^2 values, exposure times resulting in signal-to-noise ratios of 50 or less were used, thereby minimizing excitation light exposure.

The correspondence between the PO_2 values indicated by the map and those applied using the gas mixer and oxygenator was used to calibrate the system to provide accurate measures of PO_2 within the vasculature. It was discovered using the *in vitro system* that the data analysis program as it existed assigned different PO_2 values to image sets taken with different gain settings and exposure times. The identification of this problem allowed the adjustment of the program parameters and the production of accurate oxygen maps.

In Vivo System

Mice used in the study were handled according to the Institutional Animal Care and Use Committee protocols. Mice were anesthetized with an avertin/saline solution and situated in a stereotaxic

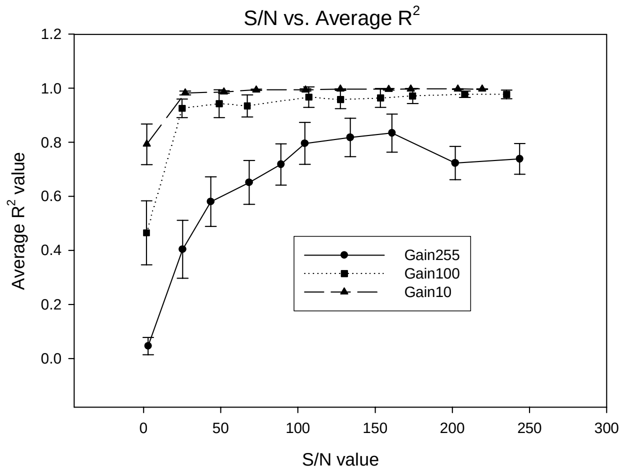

Figure 4—Average R^2 value versus SNR for gain settings 10, 100, and 255

head holder to prevent movement during experimentation. Mouse eyes were dilated, hydrated with an ophthalmic ointment, and shielded with a cover glass to allow observation of retinal vessels at the back of the eye. A solution of Pd meso-Tetra (4-carboxyphenyl) Porphrine probe was injected into the femoral vein in the amount of 10 mg/kg.

Gain and exposure time settings were determined *in vivo* using the *in vitro* experiments as a guide. SNR values were calculated using gain settings 10, 40, 70, and 100. Quality of oxygen maps (determined by average R^2 value) improved with SNR of up to about 15, after which quality remained constant. When ranges of exposure times yielding SNR between three and 15 were used for each gain, it was determined that exposure times of greater than one second caused damage to the retinal vessels (indicated by lack of blood flow). As such, a new range of exposure times resulting in SNR between three and 15 without exceeding one second was determined (Table 1).

Gain setting	Exposure time range (seconds)
100	0.058 - 0.402
70	0.15 - 0.79
40	0.32 - 1.0
10	0.4 - 1.0

Table 1—Exposure times yielding a range of SNR between approximately 3 and 15, without exceeding 1.0 seconds

Experiments were also conducted with repeated exposures of 0.23 seconds at gain 100 and 1.0 seconds at gain 40. Average PO_2 was plotted versus accumulated light exposure, and it was determined that extended light exposure (greater than 1000 mJ/cm^2) actually cause a decrease in vessel PO_2. Such decreases were not observed with shorter terms of light exposure.

Conclusions

The phosphorescence lifetime imaging system may be used on the mouse eye with accurate and reliable results. Gain settings between 10 and 100 will yield acceptable intensity images and oxygen maps. Exposure times have been determined for each gain setting. Longer exposure times yield intensity images and maps of better quality—however, care must be taken not to exceed cumulative light exposure of 1000 $mJ/\ cm^2$ over the course of the experiment due to the risk of retinal damage and decrease in retinal PO_2. If longer exposure times are necessary, power of excitation light must be decreased.

The phosphorescence lifetime imaging system will be used to study retinal oxygenation changes in mouse models of diabetic retinopathy. Understanding the changes in oxygenation at different stages of this serious disease may assist in developing and administering treatments and cures. The noninvasive nature of the technique makes its application to human patients a potential option. Detection of hypoxia using phosphorescence lifetime imaging may allow for early detection and treatment of diabetic retinopathy, potentially preventing blindness.